Insights into simple crater formation: The Hummeln impact structure (Småland, Sweden)

Johanna Granbom

Dissertations in Geology at Lund university
Master's thesis, no 665
(45 hp/ECTS credits)

Department of Geology
Lund University
2023

Insights into simple crater formation: The Hummeln impact structure (Småland, Sweden)

Master's thesis

Johanna Granbom

Department of Geology
Lund University
2023

Contents

1 Introduction **7**
2 Background **7**
2.1 Crater formation 9
2.2 Shock metamorphism & impactites 11
2.2.1 Shock-metamorphism 12
2.2.2 Spatial distribution of impactites 13
2.3 Impact-induced hydrothermal activity 14
2.4 The Hummeln structure 14
2.4.1 The Lake Hummeln Enigma 14
2.4.2 The Hummeln-1 drill core 15
2.4.3 Age of the Hummeln event 15
3 Method **16**
3.1 Field studies 16
3.2 Map-making and analysis of field notations 16
3.3 Core mapping 16
3.4 Petrography 17
4 Results **17**
4.1 Field observations and samples 17
4.1.1 Macroscopic fractures 17
4.1.2 Distribution of breccia types 18
4.1.3 Field samples 18
4.2 The Hummeln-1 drill core analysis 20
4.2.1 Mapping of drillcore 20
4.2.2 Petrographic analysis of drill core 20
5 Discussion **21**
5.1 Field observations & the Hummeln-1 drill core 21
5.1.1 Impactites of the Hummeln structure 21
5.1.2 Landforms of the Humlenäs-shoreline 24
5.1.3 Glacial trail of sedimentary blocks 24
5.1.4 Post-impact sedimentary infill (157.3-17.0 m) of the Hummeln-1 drill core 24
5.1.5 Crater-fill (164.25-157.3 m) of the Hummeln-1 drill core 26
5.1.6 Target rocks and sediments 28
5.2 Propagation of shock wave 28
5.2.1 Traces of shock metamorphism 28
5.2.2 Shock wave behavior in a sedimentary target 30
5.3 Evidence of impact-induced hydrothermal activity 31
5.4 Suggestions for future studies 32
6 Conclusions **33**
6.1 Conclusions about the Hummeln structure 33
6.2 Conclusions about small, simple, and old, impact structures 33
7 Thanks to **33**
8 References **33**
9 Appendix **37**

Cover photo: Photo of impact breccia at the Hummeln impact structure, toes and hammer for scale.
Photo: Johanna Granbom

Nedslagskraterbildning — en studie av Hummeln-strukturen (Småland, Sverige)

JOHANNA GRANBOM

Granbom, J., 2023: Nedslagskraterbildning — en studie av Hummeln-strukturen (Småland, Sverige). *Examensarbeten i geologi vid Lunds universitet*, Nr. 665, 37 sid. 45 hp.

Sammanfattning: Hummeln-strukturen har varit föremål för geologiska undersökningar under nästan två hundra år. Den udda förekomsten av paleozoiska block och en cirkulär djupanomali i den i övrigt förkastningsdominerade sjön har gett upphov till många teorier. Det var faktiskt inte förrän 2015 som fynd av chockad kvarts kunde bekräfta att den märkliga formen skapades av ett meteoritnedslag. Den här studien är den första karteringen av Humlenäs-halvön och Hummeln-1 borrkärnan som gjorts utifrån vetskapen om att djuphålan har bildats av ett nedslag och att de deformerade stenarna verkligen är impaktiter. Viktiga fynd är impaktsmälta och suevitisk breccia som liknar litologier vilka tidigare beskrivits i nedslagsstrukturer med blandad eller sedimentär målberggrund. Kombinationen av chockbildade mikrostrukturer – PDF:er är ovanliga medan PF:er är vanliga – är karaktäristisk för den låga chocktrycksregimen, vilket också pekar på att berggrunden var täckt av sediment eller sedimentära bergarter vid nedslagstillfället. Detta är också den första beskrivningen av hydrotermala omvandlingar i Hummeln-strukturen. Dessa indikerar förekomsten av nedslags-initierad hydrotermal aktivitet. Fortsatta undersökningar vad gäller tid-punkten för meteoritnedslaget är nödvändiga. Att datera primära mineral är en möjlig väg till att få en ålder på den hydrotermala aktiviteten, och därmed en minimiålder på nedslagseventet som bildade Hummeln-strukturen.

Nyckelord: Nedslagskrater, hydrotermal omvandling, chockmetamorfos, sedimentär målberggrund

Handledare: Sanna Alwmark och Carl Alwmark

Ämnesinriktning: Berggrundsgeologi

Johanna Granbom, Geologiska institutionen, Lunds universitet, Sölvegatan 12, 223 62 Lund, Sverige.
E-post: granbomjohanna@gmail.com

Insights into simple crater formation: The Hummeln impact structure (Småland, Sweden)

JOHANNA GRANBOM

Granbom, J., 2023: Insights into simple crater formation: The Hummeln impact structure (Småland, Sweden). *Dissertations in Geology at Lund University*, No. 665, 37 pp. 45 hp (45 ECTS credits)

Abstract: The Hummeln structure has been subject to geological investigations for nearly two centuries. The odd occurrence of Paleozoic blocks and a circular depth-anomaly in the otherwise fault dominated lake sparked plenty of theories. It was however not until 2015 that findings of shocked quartz could confirm that the structure originated from a hypervelocity impact event. The present study is the first mapping of the Humlenäs peninsula and the Hummeln-1 drill core done with the certain knowledge that the depression has impact origin, and that the deformed rocks are in fact impactites. Important findings of this work are impact melt and suevitic breccia that resemble lithologies previously described in impact structures with mixed or sedimentary target. The assemblage of shock-induced microstructures – planar deformation features are rare while planar fractures are abundant – is characteristic of the low shock-pressure-regime. These observations points in the direction of a sedimentary cover at time of impact. This is also the first description of hydrothermal alterations at the Hummeln structure, providing indications for impact-induced hydrothermal activity. Further investigations are required at the Hummeln impact structure regarding the age. Dating secondary minerals is a possible way to achieve the age of the hydrothermal activity and therefore a minimum age of the Hummeln impact event.

Keywords: hypervelocity impact event, impact-induced hydrothermal activity, shock-induced microstructures, sedimentary target, simple impact crater, mapping, lake of the week

Supervisors: Sanna Alwmark och Carl Alwmark

Subject: Bedrock Geology

Johanna Granbom, Department of Geology, Lund University, Sölvegatan 12, SE-223 62 Lund, Sweden.
E-mail: granbomjohanna@gmail.com

1 Introduction

The extent to which huge space rocks influence Earth by collision was not accepted in the scientific community before high resolution pictures of the surface of the Moon (French, 1998). Since the 1960's, hypervelocity impact events and the scars they create have gotten more appreciated. Consequently, 25 years ago, Bevan M. French stated that the importance of impact events was finally established – the scientific community agreed that the process of collision had shaped the solar system and reshaped the Precambrian Earth. The potential role in creating habitats for early life (e.g., Maher & Stevenson, 1988; Osinski et al., 2020) and their ability to initiate global extinction events (e.g., Alvarez et al., 1980; Schulte et al., 2010) indicate that impact events have greatly influenced the Phanerozoic Earth as well. French further claimed that the important assignment for geoscientist consequently was to use "preserved terrestrial impact structures to better define the complex mechanics by which impact structures form on Earth and other planets" (p.4, 1998).

To this day, about 200 impact structures have been confirmed on Earth (Osinski et al., 2022). Most of these are found in areas where old, crystalline bedrock is exposed, e.g., Australia and the Baltic and Canadian shields. Even though the majority of the impact structures on Earth (hidden under 4 kilometers of water in the oceanic crust) will never be found, many more await discovery. Plate tectonics and erosive forces like weathering and vegetation makes the study of ancient impact structures difficult. However, distal studies of other planets and the Moon as well as studies of terrestrial craters have shown that impact craters vary in morphology, and that the shape depends on the size of both projectile and target (Fig. 1; French, 1998). The most important factor regarding preservation of craters is burial and the presence of long-living marine conditions, explaining why some craters are better preserved than others (e.g., Suuroja et al., 2002).

The Hummeln impact structure is located in southeastern Sweden (Fig. 2). It has a simple crater geometry and is relatively small – its current diameter is less than 2 km wide. The most quoted age of the impact event is based on biostratigraphic studies of post-impact sedimentary infill and set to 470-460 Ma (Lindström et al., 1999). During most of the Early Paleozoic the Baltoscandian shield was covered by epeiric seas (e.g., Jaanusson, 1973), and the structure has most likely been preserved thanks to millions of years of marine conditions. As smaller impact structures have less chance of lasting over time, the Hummeln impact structure offers a great opportunity to better understand simple impact structures and the traces of relatively small impact events. The objective of this study is to carry the torch of Bevan M. French and re-visit the Hummeln impact structure. Through careful mapping of the remnant crater, the aim is to increase our understanding of the Hummeln impact structure and with that contribute to the knowledge about small, simple, ancient impact structures.

2 Background

Erosive forces constantly change the surface of Earth. This is why our planet does not look spotty from bombardment, like the Moon (Fig. 1). Two confirmed impact structures are here used to illustrate the importance of time and erosion when dealing with the collision-history of our planet: Meteor Crater and the Gardnos impact structure (Fig. 3).

One of the most exceptionally preserved impact structures on Earth is the Meteor Crater (Arizona, Fig. 3; Barringer, 1914). It is only 49.000 years old and the

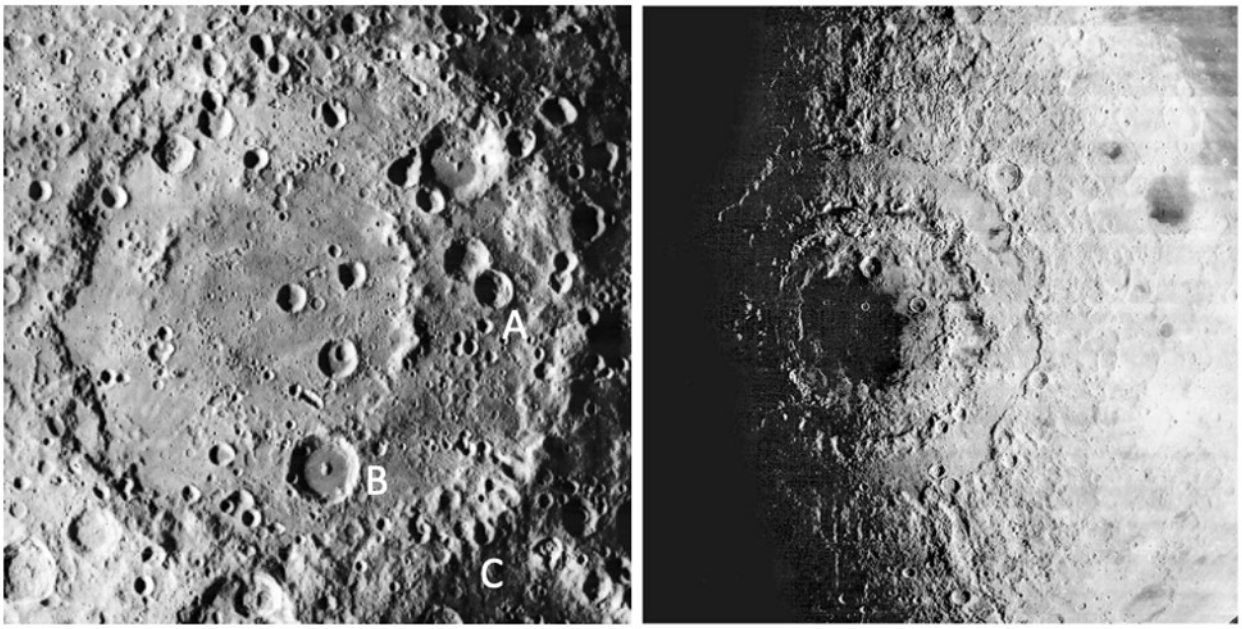

Figure 1. Examples of different crater morphologies from impact structures on the Moon. To the left: A) Small, bowl-shaped simple crater. B. Complex peak-basin crater. C. Vague, multi-ring crater that is older than all the small ones (from James Stuby (NASA) via Wikimedia Commons). The photo to the right shows Mare Orientale, a 900 km wide multi-ring basin (photo from NASA).

general lack of vegetation in the Arizona desert, among other erosive processes, gives this impact structure favorable prerequisites. When seen in profile, Meteor Crater has the typical shape of a simple crater: a bowl-shaped, more or less circular hole, with a steep crater rim (Barringer, 1914; Kring, 2017.

For comparison, the Gardnos impact structure (Norway) has suffered ~546 million years of erosive forces (Kalleson et al., 2009), among these the Caledonian orogeny (Fig. 3; French et al., 1997). What is left today of the initial crater is the vague topography of the central uplift. Impact origin could however be confirmed (Dons & Naterstad., 1992) thanks to microscopic shock-metamorphic features (see section 2.2.1).

To be able to find, confirm, investigate, and learn from ancient impact structures which no longer retain their obvious crater-shapes (Fig. 3), it is essential to extend our understanding of the various traces of deformation caused by impact events. This includes characterizing shock-metamorphic features (section 2.2.1), the distribution of impact-deformed rocks

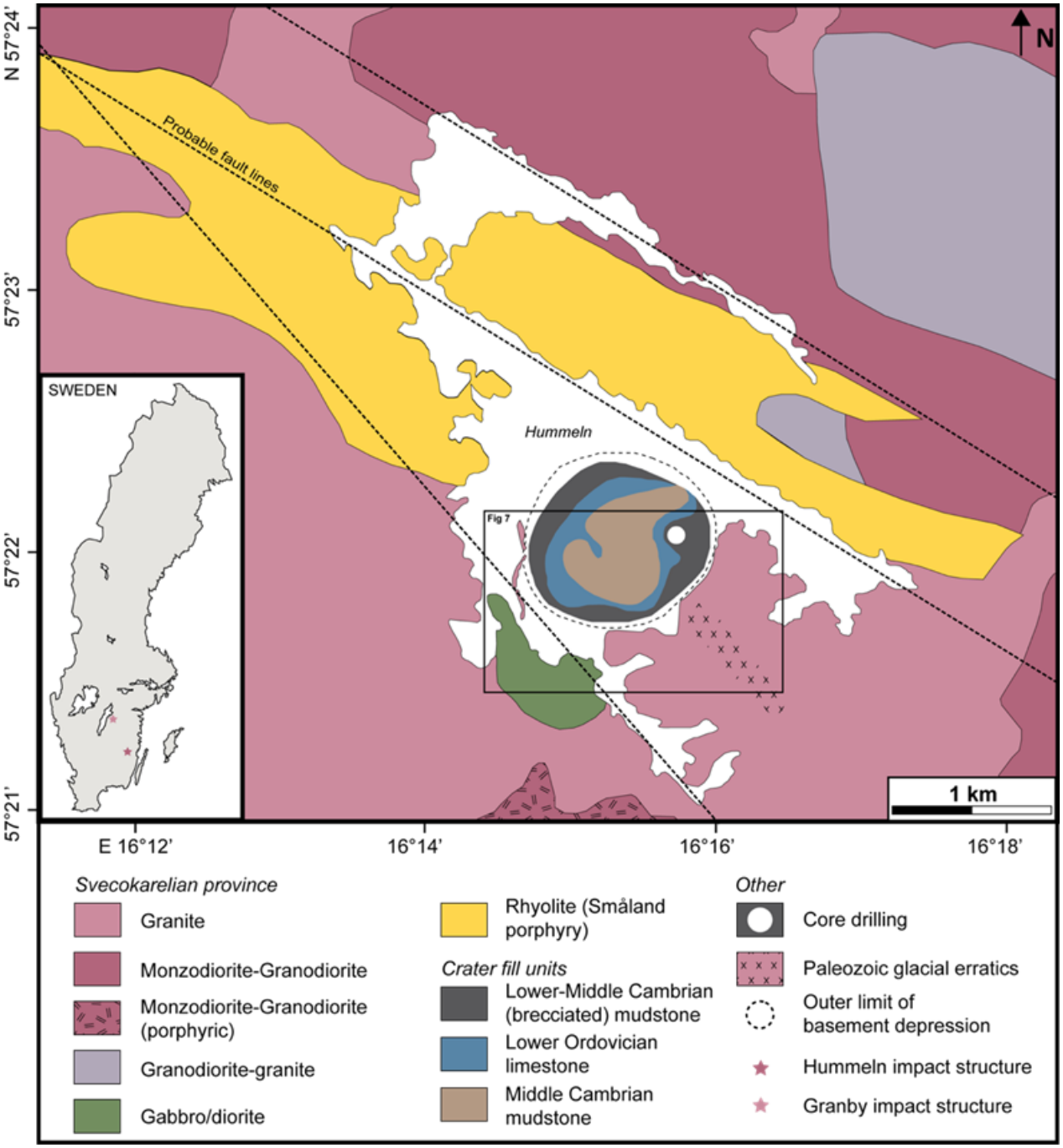

Figure 2. Geological map showing bedrock surrounding lake Hummeln, distribution of Paleozoic sedimentary rocks in the depression (after Lindström et al., 1999) and the glacial trail SE of lake Hummeln. The coordinates for the Hummeln-1 drill core is marked, how the Hummeln impact structure as well as the Granby impact structure are located in Sweden. The rectangle refers to the field map Fig. 7. Map modified after Holm-Alwmark (2021) using Adobe Illustrator). NE- and NNE-oriented probable fault lines (- - - - -) after Svensson (1966).

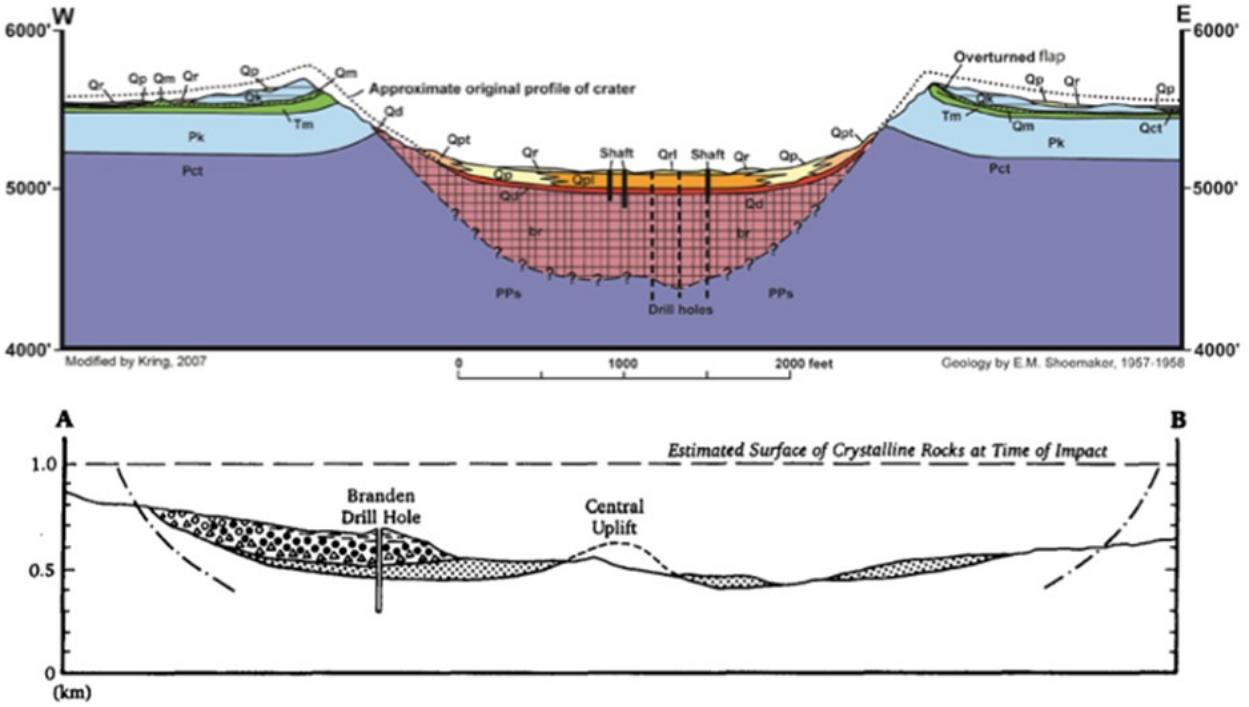

Figure 3. Comparison of impact structures of different ages. The upper profile shows the bowl-shaped Meteor crater (49.000 years old, Arizona) and the lowermost profile shows the older, complex and more eroded Gardnos impact structure (546 Ma, Norway). The upper is from Shoemaker (1957) and modified by Kring (2007), the lower is from French (1997).

("impactites", section 2.2.2), and traces of impact-induced hydrothermal activity (section 2.3), in impact structures of different ages, sizes, and geometries. Unique shock-metamorphic features have proven vital for recognizing and confirming impact structures (e.g., Melosh, 1989; French & Koeberl, 2010). The energy produced at celestial body collision far exceeds any endogenic processes, and the resulting shock wave cause unique deformation features in the target rocks and minerals (e.g., French & Koeberl, 2010). Specific shock-features have been experimentally linked to pressure-ranges. However, these experiments usually start at >10 GPa (Poelchau & Kenkmann, 2011). Shock-metamorphic features that originate from the low-shock-pressure-range (<10 GPa) are therefore not as well understood relative to intermediate to high-pressure shock metamorphic features (Poelchau & Kenkmann, 2011). This is especially problematic when studying highly eroded impact structures, since the lithologies affected by high-shock-pressure (e.g., ejecta) are often located in the shallow part of a crater – i.e., erodes first.

It is not only the search for small impact structures that benefits from better understanding of the low-shock regime. When the shock wave radiates outward the energy is lost fast, i.e., even when it comes to huge impact structures, a majority of the affected target lithology only ever experience pressures of the lower shock-regime (Melosh, 1989; Poelchau & Kenkmann, 2011). Increasing the knowledge about low-pressure shock-regime features is essential to confirm old and highly eroded impact structures on Earth. The Hummeln impact structure (Småland) is less than two kilometers in diameter and assumed to be at least 460 million years old (Fig. 2; Lindström et al., 1999). The traces of impact that have until now been discovered in the Hummeln structure – by Alwmark et al. (2015) and in this study – are in the low-pressure range, adding important pieces to this puzzle.

2.1 Crater formation

When an object only a few meters in diameter passes through the Earth's atmosphere it will disintegrate, lose kinetic energy, and strike the surface with a velocity of a few hundred meters per second (French 1998). The crater produced is of the same scale as the projectile itself and often referred to as a "pit" (Osinski et al., 2022). This crater is created only through mechanical excavation (French, 1998).

A larger object that collides with Earth at cosmic velocities (>11.2 km/s) creates a hypervelocity impact crater (Osinski et al., 2022). The shock waves produced at the point of impact are high tension stress waves. They travel through both the target rock and the projectile with a velocity much higher than the speed of sound in rocks, resulting in a shock wave (French, 1998). Diagnostic for hypervelocity impact structures, from here on referred to as "impact structures" is evidence of shock metamorphism on a rock- or mineral scale (see section 1.2.1). The minimum size for an iron object to travel through the atmosphere without disintegrating and also retaining its cosmic velocity is 20 meters in diameter, while a stony object to reach the Earth's surface at its original cosmic velocity needs to be at least 50 meters in diameter (French, 1998).

The crater formation process is traditionally divided into three different stages: 1) contact and compres-

sion stage, 2) excavation stage and 3) modification stage (Fig. 4). The latter is followed by "conventional" geological processes, like slumping and erosion (French, 1998).

1. **The contact/compression stage** starts when the projectile collides with Earth's surface. Depending on the target, it penetrates <2 times its own diameter into bedrock or sediments (O'Keefe & Ahrens, 1993). Shock waves are generated when the projectile hits the target. One set of shock waves propagates outward into the target rocks while a reflecting set of waves go through the projectile (Melosh, 1989). When the shock wave reaches the back end of the projectile, it generates a release wave (sometimes referred as tensional- or rarefaction wave) that travels back through the projectile (French, 1998). When the release wave reaches the point of impact it releases the projectile of the immense pressures induced by shock compression, resulting in near complete melting and vaporization (Melosh, 1989), The contact/ compression stage ends when the projectile is unloaded – it is destroyed and no longer plays a part in forming the crater (French, 1998).
2. The contact/compression stage is **followed by the excavation stage**. During this stage, material is ejected up and out of the transient crater, which is what causes the crater to be 20-30 times bigger than the projectile. The shock waves travel outward and upward from the point of impact (and sets off release waves when reaching the ground surface), it fractures and shatters the target but also forces it downward, upward, and outward from the impact point. The transient crater is formed: a bowl-shaped circular hole with a steep crater rim. When the transient crater reaches its maximum diameter, the excavation stage ends. For large impact events, the transient cavity is gravitationally unstable, and a complex impact crater will start to form (e.g., Kenkmann et al., 2012).
3. During the **modification stage** the dominating forces are gravity and rock mechanics. Depending primarily on the size of the transient crater, but also on target lithology, the extent of these processes will differ (Fig. 4.; Osinski et al., 2022). The types of resulting morphologies are generally divided into the following categories: simple crater, complex crater or multiring basin (Fig. 1, Fig. 5; French 1998). The discussion regarding the diameter at which the transition from a simple to a complex crater occur on our planet is still ongoing (e.g., Osinski et al., 2022; Dence, 1972) and several terrestrial impact structures are currently assigned "transitional" between the two categories, e.g., the Gow Lake impact structure (5 km; Thomas & Innes, 1977; Pickersgill et al., 2020). The numbers generally cited for the simple- to complex impact crater transition are 2 km diameter in sedimentary targets and 4 km in crystalline targets (French, 1998).

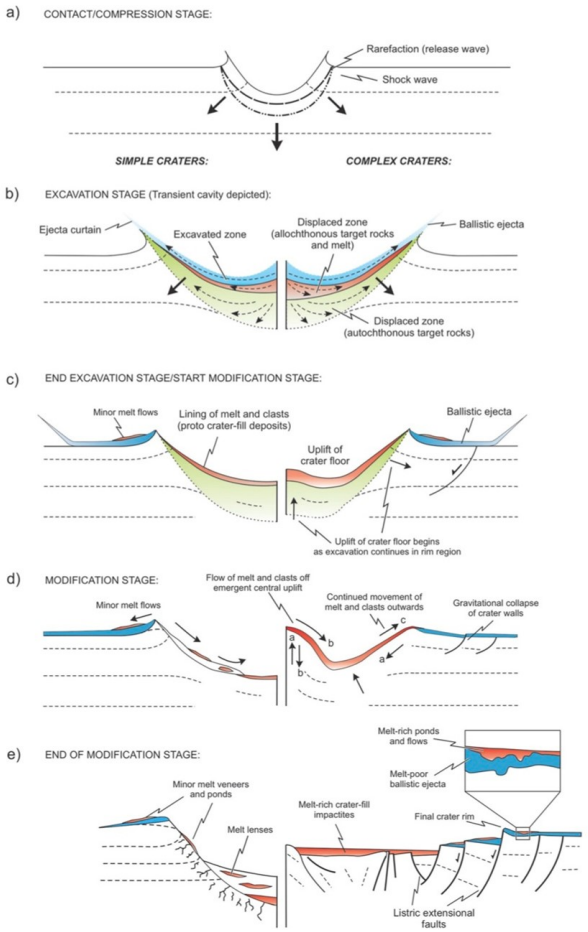

Figure 4. Crater formation process step by step of a simple crater (to the right) and complex crater (to the left). (From Osinski et al. 2022).

The simple crater is bowl-shaped with a depth between 1/3 and 1/5 of its diameter (Melosh, 1989). There is no central uplift and modifications primarily involve collapse of the crater rim resulting in debris partially filling up the interior (Fig. 4). The lens of debris, melt and breccias generally make up half the crater volume (Melosh, 1989). See section 1.3 for the description of where each lithology is expected to be found in a simple crater.

The complex crater has, as implied by the name, a more complex modification stage (Fig. 5). The bigger transient crater is less stable and suffers a more severe collapse, resulting in a central uplift and faulting of the crater wall (French, 1998). The uplift of deep-seated rocks begins at the end of the excavation stage as a result of gravitational collapse (Melosh, 1989; French, 1998). The steep crater wall collapses through normal faulting, slumping debris into the crater interior. During complex crater formation melt production is larger than during simple crater formation, and complex craters typically have a blanket of impact melt rock overlying the crater floor. Together these processes collaborate to make the final complex crater shallower than the simple crater.

Complex craters are further divided based on differences in morphology (Central-peak structures, Central -peak-basin structures and Peak-ring-basin structures; French, 1998). Thanks to crater-morphology-studies of

other planets and moons, we also know that there are multiring basins (French, 1998). The exact transitional diameter between peak-ring craters and multiring basins is not known for Earth but on the Moon it occurs at 150-200 km in diameter (French, 1998). A multiring-structure does not have a central peak, instead it has several rings (Fig. 1).

2.2 Shock-metamorphism and impactites

The velocity of the shock wave decreases rapidly with increased distance from the point of impact. Since the shock wave travels in half a sphere it will affect an exponentially larger volume of rock (O'Keefe & Ahrens, 1993), and energy is also lost through heating and mechanical deformation of the target. By studying the grade of shock-induced deformation, it is possible to study this pattern of shock wave loss of energy. Where shock-pressures are highest, close to the point of impact, target rocks will transform into vapor or melt (French, 1998). In the zone where pressures are not high enough to cause whole-rock melting and vaporization, rocks and minerals will experience shock-metamorphism, resulting in the formation of distinctive shock-metamorphic features (see section 2.2.1). The shock wave eventually reaches normal seismic

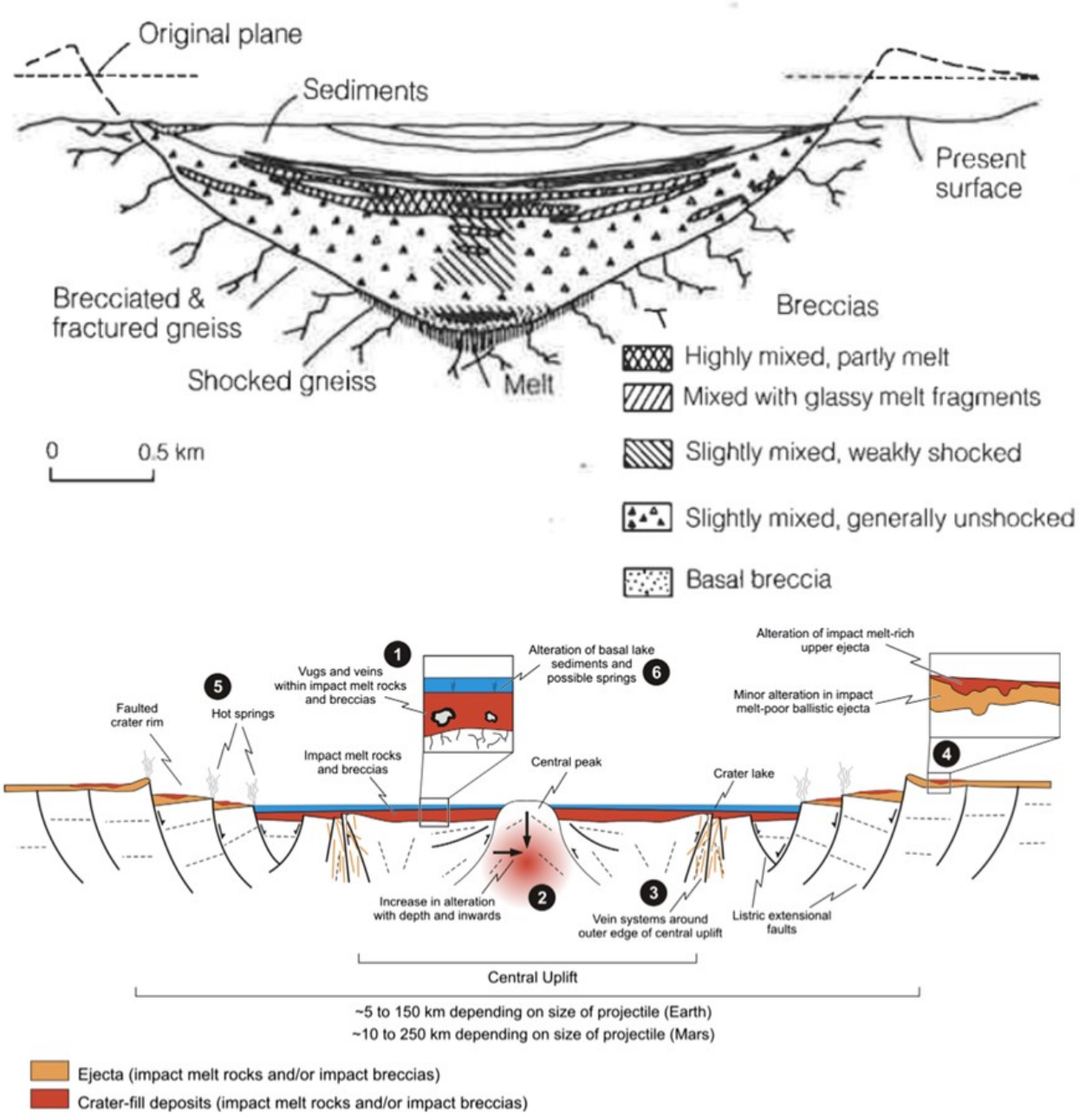

Figure 5. End-result morphologies after modification and erosion, simple and complex craters compared. The upper profile is an interpretation of the eroded Brent impact structure (modified after Melosh 1989), red numbers showing the morphology and spatial distribution of impactites: 1) crater wall 2) crater fill 3) ejecta material. The numbers in the illustration of the complex crater refers to potential locations for impact-induced hydrothermal systems, see also Fig. 21. (From Osinski et al., 2013).

velocities, forming features associated with e.g., earthquakes (breccia, fractures etc.) as a result of brittle deformation. This is approximately at the distance from the point of impact where the crater rim is located (p.18, French, 1998).

All rocks that display deformation caused by impact events are called "impactites" (Stöffler et al., 2018; section 2.2.2). As described above, their characteristics vary with shock-pressure, but their appearance naturally also depends on target material. By understanding the distribution of impactites in an impact structure it is possible to better understand the different stages of how the crater was formed.

2.2.1 Shock-metamorphism

Many features of an impact structure, such as a circular morphology, traces of extensive melting and the occurrence of breccia, are not diagnostic for impact. Volcanoes and salt-diapirs cause circular landforms, and brecciation of rocks is also produced by for instance fault movements (French & Koeberl, 2010). Hypervelocity impact structures are therefore confirmed based on findings of unequivocal evidence of shock-metamorphism (Or alternatively, more rarely, by findings of physical pieces of the impacting projectile or geochemical approaches pinpointing atypical isotopic ratios or element abundances; Melosh, 1989; French, 1998). The extreme pressure and temperature conditions which the target rocks are subjected to cause unique shock-effects on both a micro- and macroscopic scale. The following section presents an overview of the different kinds of shock-metamorphic features that can be expected, from low- to high grade, and are from here on referred to only as features of "shock".

Shock pressures <2 GPa generate no diagnostic impact features (French, 1998). Fractures and brecciated target rocks can occur over a great distance from the point of impact but their origin is, on their own, impossible to distinguish from endogenic processes at these low shock pressures.

At the **lower end of the shock-pressure-regime (2 -10 GPa),** shock-features occur on both megascopic scale (shatter cones), and microscopic scale (basal planar deformation features, planar fractures, and feather feature lamellae (French, 1998). Features that form in the low-shock-pressure-regime are commonly found in (par)authochthonous target rock that has experienced <10 GPa and in the crater-fill. Out of the total volume of an impact structure, traces of lower-shock pressures usually occur in at least twice (and sometimes three times) as much of the affected target rock (Poelchau & Kenkmann, 2011).

Shatter cones are the only diagnostic impact feature than can be seen without a microscope (French & Koeberl, 2010). They can be from one centimeter to several meters in size. Their typical shape is often referred to as "horsetail", with conical striations (French, 1998). Shatter cones are easier to recognize in fine-grained rocks such as carbonates, and more difficult in coarse grained granite. As they are usually formed below the crater-floor (sub-crater) they can often be found in deeply eroded impact structures, providing important evidence for impact origin.

Basal planar deformation features (basal PDFs) are not "true" PDFs (see section below), but mechanical twins parallel to the basal plane (0001) in the quartz crystal (Fazio et al., 2018). Often referred to as basal Brazil twins, they form at shock-pressures <10 GPa as a result of high differential stress (French & Koeberl, 2010; McLaren et al., 1967; Trepmann, 2008).

Planar fractures (PFs) are produced at 5-8 GPa and appear as parallel open fractures with >3 μm spacing (French & Koeberl, 2010). These fractures can be filled with secondary minerals such as quartz or montmorillonite and commonly form along rational crystallographic planes, like (0001) and {101} (Engelhardt & Bertsch, 1969; Stöffler & Langenhorst, 1994). Similar microfractures can also form in endogenic settings, but PFs are considered diagnostic for impact origin when occurring in multiple sets in the same (quartz) grain (e.g., French, 2004; Osinski et al., 2022).

Feather feature lamellae (FFL) occur as subparallel to parallel lamellae attached to planar fractures in quartz at an angle >35° (Poelchau & Kenkmann, 2011; Osinski et al., 2022). They are not very well understood but develop at ~7-10 GPa and are thought to form as a result of deviatoric stress. Since they have only been found in impact structures and never in endogenic settings they have been proposed to be unique for shock-metamorphism.

High differential stress is common in the low-pressure regime (<10 GPa, Poelchau & Kenkmann, 2011), explaining findings of **kinked amphiboles and micas** in impact settings (e.g., Engelhardt et al., 1968; Trepmann, 2008). While the overall shock-pressure decrease with time and distance from the point of impact, the deviatoric stress component increases as an effect of anisotropy in rocks and minerals (Poelchau & Kenkmann, 2011). Because of this, neither kink bands nor FFLs are expected to be found together with microscopic features indicating shock-pressures >20 GPa, e.g., planar deformation features indicative of high shock pressure levels. Kink bands in biotite are also known to form in tectonic settings as a result of pressure-induced gliding, i.e., they are not considered diagnostic for impact (Ebert et al., 2021).

Intermediate shock-pressure features (10-35 GPa) primarily includes Planar Deformation Features (PDFs) and high-pressure polymorphs of rock forming minerals.

PDFs in quartz are the most frequently used features to confirm impact structures where no meteorite can be found. They appear as thin (<3 μm) and narrowly spaced (2-10 μm) planes parallel to rational crystallographic planes (French, 1998). At first interpreted as glide planes (Engelhardt & Bertsch, 1969) and later as lamellar melts (Grady, 1980), PDFs are still not completely understood. The quartz crystal gets compressed by the passing shock wave and, only along specific crystallographic planes, transform into a dense, amorphous phase (Goltrant et al., 1992; Stöffler & Langenhorst, 1994).

Since the orientation of PDFs can be linked to shock-pressures, they can be used as shock-barometers. Oriented 23° from the C-axis, ω{103} forms at 7-10 GPa, while pressures >14 GPa are indicated by the appearance of {221}. At pressures >16

GPa PDFs will also form along μ{102} (French, 1998). Increasing pressure is also accompanied by an **increasing number of PDF-orientations in quartz crystals** (French, 1998). At pressures >35 GPa, PDFs are not formed. One theory is that when too much of the crystal is turned into the amorphous phase, the entire crystal is transformed into diaplectic glass (see section on diaplectic glass below; Stöffler & Langenhorst, 1994).

PDFs most commonly appear as "decorated PDFs". As a result of hydrothermal activity or other alteration processes, the originally glassy planes are recrystallized back to quartz. Since fluid-inclusions appear along the same plane as the glass used to be, PDFs are still visible and measurable (French, 1998).

The presence of **high-pressure mineral polymorphs** has been used to confirm impact structures since the 1960's, for instance The Ries impact structure (Shoemaker and Chao, 1961). At shock-pressures >12 GPa quartz can be converted into stishovite, and at shock-pressures >30 GPa, coesite can be formed. This is also why it is sometimes possible to find diamond at impact structures, having converted from graphite. Since these high-pressure polymorphs also form in endogenic settings, they are not diagnostic for impact origin in themselves but require the additional occurrence of e.g., PDFs or shatter cones in order to confirm an impact origin.

The highest shock pressures (35-100 GPa) produce several shock features: diaplectic glasses, melting, and vaporization. The highest shock pressures occur near the point of impact, right below and around the interface of the two colliding bodies of rock (French, 1998).

Above 30 GPa **diaplectic glass forms**. Unlike normal glass formed as a result of high temperatures, shock-produced diaplectic glass have not melted to liquid state (Stöffler, 1984). Since the formation does not include any flow-movements, the original crystal fabric can often be preserved (Stöffler, 1984). The formation of diaplectic glass is hypothesized to be linked to increasing density of PDFs in affected crystals, at higher shock-pressures (Stöffler & Langenhorst, 1994).

Complete melting of rocks indicates shock-pressures >60 GPa (French, 1998). It is during decompression from the high shock-pressures that the remaining waste heat causes melting as well as vaporization (Osinski et al., 2018). Impact melt bodies occur in different settings within and outside of impact structures depending on morphology and crater size (Osinski et al., 2018). In small, simple impact structures most of the melt is found in impact breccia in the crater-fill while complex impact structures often have coherent impact melt sheets on their floors as well as in ejecta, alongside other impactite lithologies that also can contain various amounts of impact melt. Complex impact structures also have both dikes of injected impact melt in the crater floor and central uplift, and pseudotachylitic breccia veins (French, 1998).

While the reason is not completely understood, it is clear that melt appears differently depending on target lithology. Until the end of the 20th century, it was not yet known if sedimentary target rocks could produce shock-induced melt (Osinski et al., 2018). In the early 80's, (Kieffer & Simonds, 1980) concluded that at least the same amount of melt should theoretically be produced in sedimentary target as in crystalline, and this is now widely accepted (Osinski et al., 2018). The reason why melt had not been found in sedimentary or mixed targets, is that it appears different from melt produced from crystalline target rocks (Fig. 6; Newsom et al., 1986; Engelhardt et al., 1995; Osinski, 2004; Osinski et al., 2018). Lithologies that had previously been described as clastic have since been reinterpreted as altered melt (Osinski et al., 2018). Newsom argue that impact induced hydrothermal activity could explain the severe alterations (1986), and Engelhardt suggested that the melts of the Ries impact structure were specifically difficult to identify due to hydrothermal alterations (1995). It has also been proposed that the faster cooling rates of sedimentary target can result in a more clast-rich melt, making it appear different than in crystalline impact structures (Fig. 6; Osinski et al., 2008).

2.2.2 Spatial distribution of impactites

All rocks that are created or deformed by impact events are termed "impactites". They are classified depending on setting in the impact structure and the occurrence or lack of shock-effects (Stöffler et al., 2018). The three main classes of impactites are shocked rocks, impact melt rocks, and impact breccias (Stöffler & Grieve, 2007).

What kind of impactites one can expect to find in an impact structure varies with both target lithology and the energy released during impact. The shock wave also propagates differently depending on target lithology which influences the resulting impactites on both a macro- and a microscopic level (Osinski et al., 2008). However, in a generalized simple crater, impactites can be expected to have the following lithologies from a proximal to distal setting (Fig. 5; p.10 in Stöffler et al., 2018):

Figure 6. Photo from an outcrop in the Haughton impact structure showing clast-rich melt rock (from Greenberger, 2020).

1. The crater floor consists of (par)autochthonous massive, fractured, and brecciated target rocks displaying low shock grade. Melt veins can accompany the fractures.

2. The base of the crater-fill is usually covered by impact melt, i.e., high grade of shock. The melt is covered by a lens of allochthonous breccia, with different grades of shock. The breccia is divided into two types depending on the presence of melt: suevitic (melt-bearing) breccia of higher shock grade, and lithic breccia not containing melt particles, i.e., lower grade of shock. Monomict breccias generally show the lowest degree of shock.

3. Outside the crater the thrown-out material is found: the ejecta blanket and air fall beds (Fig. 4; French, 1998). Closer to the crater lies restricted strewn fields of high shock material, and more distal ejecta display a variety of shock grades. These impactites are vulnerable to erosion over time and they stand little to no chance of getting preserved in ancient impact structures.

The higher energies involved during complex crater formation results in the formation of different types of impactites and a different spatial distribution of impactites than in simple impact structures (French, 1998).

2.3 Impact-induced hydrothermal activity

Impact cratering leads to fracturing and increased permeability in target rocks. If water is present, the hot impact melt may cause circulation of hot water in the crater: an impact-induced hydrothermal system is born (Osinski et al., 2020). Hydration of minerals, such as clay-altered glass, can form potential habitats for simple bacteria, which is why impact craters are considered prime environments for the rise of life or early life forms (Osinski et al., 2020). For an impact crater to form and sustain a successful hydrothermal system, a continuous presence of water must be combined with a long-lived heat source (e.g., Osinski et al., 2013). The circulation of fluids is driven by the difference between the elevated post-shock-temperatures of rocks close to the point of impact and their much cooler surroundings.

In complex impact craters, hydrothermal systems appear to form in several variable settings, representing areas affected by different heat-sources. From proximal to distal setting: in the central uplift, in melt bearing rocks and breccias in the crater-fill, in fractures and faults in the crater rim and in ejecta deposits (Fig. 5; Kirsimäe & Osinski, 2012; Osinski et al., 2013). On the contrary, traces of hydrothermal activity in simple craters seems to be less common: in a study of the ~60 impact structures on Earth displaying hydrothermal alterations, only 10 have a diameter less than 5 kilometers (Osinski et al., 2013). When found in simple craters, the hydrothermal alteration products primarily occur adjacent to melt pockets (Fig. 5; Kirsimäe & Osinski, 2012). The smallest impact structure found this far showing evidence of hydrothermal activity is Lonar Lake (1.8 km, India), where the basaltic target rocks display chloritization (Hagerty & Newsom, 2003), as well as clay and secondary calcite.

The altered rocks and minerals of an impact-induced hydrothermal system are products of low-P-high-T-metamorphism and as the temperature decreases over time it evolves into a low-P-low-T-system. Kirsimäe & Osinski (2012) describes a mineral paragenesis sequence indicating that a vapor-dominated stage is followed by a water-dominated stage as temperature decreases with time, explained below. By studying the different parageneses it is possible to understand the different phases of the impact-induced hydrothermal activity (e.g., Versh et al., 2005; Kirsimäe & Osinski, 2012):

In the **early, vapor-dominated stage** (350-500°C), low- to medium grade metamorphic reactions take place, forming e.g., garnet and epidote (Kirsimäe & Osinski, 2012). Feldspar alterations generally occur at an intermediate, vapor-liquid-dominated stage (100-300°C), as part of a quartz-sericite-pyrite-assemblage (QSP; Wallace & Maher, 2019).

Chloritization is one of the most common features of hydrothermally altered rocks, especially in target rocks of mafic composition, and can be connected to all stages of hydrothermal activity (e.g., Kirsimäe & Osinski, 2012). At high temperature ore-forming processes, chlorite is associated with epidote and albite. At intermediate temperatures chlorite can be part of the QSP-alteration assemblage (Wallace & Maher, 2019), and also in association with clay alteration products like illite and smectite (Hagerty & Newsom, 2003; Osinski et al., 2013). Studies of the paragenesis of clay minerals in several impact structures indicated low-grade metamorphic reactions over time and concluded that most impact structures probably have interacted with either ground water or marine waters during cooling (Kieffer & Simonds 1980).

Secondary minerals like calcite and sulphates are important during the **late stage (<100°C), water dominated,** hydrothermal activity. Other minor phases like apatite can also precipitate as the temperature of the hydrothermal system decrease towards normal Earth-surface temperatures (Kirsimäe & Osinski, 2012).

2.4 The Hummeln Structure

2.4.1 The Hummeln Enigma

Lake Hummeln is situated in the Småland province of south-eastern Sweden (Fig 1a). The Proterozoic bedrock is called *Växjö granite*, dated to ~1800 Ma (Mansfeld, 1991) and part of the Transscandinavian Igneous Belt (TIB). The shape of the lake primarily originates from NE and one NNE fault lines (Fig. 3) that share orientation with several other joint valley lakes in Småland, e.g., Lake Sommen and Lake Åsunden (Svensson, 1966). About one third of the lake Hummeln is however made up by a circular anomaly.

The area round the Humlenäs-farm is a nature reserve since 1972 and protects the rare and limestone -dependent flora of the peninsula (Fig. 3; Einarsson & Axelsson, 2001). Relics of lime kilns, once used by farmers for making quicklime, is also an unusual sight in this area which otherwise completely consists of TIB granites (Einarsson & Axelsson, 2001). The Swedish chemist and physicist Hisinger (1826) was familiar with the crystalline basement rock in the Hummeln area. When faced with limestone samples and told of local limestone-quarrying in Humlenäs he was surprised and decided to investigate it further.Hisinger described limestone blocks of Öland-type (i.e., rich in orthocones, brachiopods and trilobites of Ordovician age; 1826). Since he did not find a pattern in dip-directions he hypothesized that sedimentary strata must occur in a minor pocket in the proximity. The theory of a hidden depression shielding Paleozoic rocks at the bottom of Lake Hummeln was further investigated by several (e.g., Linnarsson, 1878) and during the late 19th and early 20th centuries. The circular depression north-west of Humlenäs was found through measuring of the bottom topography in 1937 *(Nordenskjöld, 1937)* (Nordenskjöld). Theories of both explosive volcanism and tectonic faulting as the origin for the depression are put forward during this time (e.g., (Asklund, 1921); (Nordenskjöld, 1944) Nordenskjöld, 1944).

The first suggestion of impact origin for the Hummeln structure arose in the 1960's (Fredriksson, 1963). At the time, only about a dozen impact structures had been verified but none in Sweden. In the book "Meteoriter" (the Swedish word for meteorites) Fredriksson and Wickman proposed a few different Swedish lakes to be of impact origin (1963), and all of these (Siljan, Mien, Dellen and Tväre n) have since been verified. The Hummeln structure also made the list due to the circular anomaly. Based on the glacial trail of Palaeozoic sedimentary rocks found in Humlenäs, the authors proposed the age to be of Precambrian or early Cambrian age (Fredriksson, 1963). The impact origin theory was further strengthened by Svensson (1966), e.g., from the lack of evidence for explosive volcanism in the area. During the 1980's and 1990's, geophysical investigations were carried out (Lindström et al., 1999; Ormö et al., 1999). A drill core of 147 meters was obtained (location marked in Fig. 3; see section 2.4.2) and described, providing further clues pointing in the direction of an impact structure (see section 2.4.3 for these authors conclusions regarding the age of the impact event). No evidence of shocked minerals or shatter cones was however found.

In 2015, findings of shocked minerals in the form of basal PDFs in quartz finally put an end to the mystery of the origin of Hummeln (Alwmark et al., 2015). Since then, no further research has been conducted to better understand Hummeln, e.g., the distribution of impactites, the age of formation, and the preservation state. In other words, the Hummeln impact structure is still not well understood.

2.4.2 The Hummeln-1 drill core

A drill-core of 132 meters was obtained from Lake Hummeln in 1995 (Ormö et al., 1999). The drill-site (N 63.60280, E 15.27300) was chosen from seismic profiles and echo sounding. To minimize water depth (14 m) and till deposits (3.1 m), the site was chosen 300 meters from shore and 400 meters from the estimated center of the impact structure (Fig. 3). Using military equipment, drilling was carried out with firmly anchored barges as a platform to the rig (Lindström,1994; Lindström et al., 1999).

The total length of the core is 147.15 meters. Most of the lithology is described as Paleozoic sedimentary rocks displaying strong slumping, except from the lowermost meters of brecciated basement rock (164.25-157.3 m; Lindström et al., 1999). Drilling was stopped due to technical and financial reasons before reaching the actual crater floor (Lindström et al., 1999). Thorough sedimentological mapping was conducted on the slumped sedimentary succession, and biostratigraphy was done on Cambrian acritarchs, Ordovician conodonts and Lower Ordovician chitinozoans (Lindström et al., 1999). The Hummeln-1 drill core has been kept safe in the dungeons of the Swedish Geological Survey in Uppsala since the 90's but is today situated at the department of Geology at Lund university.

2.4.3 Age of the Hummeln Event

The most cited age of the Hummeln impact event is 470-460 Ma (Lindström et al., 1999; Grahn et al., 1996). This is based on stratigraphy of the Palaeozoic rock, biostratigraphy, and deformation of the sedimentary infill. When analyzing the Hummeln-1 drill-core, Lindström et al. concluded that the oldest sediments of the crater-infill are of Early Cambrian age, but that the event probably took place in the late Early Ordovician or early Middle Ordovician (1999). The authors argue that the Ordovician carbonate rocks of the strata do not seem to have been deposited in a protected environment. They further suggest that all the slumping of Paleozoic sediments happened at the same time, in the latest Kundan (Middle-Ordovician; Lindström et al., 1999). They explain that crystalline basement was at the time of impact covered by >100 meters of unconsolidated Cambrian sediments, overlain by >10 meters well lithified Lower Ordovician limestone. Due to the soft sediments, the rim that was built up during crater formation collapsed and caused slump structures in the unconsolidated sediments.

Numerous impact structures with confirmed or suspected ages in the same range as proposed for Hummeln exist (ref.). One of these is the Granby impact structure, 140 km north-west of Lake Hummeln (Fig. 3), formed 465 Ma (Grahn, 1996) based on chitinozoan biostratigraphy. The same author set several ages of impact events to early Late Ordovician: Tväre n (457 Ma), Lockne (455 Ma) and Brent (452.8+-2.7 Ma). The most recent isotope datings for the Swedish impact structures mentioned are: Hummeln 465 Ma, Granby 468-467 Ma, Tväre n 458-456 Ma, and Lockne 455±1 Ma (all ages from Osinski et al., 2022).

In Canada there are several other impact events within the same age, e.g., Pilot (445+-2 Ma), Clearwater East (470-460 Ma), Decorah (467-464 Ma). The ongoing discussion about a possibly increased influx of crater-forming bodies to Earth during the Middle Ordovician is worth noting (e.g., Meier & Holm-Alwmark, 2017; Lindskog & Young, 2019; Holm-Alwmark, 2021; Lagain et al., 2022).

3 Method

3.1 Field studies

Field work at Lake Hummeln was carried out during the 23-25th of August and the 5-7th of October in 2022. Tools: compass with clinometer, hand lens, measuring tape, measuring stick, and zoomed-in maps printed in A3-format (Fig.7). The working plan was to map the south-eastern shoreline of the lake (Fig. 3, Fig. 7). Mapping was done by drawing, writing, audio-recording, taking photos and collecting hand samples. Primary focus was on the semi-circular sector that parts of the south-eastern shoreline of Lake Hummeln follows (Fig. 7). The shape of the shoreline stands in clear contrast to the majority of the shore of the lake, which are generally straight and seemingly fault-related (Fig. 3), and therefore suggests impact origin.

Hand samples were collected at some of the localities and brought to the Department of Geology at Lund University for further analyses. The H22-samples are listed in Tab. A5 and divided into three categories: the series H22-F contain in-situ hand samples, H22-B refer to lose blocks and H22-S are sedimentary rock (not in-situ). Out of the 29 hand samples three were cut for thin section production.

3.2 Map-making and analysis of field notations

To distinguish different levels of brecciation and presence of other deformation features in field, a breccia-index was defined and applied on all localities containing breccia or other types of fractured rock (Tab. A2). During post-field analysis the breccia-index was rearranged in order to show the interpreted grade of deformation, from intact to fractured to brecciated and possibly melted. Three categories are chosen to illustrate an increasing grade of deformation: 1. intact and/or semi-intact rock, 2. fractured but not brecciated rocks (little or no transport), 3. crushed and transported rocks (monomict to polymict breccias). These are used to show the distribution of impactites in both maps and close-up sketches from field localities.

3.3 Core mapping

Within the frame of this project, the lowermost seven meters of the Hummeln-1 drill core (164.25-156 m, box 22 and 21) was remapped. This is the part of the drill core that are interpreted as impactites. Also, the above-lying stratigraphy was subject to careful analysis in 1999 (Lindström et al.). General descriptions on

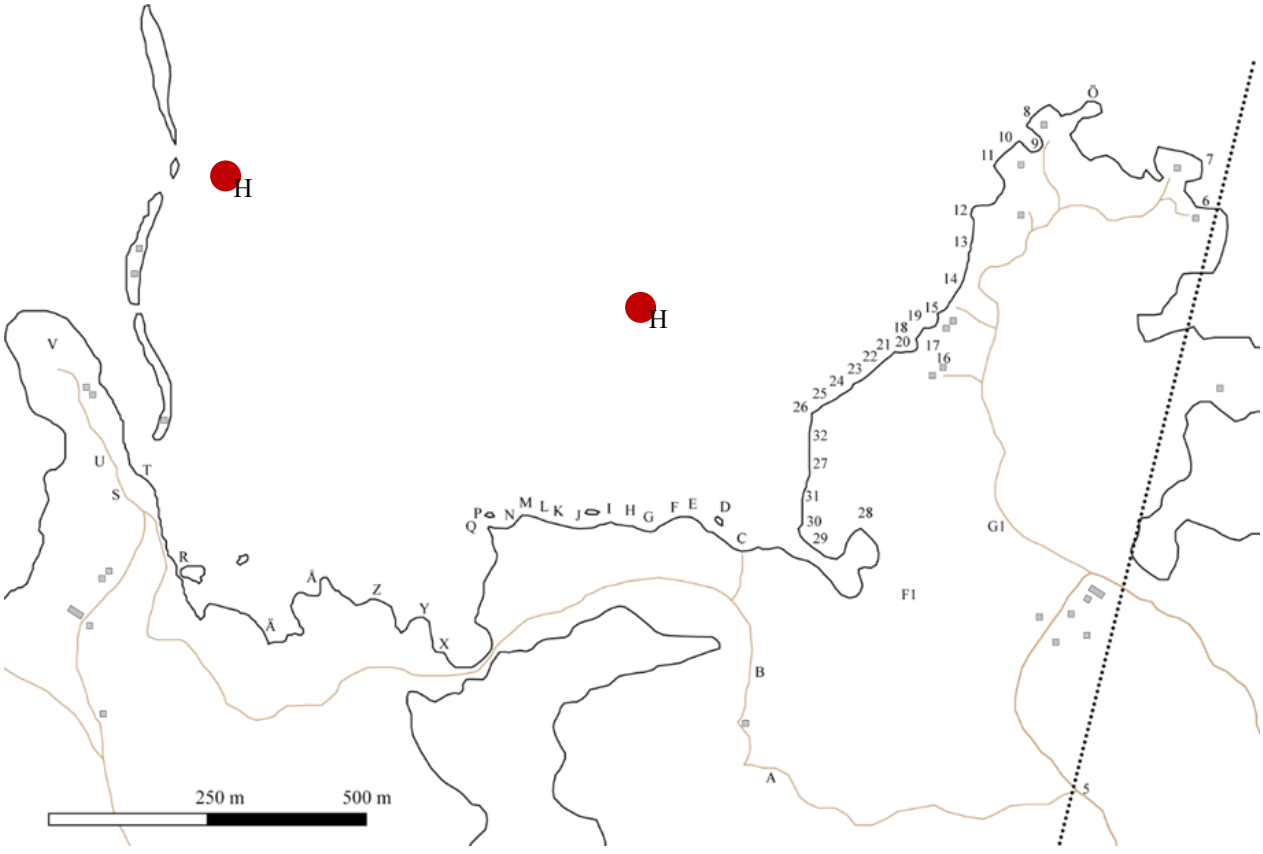

Figure 7. Field map showing the Humlenäs peninsula and the localities visited in August and October of 2022. The red circles mark the suggested sites for future drilling campaigns: (57°21'57.6"N, 16°15'08.5"E) and (57°22'00.9"N, 16°14'28.7"E) respectively. (Drawn after SGU Berggrund 1:50 000-250 000)

lithology were based on ocular studies and detailed descriptions on e.g., mineralogy from petrographic studies (see section 3.4).

3.4 Petrography

In total, 51 thin sections were made and studied for this project: 13 from hand samples collected during field studies in 2022, and 28 from the Hummeln-1 drill core.

All thin sections were studied in polarized light microscope. Some of the samples were also analyzed using the scanning electron microscope: 160.68, 160.69, 161.3A, 161.3B and 162.15B. Photos were taken with the Tescan Mira3 High Resolution Schottky FEG-SEM (field emission gun and scanning electron microscope) that resides at the Department of Geology of Lund University. For EDX-analysis (energy dispersive spectroscopy) the X-MaxN 80 from Oxford Instruments, linked to the previous instrument, were used.

4 Results

4.1 Field observations and samples

The distribution of different kinds of brecciated rocks is shown in Fig. 8, the findings of sedimentary rocks and most common mineralogy in Fig. 9, and the general orientations of parallel fractures in Fig. 10 (see Tab. A1 for detailed field notes for every locality). In-situ rock – brecciated, fractured or intact – is only found at some of the studied localities (listed in Tab A4). Notes on lithology, mineralogy, the appearance of fractures and other features are therefore also based on lose blocks found along the shoreline.

Granite is the most common rock type in the area (Fig. 9), often the red TIB-granites but with a whiteish rim. There are also patches of basalt throughout the coastline, less in the northeastern area. Basalt often occurs as xenoliths in the granite. No in-situ sedimentary rocks were found but blocks of sandstone and limestone were noted (Tab. A1). Blocks of sandstones are more evenly distributed along the Humlenäs shoreline than limestones, which is concentrated to the "glacial trail" mentioned in the literature (Fig. 9.)

4.1.1 Macroscopic fractures

Fractures were categorized into three different types when identified during field studies: sets of fractures showing a trend in orientation [Bi3] (Fig. 10), networks of fractures without any common orientation [Bi1], and "weak fractures" [Bi1w]. The first two types appear in close proximity to different kinds of breccias, and only differ in the pattern of orientation. The [Bi1w] is used to note fractures that are weak (thin and vague).

[Bi3] parallel sets of fractures were noted in both in blocks and in-situ outcrops, in total at 10 localities (Fig. 10, Fig. 11, Tab. A1). They are often found in close proximity to both non-deformed rocks and breccias (Fig. 12). The measured long axis of in-situ paral-

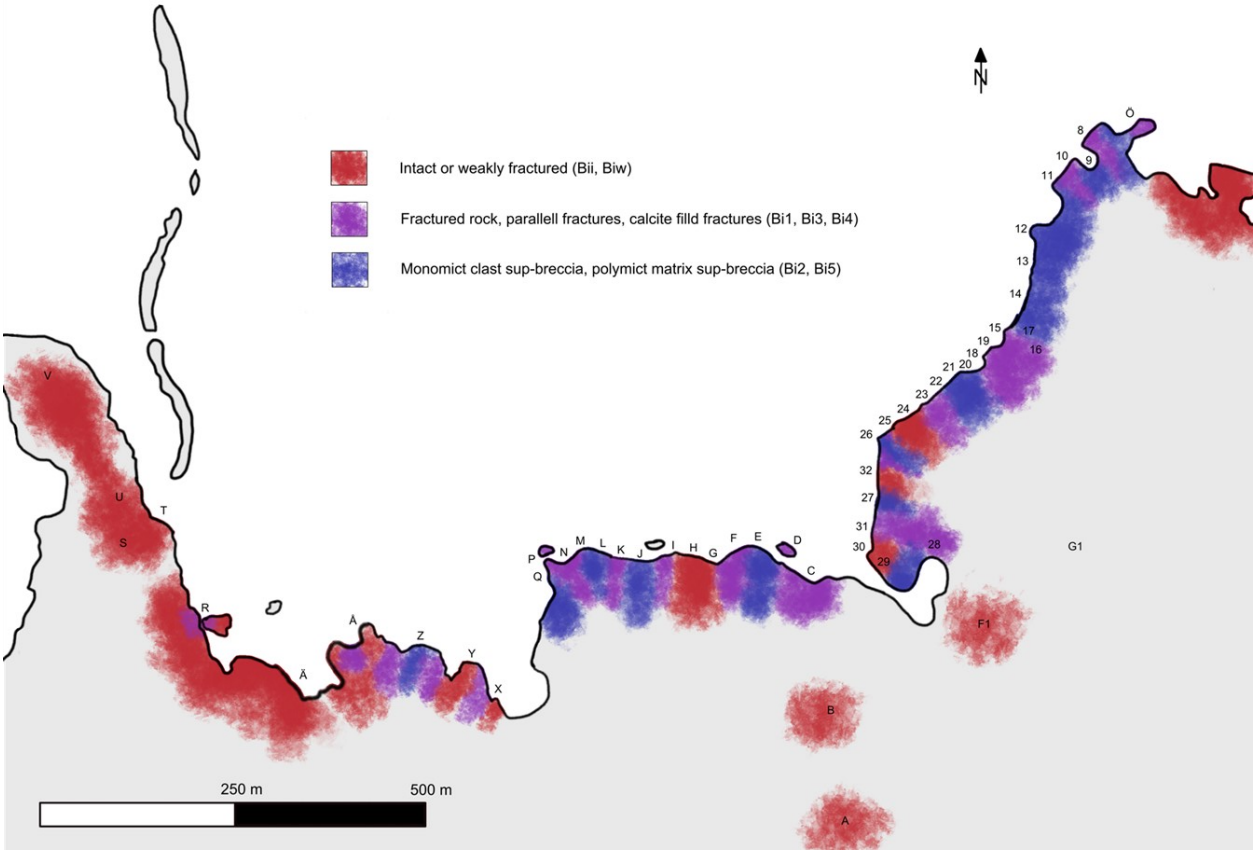

Figure 8. Map drawn from field notations showing general grade of deformation in the mapped area. The amount of deformation increases from red (intact) to purple (fractured) to blue (brecciated), corresponding to breccia-index in Tab. A1.

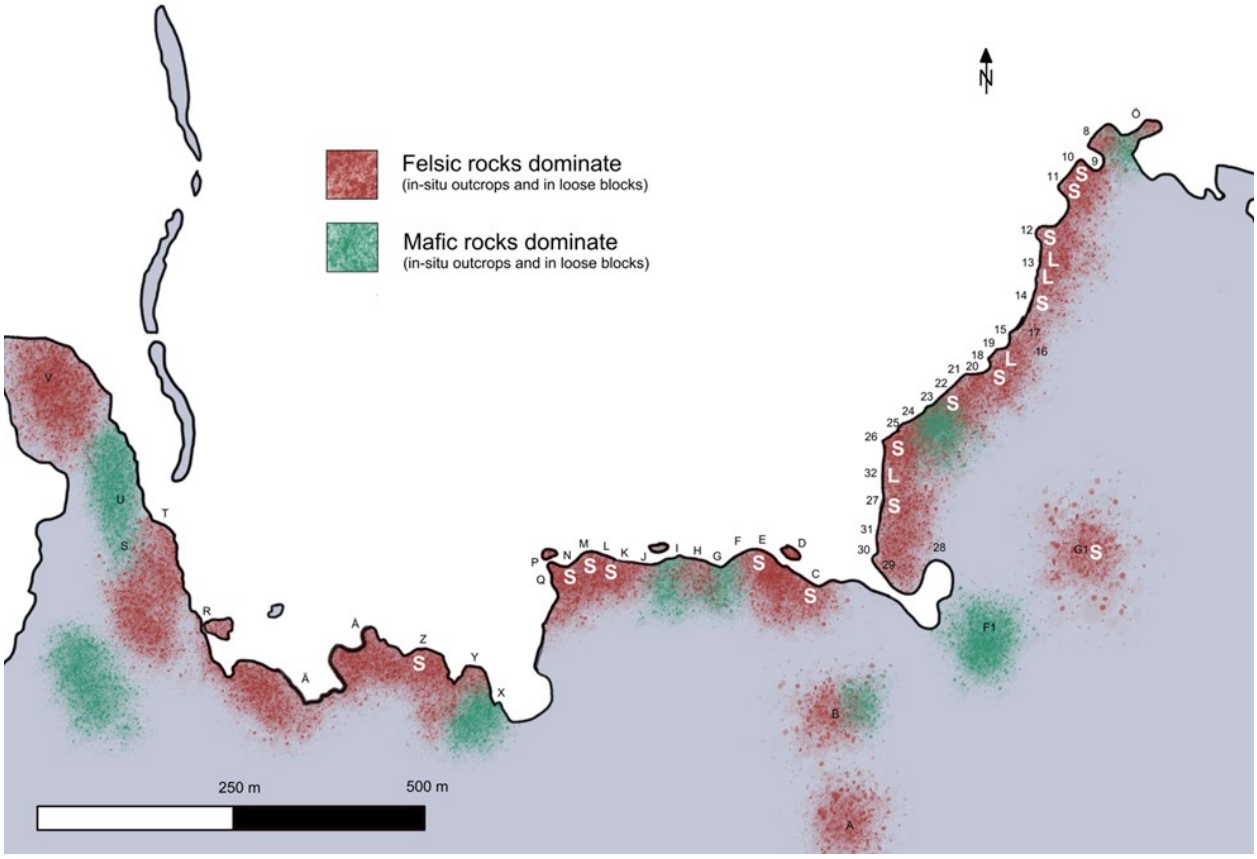

Figure 9. Rock types mapped along the south-east shore of lake Hummeln. Red and green show the distribution of felsic and mafic rocks, based on both in-situ outcrop and dominating block lithology, in the area. White letters show dominating findings of sedimentary blocks, sandstone (S) and limestone (L) respectively.

lel fractures together show a trend of NW and N orientations (Fig. 10).

Fractures in the Hummeln bedrock are commonly filled with calcite (Fig. 13), which is also in some instances making up the cement of primarily monomict breccias.

4.1.2 Distribution of breccia types

The level of deformation and alteration is in general heterogeneously distributed in the mapped area, both on a kilometer-scale (Fig. 8) and within specific localities. As seen in close-up sketches from two of the localities with in-situ rocks (locality E and locality 26, Fig. 12), different grades of deformation are often located close to each other. The generalized map of deformation grade (Fig. 8) is based on the dominating grade of deformation found at each locality. In-situ rock was prioritized, but as this could not be found without digging in many localities, generalizations are based on lose blocks as well. See Tab. A4 for notations on which localities have in-situ rocks.

Several types of fractures and breccia are found at the shore of Lake Hummeln, namely: Fractured granite, fractured granite with calcite in fractures (Fig. 13a), monomict clast supported breccia, monomict matrix supported breccia (mostly of granite composition), polymict matrix supported breccia with a matrix that sometimes appears as fine-grained "igneous" (Fig. 14a-b) and sometimes more like clay (Fig. 14c-e; see Tab. A1 for notations on each locality).

In-situ, it is more common with monomict, clast-supported granite breccia (Fig. 13) than polymict, clast - or matrix-supported breccia (Fig. 14). The polymictic breccias either have a coarse-grained matrix or a blueish, clay-rich matrix (referred to as "blue breccia" in field notes, Tab. A1). Precipitated calcite, quartz and epidote fill out fractures and sometimes aid in cementing the breccias (Fig. 13).

One pattern that is clear from mapping the Humlenäs peninsula is that the grade of fracturing and brecciation is less, almost non-existing, west of the NNW trending fault at locality Ä (Fig. 3, Fig. 8, Tab. A1).

4.1.3 Field samples

The samples collected at Lake Hummeln during the autumn of 2022 (Tab. A5) reflect the lithologies, mineralizations, and deformation types mapped (Fig. 8) and described above (section 4.1.2). The grade of deformation varies from fractured granitic rocks with and without cementing minerals (e.g., H22B02 and H22-B13), and breccias of different constitution. The major groups of breccias are monomict clast supported breccias (e.g., H22-B06), and polymict matrix supported breccias (e.g., H22-F01). The latter type is often cemented by a matrix which looks clay-like (e.g., H22-F04). The clasts in breccias are primarily of granitic composition but there are also clasts of mafic rocks and angular mudstone-fragments (Fig. 15a).

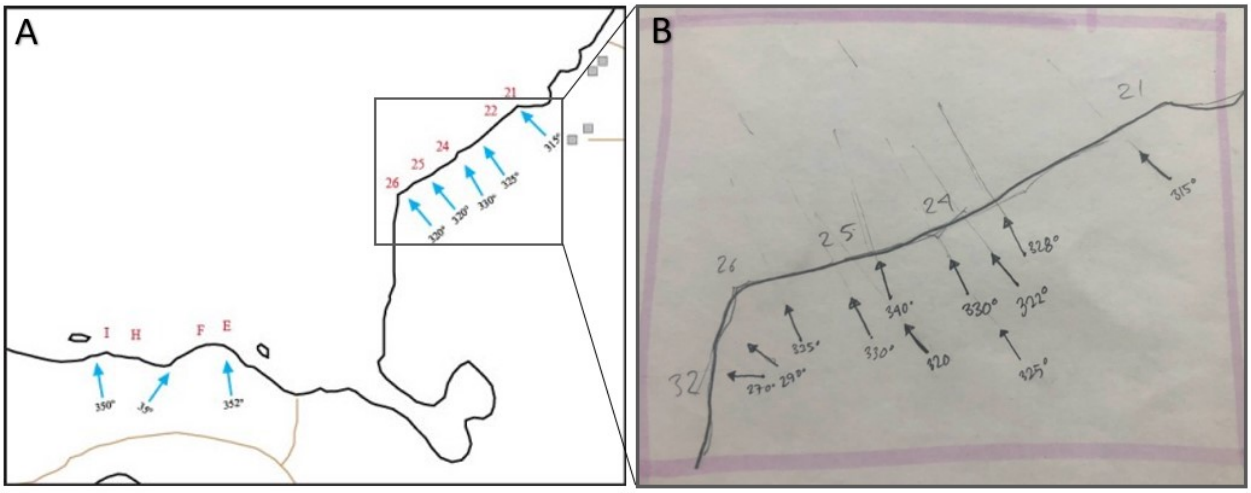

Figure 10. Measured orientations of parallel fractures at localities 21-26 and E, F, H and I. **A.** The mean orientation measured at each locality. **B.** Close-up illustration showing detailed measurements of Bi3-fracture orientations at locality 21-26.

Petrographic analysis of three of the field samples (H22-F04, H22-F06 and H22-B08) reveal PFs in rounded quartz grains (Tab. A5, Tab. A8). The field samples that contain these rounded quartz grains with PFs are all of polymict, matrix-supported breccia with blue clay-matrix. When studied through the petrographic microscope, many rock fragments show traces of alteration: micas are chloritized, and plagioclase show sericitization. Minerals of felsic composition are less altered than mafic, but fractures are common in microcline and quartz, often filled with calcite and other precipitated minerals. Matrix is not homogenous in the breccias from Hummeln: clay-alteration minerals make up the bulk in some breccias while calcite and quartz cement others (Fig. 13, Fig. 14, Fig. A1-3).

Rock fragments and clasts in the breccias picked in -situ localities are granite and mafic rock fragments of varying degree of alteration, a lot of sand grains displaying shock, angular mudstone-fragments showing alterations and one (1) fragment of limestone (H22-F04:3, Tab. A8). SEM-analysis of the fragment reveal no signs of fossils. The fractured surface has a close to rhombohedral pattern and consists primarily of calcium. Sedimentary rocks collected during field work (H22-S-series) consist of both sand- and limestone, which contain fossils and ichno fossils (Fig. 15b, Fig. 15c). No petrographic analysis was conducted on sand - or limestones.

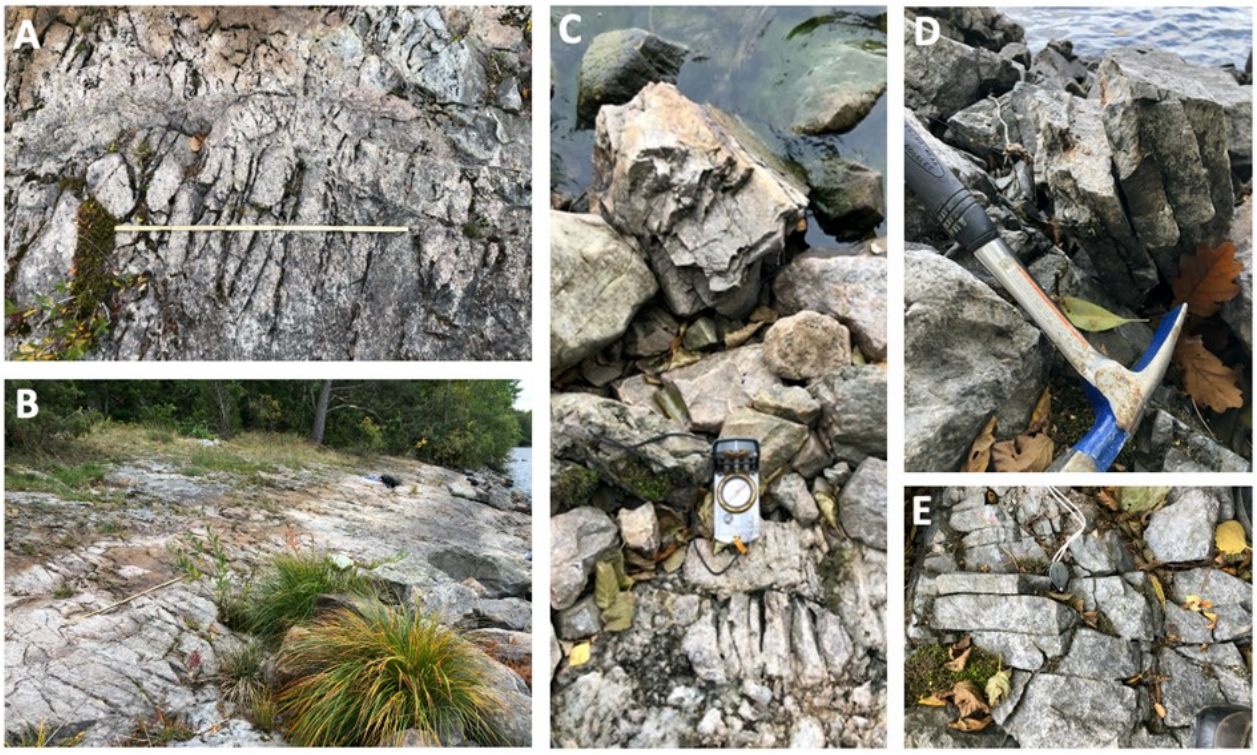

Figure 11. Field photos of parallel fractures (Bi3-breccia). **A.** and **B.** locality 24 (measuring stick for scale), **C.** locality 21 (compass for scale and orientation), **D.** locality H (hammer for scale), **E.** locality I (hand lens for scale).

4.2 The Hummeln-1 drill core analysis

4.2.1 Mapping of drill core

The Hummeln-1 drill core (Fig. 17) is 147.15 m long and contains a variety of lithologies (Fig. 16, Tab. A6): sandstone, mudstone, limestone, and different kinds of breccia. This study is primarily focused on the lowermost 7 meters containing breccia, however this section starts with a general description of the sedimentary lithology overlying it.

The uppermost level represents the lake bottom, 17 meters below lake surface at the time of retrieval (Lindström, 1999). Between 17-157 meters (box 1-19, Tab. A6) the core consists of sedimentary rock of varying lithologies (Fig. 16a-d). The bulk of it (from 157 to 150 meters) is made up of sandstone interlayered with mudstone and displays frequent slump structures (Fig. 16a) but also micro-faulting (Fig. 16b). Between ~40-50 meters the core consists of fine -grained carbonate rock, varying from gray to red in color and similar to the well-studied cold-water carbonates at the island Öland which is of Ordovician age (Fig. 16c; Lindström, 1999). The carbonate section both starts and ends with carbonate breccia (Fig. 16d).

The detailed mapping of the **lowermost 7 meters** of the Hummeln-1 drill core started from the bottom of the core, at 164.25 meters below lake surface. This part of the core consists of fractured and brecciated bedrock that is interfingered with lith-arkosic sandstone (Fig. 16e-j, Fig. 17). Fractures, grade of brecciation, grain-size of clasts and matrix, mineral alterations and microscale deformation features show a heterogenic distribution throughout this part of the core (Tab. A7).

The most common rock is granite of local TIB-type, often with a bleached rim that is visible both in microscope and by eyesight (Fig. 16j). Some granite blocks are >20 cm long. Fragments of mafic rock occur (Fig. 16h). The amount of clay and sand in the matrix vary throughout the section. Arkosic sandstone overlies the section but is also found as lenses in the breccia between (see section below). There are breccias of both monomict and polymict composition and a variation between clast-supported and matrix-supported (Fig. 16; Tab. A7 and Tab. A9 for detailed descriptions on matrix, mineralogy etc.). They vary as follows:

Monomict, clast supported granite breccia (164.3-163.5 m), polymictic matrix supported breccia (163.5 -163.2 m), monomict matrix supported granite breccia (163.2-163.0), fractured granite block (163.0-162.5 m), polymict matrix supported breccia (162.5-162.3 m), dark, dense, fine-grained, igneous-looking rock (primarily plagioclase and chlorite) cut by a granitic vein displaying flow-patterns, and calcite filled fractures which end abruptly towards overlying lithology (162.3-161.8 m), polymictic matrix supported breccia (161.8-160.9 m), arkosic sandstone with flow patterns of clay (160.9-160.6 m), matrix supported monomict granite breccia (160.6-160.3 m) fractured granite block (160.3-160.0 m), clast supported breccia, overlain by fractured massive granite block

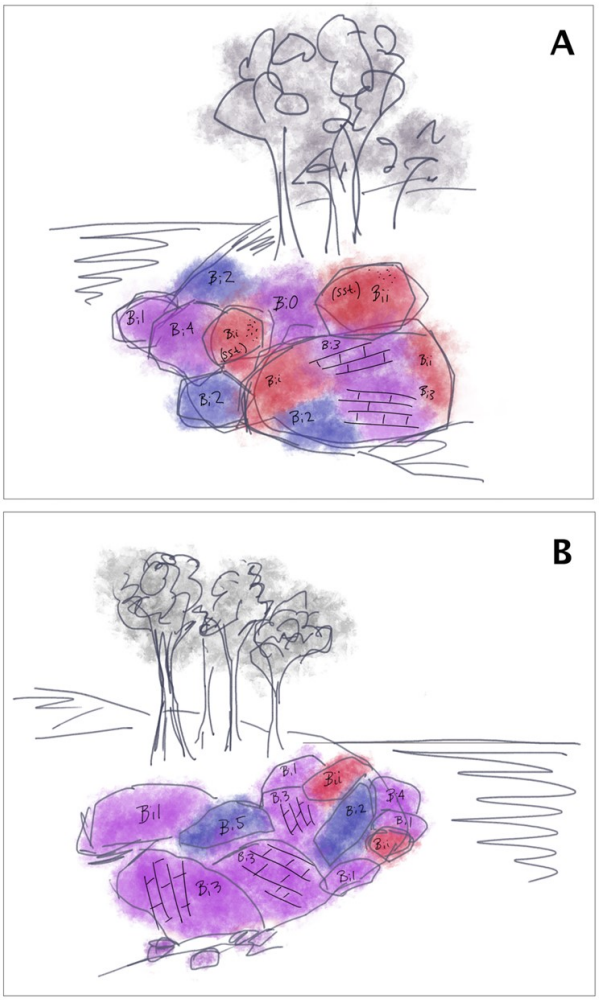

Figure 12. Sketches of locality E (A) and locality 26 (B) showing the heterogenous spatial relations between breccia types in the Hummeln impact structure. Trees (for scale) are ~2-4 m high.

(160.00-159.9 m), clast supported monomict granite breccia (159.9-159.1 m), clast supported monomict granite breccia with clay in matrix and the content of sand increasing upward (159.0-158.4 m), arkosic sandstone with flow patterns of clay (158.4-158.1 m), monomict clast supported granite breccia (158.1-157.8 m), granite block with fractures that contain monomict clast supported breccia (157.8-157.3 m), monomict clast supported breccia which gradually becomes matrix supported upwards (157.3-157.1 m), light-yellow but gradually more gray, coarse-grained arkosic sandstone with rock fragments of quartz and feldspar, no flow patterns visible (157.1-156.6), fine-grained dark gray and coarse-grained light gray arkosic sandstone interfingering in flow patterns. Some of these patterns have a more massive texture and contains round, light-colored grains (156.6-156.0 m).

4.2.2 Petrographic analysis of drill core

Thin sections were made from the following levels of the Hummeln-1 drill core: 164.25, 163.21, 162.45, 162.43, 162.15, 161.80, 161.30**, 160.69*, 160.68*, 160.36, 158.29, 158.28, 158.27*, 154.60*, 153.85*,

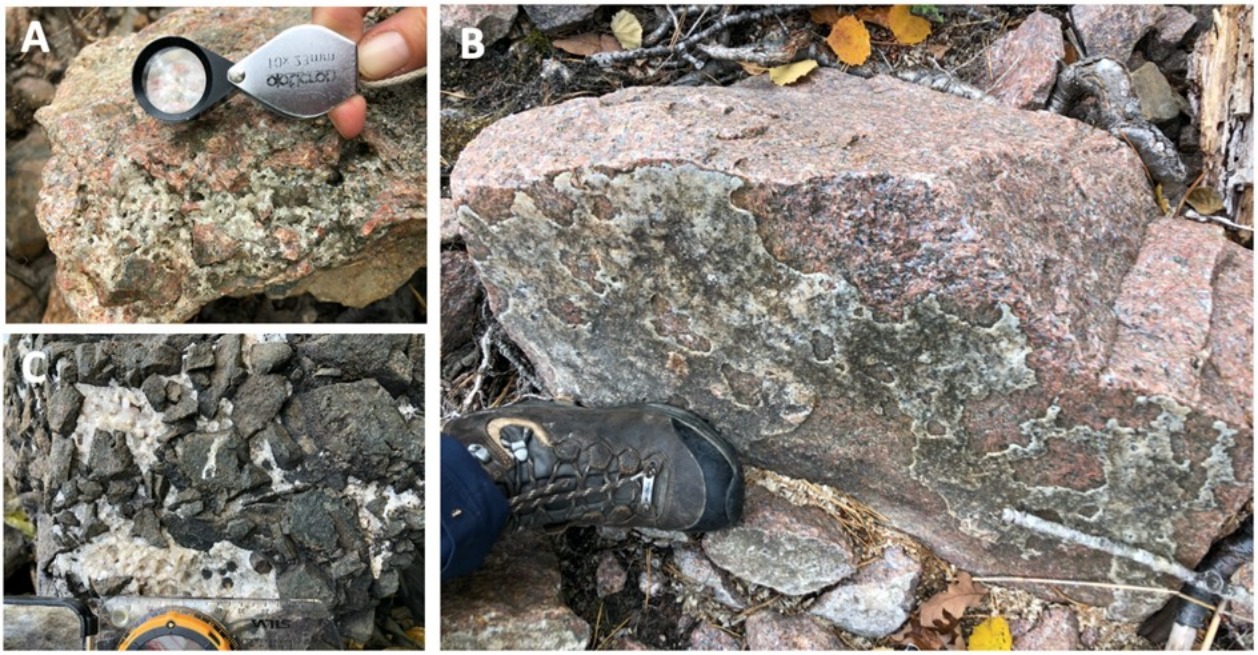

Figure 13. Calcite is the most abundant fracture filling mineral in the Hummeln impact structure. **A.** Granitic clast supported monomict breccia cemented by calcite at locality 31 (hand lens for scale). **B.** One side of a granite block is covered in calcite as a remnant of a calcite filled fracture at locality 30 (shoe size 38 for scale). **C**. Matrix supported monomict breccia with calcite filling out voids and fractures, locality F (compass for scale).

153.30 and 139.90* (Fig. 17). Quartz with PFs occurs in levels marked with an asterisk (Tab. A9), almost exclusively in rounded quartz grains (Fig. 18a-b), while double-asterisk marks kinked biotite.

The most common shock features observed in this study are planar fractures in quartz (PFs; Fig. 18a, Fig. 18b) which occur in sand-grains which range in size from ~200 to 1100 µm. PDFs in quartz are rare and oriented parallel to the basal plane in the crystal (Fig. 18c). This is inferred from the extinction of the crystal in relation to the orientation of the PDFs, and not confirmed from U-stage measurements which are beyond the scope of this work. Some PFs host feather feature lamellae (FFL, Fig. 18d). Kink bands are found in biotite in rock fragments in sample 161.30B (Fig. 19a; Tab. A9; Fig. A1).

Unaltered minerals in the brecciated part of the drill core are primarily quartz and feldspars with minor constituents of micas and opaques. Chloritization and sericitization of plagioclase are common alterations (Fig. 18e-h). The most abundant fracture filling mineral is calcite, cross cutting both rock fragments and matrix (Fig. 16i). Calcite also occurs in voids between crystals (Fig. 19a), sometimes in paragenesis with pyrite and quartz and minor crystals of zircon and a TiO_2-polymorph, maybe rutile (Fig. 19b-d).

The matrix of the sampled breccia does not have a homogenous mineralogy. In the monomict, clast supported sections, matrix primarily consists of granite fragments and lack both clay-particles and rounded quartz grains (Fig. 13). In sections with polymict breccia, and in those that primarily consist of rounded quartz grains, clay-minerals are more common. A flow-pattern of elongated clay-minerals is visible from electron backscatter imaging (Fig. 19e, Fig. 19f).

5 Discussion

This is the first detailed study of impact-related features of the Hummeln impact structure since its impact origin was confirmed in 2015 (Alwmark et al., 2015). Geological examinations of Lake Hummeln have been carried out over almost two centuries but – until now – without the certain knowledge that an impact event formed the structure. When the Hummeln-1 drill core was retrieved in the 1990's (Lindström et al., 1999), an impact origin for the structure was suspected but could not yet be confirmed. Since then, the low-pressure range of shock-metamorphic features has been further understood. For instance, multiple sets of planar fractures are today regarded as diagnostic for shock metamorphism (e.g., French, 2004).

By mapping the Humlenäs shoreline and studying the Hummeln-1 drill core in the light of the confirmed impact origin, this study extends our knowledge about the Hummeln impact structure. From landforms remnant of the eroded impact structure and the distribution of lithologies to the appearance of shock-induced microstructures and traces of impact-induced hydrothermal activity – re-visiting the Hummeln impact structure contributes to our understanding of small, old, impact structures.

5.1 Field observations & the Hummeln-1 drill core

5.1.1 Impactites of the Hummeln structure

Several impactite lithologies that one can expect in a simple impact crater (Melosh, 1989) can no longer be found in the Hummeln impact structure. Comparing it to the Meteor Crater (Fig. 2), several features probably

never will be found in the Hummeln structure. There is no overturned flap, no ejecta blanket and the only trace of a steep crater-wall is the 60 m deep lake (Fig. 5, Fig. 20). What is left of the Hummeln structure shows more resemblances with the much bigger, and complex, Gardnos impact structure (Fig. 2). However: considering the supposed age of the Hummeln impact structure, a surprising amount of the structure is still preserved, se list 1-3 below (with the different settings illustrated in Fig. 20).

Figure 14. Field photos showing different types of in-situ impact breccia at the Hummeln structure. **A.** and **B.** from an outcrop at a small island 3 m from land (locality D), displaying coarse matrix supported in-situ breccia (hammer and feet for scale). **C.** **"**Blue-breccia" (Bi5) – polymict matrix supported breccia with clay (locality 14, shoe for scale). **D. "**Blue-breccia" (locality J, hand lens for scale). **E.** In-situ "blue-breccia" at locality 14 (shoes for scale). **F.** Polymict matrix supported breccia at locality Q (Bi7, hand lens for scale). **G.** Monomict clast- and matrix supported breccia with small granitic fragments (locality 8, fingers for scale). **H.** Polymict matrix supported breccia with coarse grained matrix (locality 26, pen for scale).

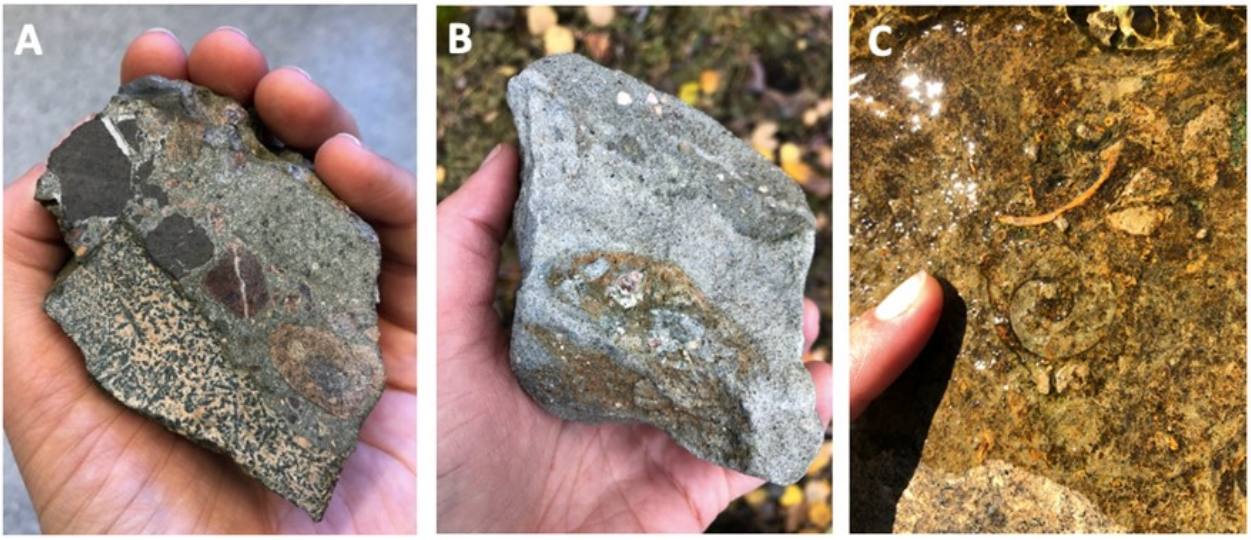

Figure 15. Photos of hand samples collected during field work at lake Hummeln August and October 2022, fingers for scale. **A.** Polymict matrix supported breccia with clasts of mudstone (H22-F06, locality 19). **B.** Arkosic sandstone with lithic granite fragments, similar to sample 139.90 m in the Hummeln-1 drill core (locality J). **C.** Close-up photo of gastropod and trilobite fossils in a limestone block at the shoreline, locality 12.

In the result-section (4.2) the field samples from Hummeln are listed and categorized as different types of breccias. In this section these breccia types are assigned type of impactite, and location in the crater setting: 1. crater wall, 2. crater-fill or 3. ejecta blanket (Fig. 20).

- Fractured basement rocks are interpreted as autochthonous crater wall.
- Monomict clast supported breccias (with matrix of either smaller fragments of the same mineralogy or of secondary minerals) are interpreted as lithic impact breccia, and part of either crater-fill or crater wall.
- Polymict matrix supported breccia with a blueish matrix are interpreted as suevitic impact breccia in the crater-fill.
- Breccia with a heavily weathered, clast rich and coarse-grained matrix (H22-F02) is interpreted as clast rich impact melt rock.

1. Several lithologies of the Hummeln-samples are thought to be **part of the crater wall.** Granitic rock that displays fractures in outcrops (e.g., locality 24) is interpreted as crater wall. Lithic impact breccias that are primarily cemented by calcite or other precipitated minerals (e.g., H22-B13, H22-F03 and H22-F09) are also interpreted to belong to the crater wall. The multiple parallel fractures, referred to as Bi3 in the field notes, are found at eleven localities in total and the orientation was measured in-situ at seven different localities (e.g., Fig. 9). The general direction measured is north-north-west, which at this part of the shoreline points towards the middle of the lake (Fig. 10). Taking in regard what is stated above about the generally heterogenic pattern of deformation, it is however necessary to note that the parallel fractures point towards the point of impact. In the idealized eroded simple crater based on the Brent structure and drawn by Melosh (1989), parallel fractures directed at the point of impact appears possible. Further studies of these fractures along the Hummeln shoreline, and a comparison with other eroded ancient impact structures, are needed in order to draw conclusions regarding this phenomenon.

2. Several types of breccia are interpreted as **part of the crater-fill.** According to Stöffler et al., typically the crater-fill of a simple crater consists of a mixture of lithic impact breccias and suevitic breccias (2018). The Hummeln samples of lithic impact breccias that are found in-situ in close proximity to suevitic breccias (e.g., locality 19 and 26), are interpreted as crater-fill close to the lower part of the crater wall. Suevitic breccias (e.g., H22-F01, H22-F04 and H22-B08) bear witness of severe movement and mixture. They contain rock fragments of several lithologies and sizes (Fig. 14c-e, Fig. A1, Fig. A3) and are therefore interpreted as allochthonous.

The in-situ breccia at locality D is made up of big, granite clasts and an unusual matrix (Fig. 14a-b, H22-F02, Tab. A5). The matrix itself resembles highly weathered coarse-grained granite, i.e., the texture looks igneous. Therefore, the breccia at locality D is interpreted as having formed from impact melt (see section 5.1.2 on how this lithology could possibly have affected the landform, and 5.2.2, about shock wave behavior in sediment or sedimentary target).

When studied under the microscope, the blue type of matrix (Bi5 in field notes) reveals both clays and sand grains. It is interpreted as sand-rich melt or glass that have suffered clay-alteration after crater formation (see section 5.1.5. for SEM-analysis of the same lithology).

Two unusual types of clasts are found in field samples of suevitic impact breccia: a fragment of carbonate rock (H22-F04) and fragments of mudstone (H22-F06:3; Fig. A3). The angularity of these clasts indicates that these lithologies was consolidated at the time of impact.

3. None of the samples collected during field work are interpreted as impact ejecta (Fig. 2). Considering the amount of erosion that Hummeln probably has endured (Fig. 5, Fig. 20), these lithologies are unlikely to be found.

5.1.2 Landforms of the Humlenäs-shoreline

Mapping of the Humlenäs shoreline reveals an eroded cut of the Hummeln impact structure. At the localities described along the shoreline (Tab. A1), the mixture of impactites and grades of deformation is interpretated as the boundary between crater wall and crater-fill of the original crater (Fig. 20).

As seen in the close-up sketches from localities with in-situ rocks (E and 26; Fig.12), different grades of deformation are often located close to each other. For example, locality 26 displays intact granite rock, fractures of different orientations, lithic impact breccia cemented by calcite, and suevitic impact breccia – all in-situ and within an area of less than 10 m^2 (Fig. 12). This general pattern of heterogeneous distribution of deformation is also illustrated on a bigger scale (Fig. 8), and has influenced the geometry of the present shoreline. The "smoothest", closest to a circumference, part of the shoreline are located where there is primarily intact and in-situ granite, fractured but not crushed (e.g., locality 24 and 25). Where polymict, matrix supported breccias are abundant, the small bays make the shoreline patchier (e.g., locality 15 and 19, Fig. 8).

In section 4.1.2 it is noted that monomict, clast-supported breccias are more common in-situ than polymict, clast- or matrix-supported breccia. Crater-fill breccias ought to be more prone to erode than the fractured crater wall (which has also been sheltered by both sedimentary infill and crater-fill). The more shock a lithology has experienced, the less weathering it can withstand (Osinski et al., 2020). This can explain why the shoreline is more patchy and rugged in areas where I found a lot of matrix-supported breccia (e.g., locality 15 and 19) than in areas where I find low-grade deformation (mainly fractures, e.g., locality 24 and 25). The narrow bay located between locality D and locality 29 could be explained by the presence of altered melt, if the matrix of the breccia found at locality D is in fact impact melt and more prone to weathering.

There are many factors to account for this heterogenic distribution of the shock wave, such as density differences between lithologies and the probability of a mixed target. It is however notable that the grade of deformation is lower altogether on the western side of the fault described at locality Ä. This suggests that the NNE-trending fault(s) was in fact older than the impact event, since the shock wave lost most or all of its energy at this boundary.

5.1.3 Glacial trail of sedimentary blocks

As frequently noted in the earliest geological investigations of the Hummeln structure (e.g., Hisinger, 1826; Linnarsson, 1878), limestone and sandstone are found along the shoreline of Humlenäs (Tab. A1). These lithologies are not common in the otherwise granite basement of the area, but fossils in limestone samples are known from Ordovician strata of Öland (Fig. 15c, Fig. 16c-d). When mapped in field, it is noted that these sedimentary lithologies are not evenly distributed along the shoreline of Humlenäs (Fig. 8). Sandstone blocks are frequent along the whole stretch, while limestone blocks are in fact concentrated to the "glacial trail" mentioned in the literature (right southeast of the lake center).

There are several mechanisms that could account for this pattern. First, because of how patches of limestone and sandstone are located differently in the lake (Fig. 3; Lindström et al., 1999) and moved by the ice. Secondly, it can be due to different rates of eroding: quartz rich sandstones have better chances of surviving the sometimes acid above-lake-surface-environment than carbonate rocks. A third theory is that the pattern comes from historical times: limestone has been picked and burnt by humans at Humlenäs for centuries, while sandstone has been left in place.

5.1.4 Post-impact sedimentary infill (157.3-17.0 m) of the Hummeln-1 drill core

The lithologies of the Hummeln-1 drill core is interpreted to represent two different parts of the impact structure (Fig. 20). The lowermost parts are considered impact breccias in the crater-fill, deposited during the modification stage of crater formation (Fig. 16f-j, section 5.1.5). The majority of the lithology is however interpreted as post-impact sediments that was deposited in the depression during the millions of years following crater formation (Fig. 16a-d, Tab. A6).

The sedimentary rocks of the Hummeln-1 drill core have been the subject of thorough analysis regarding biostratigraphy and sedimentology prior to this study (Lindström et at., 1999). Through correlation with e.g., similar lithologies in the island of Öland, the "chronostratigraphic ages" of the different lithologies in the sedimentary infill was acquired (Lindström et al., 1999). Without questioning the biostratigraphics of Lindström et al. (1999), the processes which deposited and deformed these sedimentary rocks are here subject to alternative interpretations. While previous studies interpreted the sedimentary structures as originating from movements during crater formation, this study concludes slumping and faulting as post-impact structures. The repetition of stratigraphic units (e.g., Cambrian mudstone overlaying Ordovician limestone) more likely formed much later as a consequence of e.g., glacial movements.

Carbonate rocks. Between ~ 40-50 meters, the lithology of the Hummeln-1 drill core consists of fine-grained, carbonate rocks. These beds lie more or less horizontally, vary in color from red to greenish gray and display a variety of deformation structures. No deformation structures of the Ordovician carbonate rocks do however indicate that the lithology has been

Figure 16. Photos of representative sections of the Hummeln-1 drill core in hand sample, the top of the stratigraphy is pointing upwards in all photos. **A.** Slump structures in a sandy mudstone (85.20 m). **B.** Faulting in sandstone interlayered with mudstone (80.10 m). **C.** Stylolite in carbonate rock (45.50 m). **D.** Carbonate breccia (48.15 m). **E.** Transition from breccia to arkosic sandstone (157.25 m, see Fig. 17). **F.** Monomict clast supported granite breccia 159.50 m. **G.** Sand-rich matrix with flow-structures (160.70 m). **H.** Polymict matrix supported breccia 161.20 m. **I.** Dark and fine-grained rock with granite fragments and calcite filled fractures (162.00 m). **J.** Monomict clast supported breccia with clay in matrix (164.10 m).

target to a high velocity impact projectile.

The carbonate section starts and ends with matrix-supported, calcareous breccia (Fig. 16d) indicating movement of already lithified carbonate rocks. Within the carbonate strata, vertical stylolites (Fig. 16c) suggest that compressional strain was at one point greater from the side than from above. Glacio-tectonics probably pushed the flat-lying carbonate rocks into the Hummeln-depression.

Sand- and mudstone. The majority of the sedimentary infill consists of sandstone interlayered with various amounts of mudstone. This lithology displays both plastic and brittle deformation structures: steep slumping (Fig. 16a) and faulting (Fig. 16b). The slump structures are interpreted to have formed while the unconsolidated sediments were deposited in the Hummeln-depression, and the cm-scale faults could have formed from shearing of overlying strata by glacio-tectonic movements.

The steep inclinations of the slumped sediments are interesting to compare to the Rock Elm impact structure (Wisconsin), where ring basin-filling sedimentary rocks are described by French (2004). The same type of sedimentary rocks is not found in the vicinity are therefore certain to have been deposited after impact (French, 2004). The strata of the sedimentary rocks in Rock Elm appear almost flat and locally displays a few degrees dipping. In sharp contrast, the sedimentary rocks of Hummeln dip between 30-50° (Lindström et al., 1999).

The difference in inclination is possibly explained by crater morphology. Where Hummeln is thought to be formed as a simple, bowl shaped, crater, Rock Elm is 6.5 km in diameter and a complex crater with a central uplift. Therefore, the ring basin of Rock Elm is shallow and shows less topography than the freshly formed Hummeln structure would have done. Sediments deposited in the Hummeln crater after formation experienced slumping down a deep and rather narrow bowl, forming steep inclinations in the strata.

5.1.5 Crater-fill (164.25-157.3 m) of the Hummeln-1 drill core

The lowermost 7 meters of the drill core generally consist of mono- and polymict breccias interfingered with arkosic sandstone displaying flow patterns. This part of the drill core is interpreted as allochthonous crater-fill deposits (Fig. 16f-j, Tab. A7). There is nothing in the lithology implying that we have reached the crater floor, and previous studies did not conclude so either (Lindström, 1999). On the contrary, the presence of polymict breccia point towards massive movements at this level.

The two main types of breccia, clast supported monomict breccia (e.g., 159.9-159.1 m) and matrix supported polymict breccia (e.g., 162.5-162.3 m) are here interpreted as lithic impact breccia and suevitic impact breccia respectively. The lith-arkosic sandstone (e.g., 160.9-160.6 m) is thought to be sand-rich impact melt rock (see section 5.3.2.), and the dense, igneous-looking rock (at 162-162.5 m) is interpreted as clast-poor impact melt rock (Fig. A1).

Generalised interpretation of the crater-fill part of the Hummeln-1 drill core: The bottom level (starting at 164.25 m) of the drill core consists of suevitic impact breccia (Fig. 16j), overlain by lithic impact breccia (163.0-162.5 m), overlain by suevitic impact breccia which gradually transitions into clast-poor impact melt rock at ~162.3 m (Fig. 16i). At 161.8 m there is a sharp transition from impact-melt rock to suevitic breccia (calcite fractures display brittle cuttings). This lithology gradually transitions into a clast-rich impact-melt rock with flow structure, containing a lot of sand-grains, at 160.9 m. Overlying this is a suevitic impact breccia that gradually transitions into lithic impact breccia at 160.3 m. The impact breccia continues until 159 m where it transitions into suevitic impact breccia, which then transitions into a clast-rich impact melt rock with sand-grains at 158.4 m. From 158.1 m the core consists of lithic impact breccia, which between 157.2-157.1 m transitions to coarse, arkosic sandstone. This is where crater-fill transitions into sedimentary fill.

The transition between impactites and post-impact sediments at 157.3 m (Fig. 5, Fig. 16e, Fig. 20) is of great importance, especially since the interpretation of this study differs from previous studies of the Hummeln-1 drill core. Lindström et al. (1999) set the age of the Hummeln impact event to Ordovician, inferring that the entire sequence of Paleozoic sediments was already present at the moment of impact. The authors stated that the sediments of the Hummeln-1 drill core did "not carry any signs of having sedimented in a protected sediment trap, like a crater." (p. 251, 1999). They further explained that the slump-structures are products of late-stage crater formation: "We assume that the rim of the transient cavity collapsed and entrained slump material from the immediate vicinity" (p. 252, 1999).

In this study, the transition from crater-fill to post-impact sedimentary infill is set to 157.3 meters in the Hummeln-1 drill core for the following reasons:

- The strata above 157.3 m differs from the lithologies below, in particular regarding maturity. Fragments in the breccias below 157.3 m are both larger and more angular than grains and fragments above.
- While the mineralogy of the breccia-fragments (e.g., potassium feldspar) does also appear in the arkose, they are much smaller and more rounded.
- The sedimentary structures in the arkosic sandstone, such as high-angle bedding, are here interpreted as consequences of forming in a sedimentary trap rather than during crater formation. This type of bedding more likely suggests uneven bottom topography than chaotic mixing (which could be expected from an impact event).
- If all of the Paleozoic sediments and lithologies would have been present at impact, the excava-

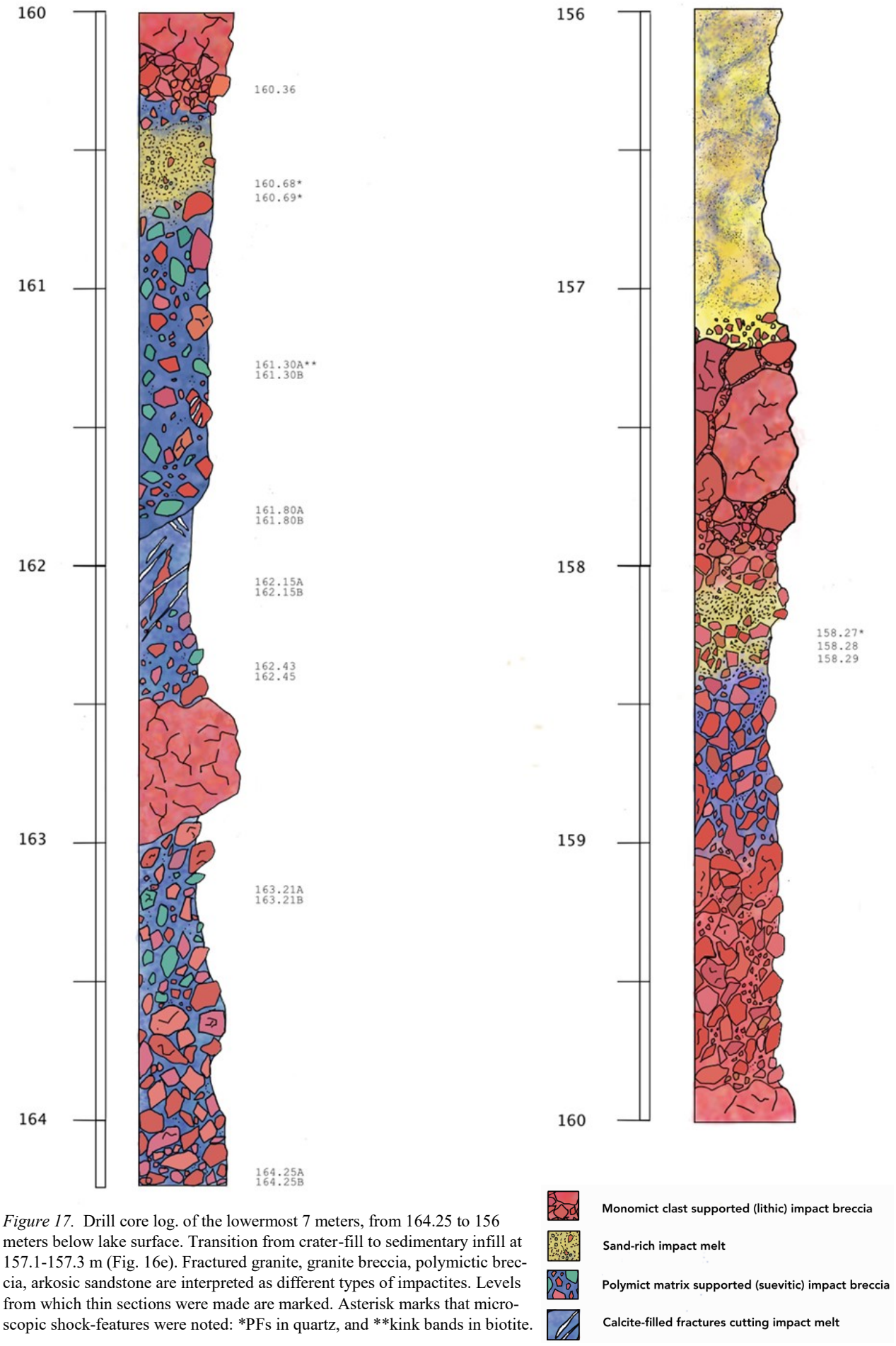

Figure 17. Drill core log. of the lowermost 7 meters, from 164.25 to 156 meters below lake surface. Transition from crater-fill to sedimentary infill at 157.1-157.3 m (Fig. 16e). Fractured granite, granite breccia, polymictic breccia, arkosic sandstone are interpreted as different types of impactites. Levels from which thin sections were made are marked. Asterisk marks that microscopic shock-features were noted: *PFs in quartz, and **kink bands in biotite.

tion stage during crater formation would have caused sand, clay and limestone to mix more.

Petrographic studies of the Hummeln-1 drill core reveal the same mineralogy as the thin sections made from field samples from the Humlenäs shoreline (H22-F04, H22-F06 and H22-B08). It shows the same mineralogy and the same types of alterations, and the clay-rich matrix is similar (Tab. A5, Tab. A7). This type of matrix was noted as "blue-breccia" (Bi5) in the field. Under the microscope it appears to consist of a mixture of clay-minerals and rounded quartz grains (Tab. A8, Tab. A9, Fig. A1-3). When studied in SEM, the elongated clay-crystals sometimes display flow-patterns indicative of melt or glass (Fig. 19e-f). The "blue-breccia" of Humlenäs is therefore interpreted as suevitic impact breccia, where the melt has later suffered clay-alteration (Fig. 14c-e).

Microstructures indicative of shock-metamorphism was found in the following thin sections from the Hummeln-1 drill core: 161.30 A, 160.69, 160.68, 158.27, 154.60 A & B, 153.85 A, B & C and in 139.9 A & B (Fig. 18a-d, Fig. A1-3). Petrographic studies revealed that the shock metamorphic features primarily occur in rounded quartz grains, especially when these grains are found in the clay-matrix interpreted as former melt or glass described above. The samples from 158.27, 158.28. and 158.29 meters illustrate this well: the lithology is homogenous except for a small portion of 158.27, where matrix is dark and contains clay (Fig. A3). This is the only part of these three samples that contain PFs (>4 in an area of 1.5 cm^2). It is worth noting that rock-fragment-building quartz crystals of the Hummeln-1 drill core rarely show any shock features.

5.1.6 Target rocks and sediments

Findings of sedimentary grains and clasts in the impact breccias of the Hummeln structure provide an opportunity to investigate which lithologies that were present at the time of impact. Since the age of the impact event is set to middle/late Ordovician, the most abundant lithologies of Öland (sandstone, claystone, and cold-water-carbonates) would be expected in the crater-fill.

As mentioned in section 5.1.5, quartz crystals in rock-fragments (e.g., granite) show less shock features than sand-grains found in suevitic breccia. Shocked quartz-grains occur on several levels in the drill core (160.69, 160.68, 158.27, 154.60, 153.85 and 139.9 m) and since they are often found in close proximity to angular clasts of different rock types, the matrix that they occur in are interpreted as not having suffered a lot of transport. Abundant sand-grains in the crater-fill means that either unconsolidated sand or sandstone was present, covering basement, at the time of impact.

No mudstone-clasts were found in the thin sections from Hummeln-1 drill core, only clay-alteration in matrix. Angular clasts of claystone were however discovered in sample H22-F06:3 (Fig. A3), why it is concluded that mudstone was at site and lithified at the time of impact. What is however alarmingly rare in the impact breccias of Hummeln are fragments of carbonate rocks. Calcite is an abundant fracture filling mineral, but during microscopic studies of the crater-fill only one (1) carbonate fragment has hitherto been found (in suevitic impact breccia, sample H22-F04:3). None of the samples from the crater-fill part of Hummeln-1 drill core contained carbonate fragments.

Considering the general lack of carbonate clasts in the polymict breccia it is unlikely that thick beds of Ordovician cold-water carbonates covered the site at impact, which provides new implications regarding the age of the Hummeln impact event. It is most unlikely that a projectile collided with a seafloor that had endured carbonate sedimentation for several millions of years, which would have been the case if the impact event took place in the late Early Ordovician (Lindström et al., 1999). The rarity of carbonate fragments in the impactites of Hummeln indicates that this impact structure is far older than 470 million years. Having endured erosion for more time than previously assumed, the Hummeln impact structure is even more exceptional than previously expected.

5.2 Propagation of shock wave

5.2.1 Traces of shock metamorphism

Previous petrographic studies of Hummeln-rocks are rare. In 2015, Alwmark et al. reported findings of decorated PDFs oriented parallel to the basal plane (0001) in quartz. The study did however not report any other findings of shock-metamorphic features. Previous studies of the Hummeln-1 drill core was prominently focused on describing the biostratigraphy (Lindström, 1999) and did not record any shocked minerals.

This study confirms that PDFs are rare but present in the Hummeln structure. They occur as basal PDFs in the sand-rich part of the Hummeln-1 drill core (e.g., sample 160.68, Fig. A3), indicating low shock pressures (<8 GPa; French 1998) but high deviatoric stress (see paragraph below). Planar fractures (PFs) are abundant in the samples from Hummeln. They occur in rounded quartz grains in the matrix of polymict, matrix-supported breccias (melt-rich impact breccias). These fractures are not, as mentioned in section 2.2.1, considered diagnostic for impact unless accompanied by other shock-features such as PDFs or shattercones. When found in multiple sets and in great numbers however, e.g., in quartzite pebbles of the Rock Elm impact structure, they are tentatively regarded as a shock-metamorphic criterion (French, 2004). The same study proposes a connection between the general lack of PDFs and the abundance of PFs, namely that they form at distinctly different shock-pressures (French, 2004). See section 5.2.2 for further comparisons and implications.

Figure 18. (Next page) Photos from the optical microscope showing shock induced microstructures in quartz (A-D) and altered minerals (E-H). **A.** Close-up of a rounded quartz grain displaying planar fractures (H22-F06:3). **B.** Several rounded quartz grains in a clay-rich matrix displaying planar fractures (160.68). **C.** Planar deformation features along the basal plane in a granitic fragment (sample 160.68). **D.** Feather feature lamellae along PF in a quartz grain (154.60). **E.** & **F.** Chloritization of micas, PPL and XPL respectively (162.43). **G.** & **H.** Sericitization of plagioclase, PPL and XPL respectively (H22-B08:A).

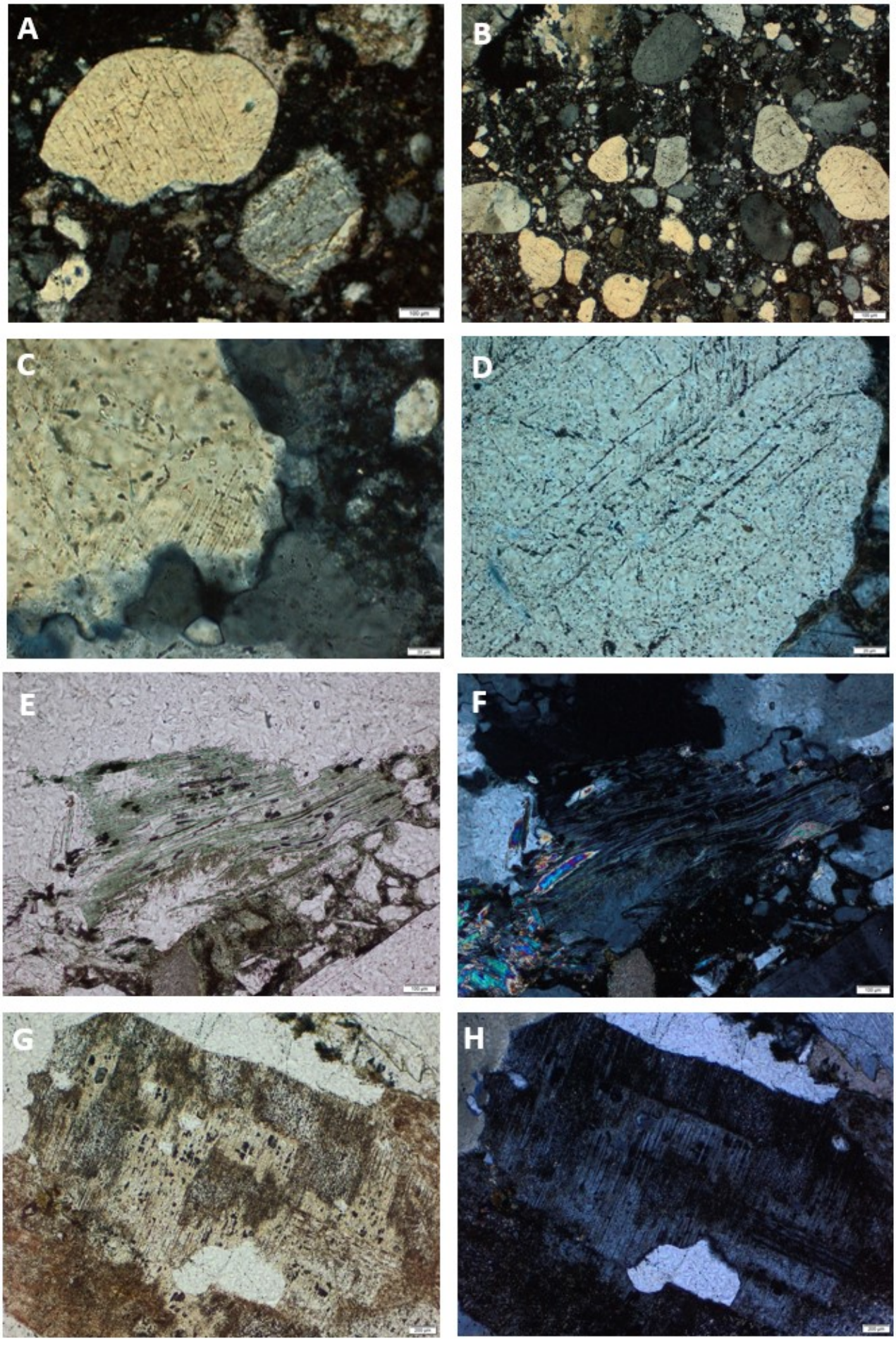
A
B
C
D
E
F
G
H

Several of the microscopic deformation features found in the Hummeln-samples are evidence of shock-induced shear deformation: mechanical twins (basal PDFs), planar fractures (PF), feather feature lamellae (FFL) and kink bands in biotite (Fig. A1). Feather feature lamellae (FFLs, Fig. 18d) are noted in a few samples from the Hummeln structure (e.g., 160.68). FFLs and the host-PF form an angle that, like an arrow, point in the direction of the shear stress (Poelchau & Kenkmann, 2011). These features can thus sometimes be used to understand the direction of strain. However, since the FFLs in the Hummeln-impactites formed before the rocks were lithified, and since all FFLs are developed in sand-grains that "float" in a melt-matrix, strain direction cannot be measured from FFLs in the Hummeln-samples. Kink bands in biotite are not considered diagnostic for impact origin (Ebert et al., 2021), but reported from several impact settings, e.g., the Ries impact structure (Engelhardt et al., 1968), the Gardnos impact structure (French 1997), and Chicxulub (Ebert et al., 2021). In Chicxulub, kinked micas have been used to determine principal axis of strain when occurring together with feather features (Ebert et al., 2021).

In conclusion, the findings of basal PDFs, PFs, FFLs and kinked biotite in the Hummeln impactites bear evidence of low shock-pressures and high shock-induced deviatoric stress.

5.2.2 Shock wave behavior in a sedimentary target

Signs of low shock pressures are also a potential sign of sedimentary target rocks (French, 2004). The combination of abundant PFs, occurrence of FFLs and absence of true PDFs is described from the sedimentary impactites of the Rock Elm impact structure (French, 2004). Since Rock Elm is a complex structure of >6 km in diameter and the microscopic features mentioned are found in the central uplift, this combination is not restricted to small, simple craters as the Hummeln structure – but possible rather an indication of sedimentary or mixed target.

Based on mesoscale modeling of impact-induced shock in porous sandstone, Güldemeister et al. (2013) calculated the connection between bulk porosity and reduction in shock pressures and proposed that shock-induced compaction is key to understanding the behavior of porous target rocks. Osinski et al. proposed that peak shock-pressures are consumed in the crushing of pore space, resulting in absence of intermediate

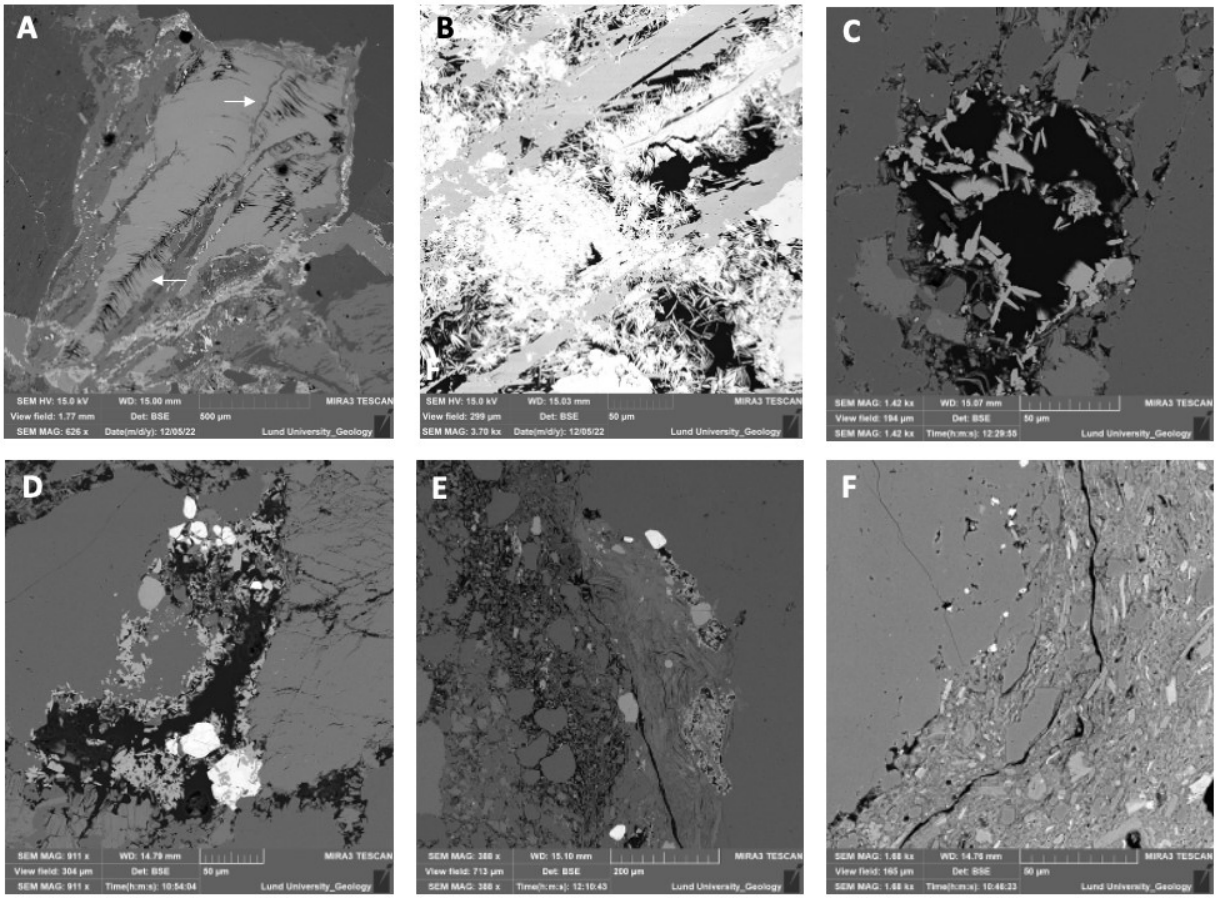

Figure 19. Scanning electron microscope-photos (SEM-EBSD) of different features in the Hummeln-1 drillcore. **A.** Kink bands, marked with arrows, in biotite (sample 161.30A). **B.** Calcite-needles grown in voids (161.30B). **C.** TiO_2-needles grown in voids (160.68). **D.** TiO_2 inter-grown with pyrite (160.68). **E.** Clay-alteration at the boundary of a feldspar-grain (160.69). **F.** Clay-minerals that display flow-structure, potentially altered glass (160.69).

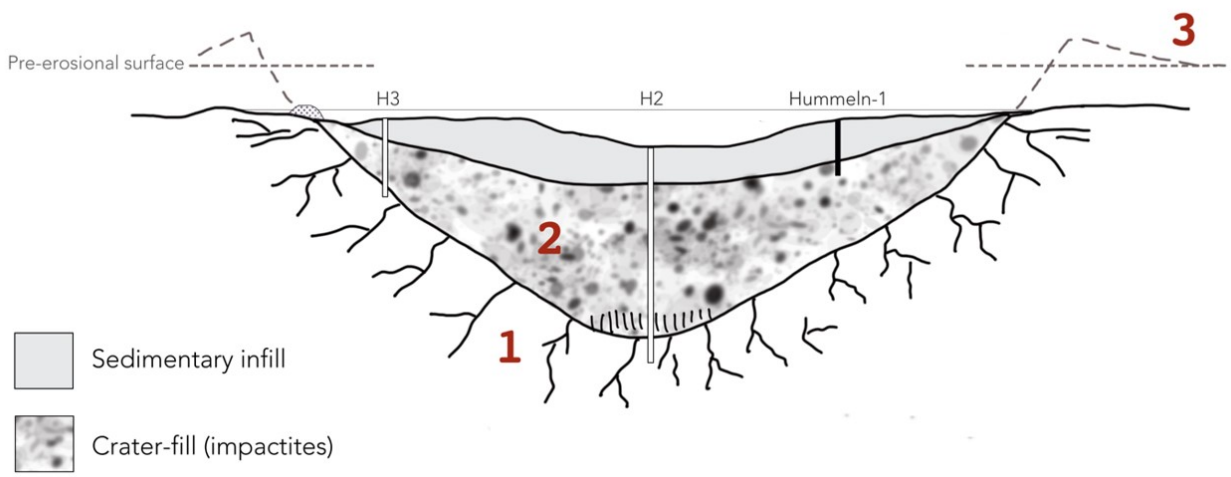

Figure 20. Interpretation of the Hummeln impact structure drawn as a profile inspired by Melosh, 1989 and (modified from Fig. 2 in (Grieve, 1979). Also loosely based on gravimetric models in Ormö et al. (p. 167, 1999). Showing interpreted spatial distribution of lithologies and pre-erosional surface (not to scale). Location of the Hummeln-1 drill core marked in black, suggestions for future drilling programs H2 and H3 marked in white. (also in Fig. 7). Photos of lithologies in Fig. 16, linked to the two parts of what is still present in the Hummeln impact structure: 1) crater wall, and 2) crater-fill. Because of erosion, there is no "3) ejecta" to be found at Hummeln.

- or high-shock pressure indicators (like PDFs) as in the Hummeln samples (2018). In essence, PDFs and PFs form in different pressure ranges. In the Hummeln impact structures however, just as in the Rock Elm impact structure, the abundance of PFs and lack of PDFs are likely an effect of porous target lithology rather than the amount of energy released at impact.

The shocked sand-grains are not evenly distributed in the crater-fill section of the Hummeln-1 drill core: PFs occur at 160.68 meters, are absent in arkosic sandstone at 153.30 meters and then again abundant in arkosic sandstone at 139.90 m. This heterogenic distribution of shock may also be explained as an effect of rarefaction waves produced by pore collapse (Güldemeister et al., 2013). Regarding shocked quartz it is also worth noting that the rounded, shocked, grains of Hummeln are often found in the clay-rich matrix (blue-breccia, Bi5, e.g., H22-F04). Since shock -deformation is evidently present in this type of matrix, this strengthens the above posed idea that the blue, clay-rich matrix is in fact clay-altered melt (see section 5.1.2). The occurrence of quartz grains in a matrix interpreted as impact melt poses the question "How come these grains did not melt?". One probable scenario is that the quartz grains that are still intact were incorporated in the melt-rich matrix when this had cooled sufficiently, maybe when the steep crater-rim of the transient crater collapsed. If the target lithology was under water, fluids could lower the temperature of the system by using energy for vaporizing. If the quartz grains were lithified as sandstone, breaking these bonds could also aid in cooling the lithology.

The unusual appearance of what is here interpreted as recrystallized impact melt can actually be regarded as yet another sign of sedimentary cover at impact. As briefly mentioned in section 2.2.1., it was not confirmed until the end of the 19th century that impact structures of sedimentary target produce melt at all (Kieffer & Simonds, 1980). It has since been proposed that the same amount of melt is in fact produced, but that it does appear different (e.g., Greenberger et al., 2020). Faster cooling rates, a more clast-rich melt, impact-induced hydrothermal activity, and widespread clay-alterations are reasons that have been discussed (Newsom 1986, Osinski, 2004; Osinski & Grieve 2008; Engelhardt, 1995). Two types of lithologies studied at Hummeln and in the Hummeln-1 drill core are interpreted as altered melt (or glass):

1. The matrix of polymict matrix-supported breccia (e.g., H22-F06, Fig. 15a) appears similar to clast-rich impact melt described in the Haughton impact structure (Canada; Fig. 6; Greenberger et al., 2020).

2. Locality D. Matrix between the big granite fragments appears similar to thoroughly weathered granite, i.e., an igneous texture which is therefore interpreted as impact melt acting as matrix around big, granite fragments (Fig. 14a, Fig. 14b).

To conclude, the absence of classic looking impact-melt, paired with the combination of PFs and FFLs as well as the occurrence of angular sedimentary rocks in impact breccia (Fig. 15a), all point towards a mixed target.

5.3 Evidence of impact-induced hydrothermal activity

Impactite samples from the Hummeln structure display several low-grade metamorphic alterations that are typically associated with hydrothermal activity (Kirsimäe & Osinski, 2012). Similar mineral paragenesis are described from volcanic settings, e.g., geysers and sub-marine hydrothermal vents (e.g.,

Trewin, 2005).

One explanation for low-grade metamorphic alterations in the Hummeln structure is the presence of impact-induced hydrothermal activity, bearing in mind that alterations of impactites happen without the influence of hydrothermal activity. In large impact structures like Chicxulub (~200 km in diameter) and Sudbury (~250 km in diameter), durations for impact-induced hydrothermal systems have been calculated to 1–2 million years (Osinski et al., 2020 and references therein). While the morphology of complex impact structures offers several heat sources for hydrothermal activity (Fig. 5., Fig. 21), studies of the 1.8 km wide Lonar Lake impact structure imply that hydrothermal activity in simple craters is probably dependent on remnant impact energy deposited in shocked rocks (Hagerty & Newsom, 2003). For how long time an impact structure of the size of Hummeln can retain sufficient heat is under debate, but impact- and geothermal modeling of the 4 km wide Kärdla structure (Estonia) suggests that the impact-induced hydrothermal flow continued for ~10.000 years (Jõeleht et al., 2005).

It is also worth noting that shock metamorphosed rocks and minerals are weakened and therefore more susceptible to all kinds of alterations (Osinski et al., 2020), and that low-grade alterations of the target rocks are common in the vicinity of Hummeln. Investigations in the Simpevarp area, 25 km from lake Hummeln, revealed low-temperature alterations that could be linked to four different orogenies (Drake et al., 2009). To be certain that specific alterations in rocks and minerals at Hummeln are a result of impact-induced hydrothermal activity, and not older, structural relations such as crosscuttings of matrix in breccia must be considered carefully.

5.4 Suggestions for future studies

Throughout this work many impact-related features of the Hummeln structure have been described. At the same time new questions arose. Several findings could be further investigated in order to shed more light on the Hummeln impact structure:

- New drillings at site 2 and 3 (Fig. 7, Fig. 20), number 2 deep enough (>300 m) to reach the crater floor. To search for potential impact melts at the deepest part of the crater to gain better understanding of the spatial distribution of crater-fill, but also to find traces of high temperature hydrothermal activity.

- Radiometric dating of secondary minerals that can be linked to impact-induced hydrothermal activity, e.g., calcite or TiO_2 (if rutile). Mineralizations in fractured impact-lithologies such as impact-melt (e.g., Fig. 16i) could provide a minimum age of the Hummeln impact event.

- Search sedimentary rocks of the drill core for hydrothermal alterations and compare to the same strata at Öland. For instance, studying illite crystallinity in the limestone-part of the drill core could shed some light as to whether the carbonate rocks are the same age as (or much younger than) the impact event.

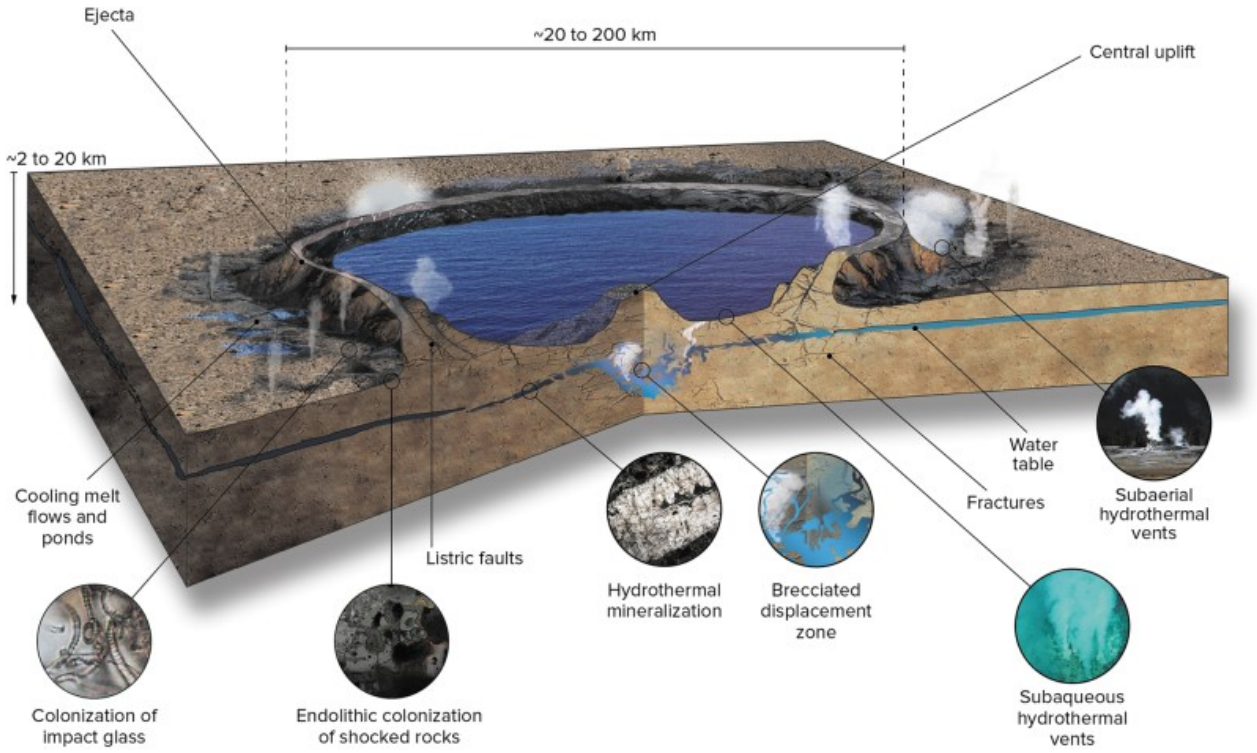

Figure 21. Artistic interpretation of impact-induced hydrothermal activity in a complex impact crater with a central uplift. (From Osinski et al., 2020). See also Fig. 5 for numbered locations and heat sources.

- Search sedimentary rocks for traces of impact trauma. Until now, no in-situ Paleozoic sedimentary rocks have been found at Hummeln. But it would be interesting to systematically search the sandstone- and limestone blocks for impact related deformation, for example shocked minerals or shattercones.

- Compare the incorporated sedimentary rocks to the Almesåkra group. If the clasts of mudstone (H22-F06, Fig. 15a) and sandstone (e.g., sample 139.90, Fig. A2) are not in fact Paleozoic, they might origin from the proterozoic Almesåkra group found in lake Vättern approximately 150 km from lake Hummeln (Rodhe, 1987).

- Further map and investigate the parallel oriented fractures along the shore of Humlenäs. To compare them to other impact structures and better understand how this feature could possibly relate to the gross crater morphology.

6 Conclusions

This study solidifies the importance of revisiting impact structures after confirmation.

6.1 Conclusions about the Hummeln structure

- The scarcity of carbonate clasts in the impact breccias of lake Hummeln could imply that that type of rock was not present at the time of the Hummeln impact event. This could have implications about the age of the event but further and more extensive studies are necessary.

- Though the uppermost parts of the crater (ejecta, rim and upper flanks) are eroded, the Hummeln impact structure is surprisingly well preserved considering its age. This is most likely a consequence of epeiric seas covering the Baltoscandian shield during the early Paleozoic.

- The Hummeln impact structure was most likely formed in a mixed target of sediments and sedimentary rocks overlying crystalline basement. Findings of impact melt and suevitic breccia resemble lithologies previously described in impact structures with a certain mixed or sedimentary target. The assemblage of shock-induced microstructures also point toward a target with high porosity.

- This is the first description of traces of hydrothermal activity in the Hummeln impact structure. New drilling campaigns aimed at locations in the structure that have experienced higher temperatures, e.g., the probable melt lens at the middle of the crater floor, are needed to document this phase of crater formation further. Radiometric dating of hydrothermally precipitated minerals would provide a minimum-age for the impact event.

6.2 Conclusions about small, simple, and old, impact structures

- Impact structures that are <2 km in diameter can be preserved for >470 million years under favorable conditions.

- Small impact structures with sedimentary or mixed target are interesting to study in order to better understand the low-grade shock-pressure-regime.

- Impact-induced hydrothermal activity in small impact structures might be more common than previously assumed.

- Re-visiting already confirmed impact structures is valuable to gain new insights in into crater formation, crater preservation and shock-metamorphism.

7 Thanks to

Surre, Matrin and Findus for having me stay with you in Småland. Twice. To Mr and Mrs Johansson for letting me roam your garden, for telling me about recent changes in lake-surface-levels and recommending the hidden treasure “Humlenäsboken”. To Ida, Daniel and Gabriel for helping out with microscope studies and discussing obscure mineral findings. To Sylvain and Anders for offering your thoughts on carbonate rocks of Hummeln. To Kristoffer for the curious questions. To Carl for coming with me to Hummeln and letting me use your office. And Sanna, thank you for the steady and kind guidance and for teaching me about shock metamorphism.

8 References

Alvarez, L. W., Alvarez, W., Asaro, F., & Michel, H. V. (1980). Extraterrestrial Cause for the Cretaceous-Tertiary Extinction. *Science*, *208*(4448), 1095-1108. http://www.jstor.org/stable/1683699

Alwmark, C., Ferrière, L., Alwmark, S., Ormö, J., Leroux, H., & Sturkell, E. (2015). Impact origin of the Hummeln structure (Sweden) and its link to the Ordovician disruption of the L-chondrite parent body. *Geology*, *43*. https://doi.org/10.1130/G36429.1

Alwmark, S. (2021). Impact cratering record of Sweden - A review. In. https://doi.org/10.1130/2021.2550(01)

Asklund, B. (1921). Nya fynd av kambrisk-silur berggrund i Sverige och deras geologiska betydelse. [New findings om cambrian-silurian rocks in Sweden and their geological importance]. *Geologiens*

grunder, *2*, 372.
Barringer, D. M. (1914). Further Notes on Meteor Crater, Arizona. *Proceedings of the Academy of Natural Sciences of Philadelphia*, *66*(3). http://www.jstor.org/stable/4063594
Dons J. A., Naterstad J. (1992). The Gardnos impact structure, Norway (abstract). *Meteoritics 27*, 215.
Dence, M. R. (1972). Meteorite impact craters and the structure of the Sudbury Basin. *(Guy-Bray, J.V., ed.) Geol. Assoc. Can*, *Spec. Paper 10*, 7-18.
Ebert, M., Poelchau, M.H., Kenkmann, T., Gulick, S.P.S., Hall, B., Lofi, J., McCall, N., and Rae, A.S.P., 2021, Comparison of stress orientation indicators in Chicxulub's peak ring: Kinked biotites, basal PDFs, and feather features, in Reimold, W.U., and Koeberl, C., eds., Large Meteorite Impacts and Planetary Evolution VI: *Geological Society of America Special Paper 550*, p. 479–493
Einarsson, B., & Axelsson, R. (2001). Humlenäsboken - En gårds och släktbeskrivning. [The Humlenäs-book – description of a farm an a family]. 286 p.
Engelhardt, von, W., & Stöffler, D. (1968). Stages of shock metamorphism in crystalline rocks of the Ries Basin, Germany. In (pp. 159-168).
Engelhardt, W. V., Arndt, J., Fecker, B., & Pankau, H. G. (1995). Suevite breccia from the Ries crater, Germany: Origin, cooling history and devitrification of impact glasses [https://doi.org/10.1111/j.1945-5100.1995.tb01126.x]. *Meteoritics*, *30*(3), 279-293. https://doi.org/https://doi.org/10.1111/j.1945-5100.1995.tb01126.x
Engelhardt, W. v., & Bertsch, W. (1969). Shock induced planar deformation structures in quartz from the Ries crater, Germany. *Contributions to Mineralogy and Petrology*, *20*(3), 203-234. https://doi.org/10.1007/BF00377477
Fazio, A., Pollok, K., & Langenhorst, F. (2018). Experimental evidence for mechanical Brazil twins as an indicator of low-pressure shock metamorphism (<17.5 GPa). *Geology*, *46*(9), 787-790. https://doi.org/10.1130/G40198.1
Fredriksson, K. Wickman., F.E. (1963). Meteoriter. [Meteorites] *Svensk Naturvetenskap*, *16*, 128-129.
French, B. M., & Koeberl, C. (2010). The convincing identification of terrestrial meteorite impact structures: What works, what doesn't, and why. *Earth-Science Reviews*, *98*(1), 123-170. https://doi.org/https://doi.org/10.1016/j.earscirev.2009.10.009
French, B. M., Koeberl, C., Gilmour, I., Shirey, S. B., Dons, J. A., & Naterstad, J. (1997). The Gardnos impact structure, Norway: Petrology and geochemistry of target rocks and impactites. *Geochimica et Cosmochimica Acta*, *61*(4), 873-904. https://doi.org/https://doi.org/10.1016/S0016-7037(96)00382-1
Gebremedhin, G.G. (2023). U-Pb geochronology of brittle deformation using LA-ICP-MS imaging on calcite veins. Master's thesis, Lund University, No. 647, 50 pp. http://lup.lu.se/student-papers/record/9111010.
Goltrant, O., Leroux, H., Doukhan, J.-C., & Cordier, P. (1992). Formation mechanisms of planar deformation features in naturally shocked quartz. *Physics of the Earth and Planetary Interiors*, *74*(3), 219-240. https://doi.org/https://doi.org/10.1016/0031-9201(92)90012-K
Grady, D. E. (1980). Shock deformation of brittle solids [Article]. *Journal of Geophysical Research*, *85*(B2), 913-924. https://doi.org/10.1029/JB085iB02p00913
Grieve, R. A. F., & Dence, M.R. (1979). Principal characteristict of the Impactites at Brent Crater, Ontario, Canada. *Lunar and Planetary Science*, *IX*, 416-418.
Güldemeister, N., Wünnemann, K., Durr, N., & Hiermaier, S. (2013). Propagation of impact-induced shock waves in porous sandstone using mesoscale modeling [https://doi.org/10.1111/j.1945-5100.2012.01430.x]. *Meteoritics & Planetary Science*, *48*(1), 115-133. https://doi.org/https://doi.org/10.1111/j.1945-5100.2012.01430.x
Hagerty, J. J., & Newsom, H. E. (2003). Hydrothermal alteration at the Lonar Lake impact structure, India: Implications for impact cratering on Mars. *Meteoritics & Planetary Science*, *38*.
Hisinger, W. (1826). Underrättelse om lager av petrificatförande kalksten på Humlenäs i Calmar Län. [Notification about layers of limestone at Humlenäs in the Kalmar area]. *Kungliga vetenskapskadademins handlingar*, *v.1825*, 180-187.
Holm-Alwmark, S. (2021). Impact cratering record of Sweden—A review. *Large Meteorite Impacts and Planetary Evolution VI*, *550*, 0. https://doi.org/10.1130/2021.2550(01)
Holm-Alwmark, S., 2021, Impact cratering record of Sweden—A review, in Reimold, W.U., and Koeberl, C., eds., Large Meteorite Impacts and Planetary Evolution VI: *Geological Society of America Special Paper 550*, p. 1–39
Jaanusson, V. (1973). Aspects of carbonate sedimentation in the Ordovician of Baltoscandia. *Lethaia*, *6*(1), 11-34. http://ludwig.lub.lu.se/login?url=https://search.ebscohost.com/login.aspx?direct=true&db=edb&AN=62193660&site=eds-live&scope=site
Jõeleht, A., Kirsimae, K., Versh, E., Plado, J., & Ivanov, B. (2005). Cooling of the Kardla Impact Crater.
Kalleson, E., Corfu, F., & Dypvik, H. (2009). U-Pb systematics of zircon and titanite from the Gardnos impact structure, Norway: Evidence for impact at 546 Ma? *Geochimica et Cosmochimica Acta*, *73*, 3077-3092. https://doi.org/10.1016/j.gca.2009.02.020
Kenkmann, T., Collins, G., & Wünnemann, K. (2012). *The Modification Stage of Crater Formation*.
Kieffer, S. W., & Simonds, C. H. (1980). The role of volatiles and lithology in the impact cratering process [https://doi.org/10.1029/RG018i001p00143]. *Reviews of Geophysics*, *18*(1), 143-181. https://doi.org/https://doi.org/10.1029/RG018i001p00143
Kirsimäe, K., & Osinski, G. R. (2012). Impact-induced hydrothermal activity. In O. a. Pierazzo (Ed.), *Impact Cratering: Processes and Products*

grunder, *2*, 372.
Barringer, D. M. (1914). Further Notes on Meteor Crater, Arizona. *Proceedings of the Academy of Natural Sciences of Philadelphia*, *66*(3). http://www.jstor.org/stable/4063594
Dons J. A., Naterstad J. (1992). The Gardnos impact structure, Norway (abstract). *Meteoritics 27*, 215.
Dence, M. R. (1972). Meteorite impact craters and the structure of the Sudbury Basin. *(Guy-Bray, J.V., ed.) Geol. Assoc. Can*, *Spec. Paper 10*, 7-18.
Ebert, M., Poelchau, M.H., Kenkmann, T., Gulick, S.P.S., Hall, B., Lofi, J., McCall, N., and Rae, A.S.P., 2021, Comparison of stress orientation indicators in Chicxulub's peak ring: Kinked biotites, basal PDFs, and feather features, in Reimold, W.U., and Koeberl, C., eds., Large Meteorite Impacts and Planetary Evolution VI: *Geological Society of America Special Paper 550*, p. 479–493
Einarsson, B., & Axelsson, R. (2001). Humlenäsboken - En gårds och släktbeskrivning. [The Humlenäs-book – description of a farm an a family]. 286 p.
Engelhardt, von, W., & Stöffler, D. (1968). Stages of shock metamorphism in crystalline rocks of the Ries Basin, Germany. In (pp. 159-168).
Engelhardt, W. V., Arndt, J., Fecker, B., & Pankau, H. G. (1995). Suevite breccia from the Ries crater, Germany: Origin, cooling history and devitrification of impact glasses [https://doi.org/10.1111/j.1945-5100.1995.tb01126.x]. *Meteoritics*, *30*(3), 279-293. https://doi.org/https://doi.org/10.1111/j.1945-5100.1995.tb01126.x
Engelhardt, W. v., & Bertsch, W. (1969). Shock induced planar deformation structures in quartz from the Ries crater, Germany. *Contributions to Mineralogy and Petrology*, *20*(3), 203-234. https://doi.org/10.1007/BF00377477
Fazio, A., Pollok, K., & Langenhorst, F. (2018). Experimental evidence for mechanical Brazil twins as an indicator of low-pressure shock metamorphism (<17.5 GPa). *Geology*, *46*(9), 787-790. https://doi.org/10.1130/G40198.1
Fredriksson, K. Wickman., F.E. (1963). Meteoriter. [Meteorites] *Svensk Naturvetenskap*, *16*, 128-129.
French, B. M., & Koeberl, C. (2010). The convincing identification of terrestrial meteorite impact structures: What works, what doesn't, and why. *Earth-Science Reviews*, *98*(1), 123-170. https://doi.org/https://doi.org/10.1016/j.earscirev.2009.10.009
French, B. M., Koeberl, C., Gilmour, I., Shirey, S. B., Dons, J. A., & Naterstad, J. (1997). The Gardnos impact structure, Norway: Petrology and geochemistry of target rocks and impactites. *Geochimica et Cosmochimica Acta*, *61*(4), 873-904. https://doi.org/https://doi.org/10.1016/S0016-7037(96)00382-1
Gebremedhin, G.G. (2023). U-Pb geochronology of brittle deformation using LA-ICP-MS imaging on calcite veins. Master's thesis, Lund University, No. 647, 50 pp. http://lup.lu.se/student-papers/record/9111010.
Goltrant, O., Leroux, H., Doukhan, J.-C., & Cordier, P. (1992). Formation mechanisms of planar deformation features in naturally shocked quartz. *Physics of the Earth and Planetary Interiors*, *74*(3), 219-240. https://doi.org/https://doi.org/10.1016/0031-9201(92)90012-K
Grady, D. E. (1980). Shock deformation of brittle solids [Article]. *Journal of Geophysical Research*, *85*(B2), 913-924. https://doi.org/10.1029/JB085iB02p00913
Grieve, R. A. F., & Dence, M.R. (1979). Principal characteristict of the Impactites at Brent Crater, Ontario, Canada. *Lunar and Planetary Science*, *IX*, 416-418.
Güldemeister, N., Wünnemann, K., Durr, N., & Hiermaier, S. (2013). Propagation of impact-induced shock waves in porous sandstone using mesoscale modeling [https://doi.org/10.1111/j.1945-5100.2012.01430.x]. *Meteoritics & Planetary Science*, *48*(1), 115-133. https://doi.org/https://doi.org/10.1111/j.1945-5100.2012.01430.x
Hagerty, J. J., & Newsom, H. E. (2003). Hydrothermal alteration at the Lonar Lake impact structure, India: Implications for impact cratering on Mars. *Meteoritics & Planetary Science*, *38*.
Hisinger, W. (1826). Underrättelse om lager av petrificatförande kalksten på Humlenäs i Calmar Län. [Notification about layers of limestone at Humlenäs in the Kalmar area]. *Kungliga vetenskapskadademins handlingar*, *v.1825*, 180-187.
Holm-Alwmark, S. (2021). Impact cratering record of Sweden—A review. *Large Meteorite Impacts and Planetary Evolution VI*, *550*, 0. https://doi.org/10.1130/2021.2550(01)
Holm-Alwmark, S., 2021, Impact cratering record of Sweden—A review, in Reimold, W.U., and Koeberl, C., eds., Large Meteorite Impacts and Planetary Evolution VI: *Geological Society of America Special Paper 550*, p. 1–39
Jaanusson, V. (1973). Aspects of carbonate sedimentation in the Ordovician of Baltoscandia. *Lethaia*, *6*(1), 11-34. http://ludwig.lub.lu.se/login?url=https://search.ebscohost.com/login.aspx?direct=true&db=edb&AN=62193660&site=eds-live&scope=site
Jõeleht, A., Kirsimae, K., Versh, E., Plado, J., & Ivanov, B. (2005). Cooling of the Kardla Impact Crater.
Kalleson, E., Corfu, F., & Dypvik, H. (2009). U-Pb systematics of zircon and titanite from the Gardnos impact structure, Norway: Evidence for impact at 546 Ma? *Geochimica et Cosmochimica Acta*, *73*, 3077-3092. https://doi.org/10.1016/j.gca.2009.02.020
Kenkmann, T., Collins, G., & Wünnemann, K. (2012). *The Modification Stage of Crater Formation*.
Kieffer, S. W., & Simonds, C. H. (1980). The role of volatiles and lithology in the impact cratering process [https://doi.org/10.1029/RG018i001p00143]. *Reviews of Geophysics*, *18*(1), 143-181. https://doi.org/https://doi.org/10.1029/RG018i001p00143
Kirsimäe, K., & Osinski, G. R. (2012). Impact-induced hydrothermal activity. In O. a. Pierazzo (Ed.), *Impact Cratering: Processes and Products*

(pp. 76-89). Wiley Blackwell.
Kring, D. A. (2017). Guidebook to the Geology of Barringer Meteorite Crater, Arizona (a.k.a. Meteor Crater) 2nd edition. *Lunar and Planetary Institute, Houston TX*, *No. 2040*.
Lagain, A., Kreslavsky, M., Baratoux, D., Liu, Y., Devillepoix, H., Bland, P., Benedix, G. K., Doucet, L. S., & Servis, K. (2022). Has the impact flux of small and large asteroids varied through time on Mars, the Earth and the Moon? *Earth and Planetary Science Letters*, *579*, 117362. https://doi.org/https://doi.org/10.1016/j.epsl.2021.117362
Lindskog, A., & Young, S. A. (2019). Dating of sedimentary rock intervals using visual comparison of carbon isotope records: a comment on the recent paper by Bergström et al. concerning the age of the Winneshiek Shale [https://doi.org/10.1111/let.12316]. *Lethaia*, *52*(3), 299-303. https://doi.org/https://doi.org/10.1111/let.12316
Lindström, M., Flodén, T., Grahn, Y., Hagenfeldt, S., Ormö, J., Sturkell, E., & Törnberg, R. (1999). The Lower Palaeozoic of the probable impact crater of Hummeln, Sweden. *GFF*, *121*, 243-252. https://doi.org/10.1080/11035899901213243
Linnarsson, J. G. O. (1878). De paleozoiska bildningarna vid Humlenäs i Småland. [The Paleozoic formations at Humlenäs in Småland]. *Sveriges Geologiska Undersökning C*(28), 1-9.
Maher, K. A., & Stevenson, D. J. (1988). Impact frustration of the origin of life. *Nature*, *331*(6157), 612-614. https://doi.org/10.1038/331612a0
Mansfeld, J. (1991). U–Pb age determinations of Småland-Värmland granitoids in Småland, southeastern Sweden. *Geologiska Föreningens i Stockholm Förhandlingar 113*, 113–119.
McLaren, A. C., Retchford, J. A., Griggs, D. T., & Christie, J. M. (1967). Transmission Electron Microscope Study of Brazil Twins and Dislacations Experimentally Produced in Natural Quartz. *Physica Status Solidi B-basic Solid State Physics*, *19*, 631-644.
Meier, M. M. M., & Holm-Alwmark, S. (2017). A tale of clusters: no resolvable periodicity in the terrestrial impact cratering record. *Monthly Notices of the Royal Astronomical Society*, *467*(3), 2545-2551. https://doi.org/10.1093/mnras/stx211
Melosh, H. J. (1989). Impact Cratering. A Geologic Process. . *Oxford Monographs on Geology and Geophysics Series no. 11*, *126*(6), 729-730. https://doi.org/10.1017/S0016756800007068
Newsom, H. E., Graup, G., Sewards, T., & Keil, K. (1986). Fluidization and hydrothermal alteration of the Suevite deposit at the Ries Crater, West Germany, and implications for Mars [https://doi.org/10.1029/JB091iB13p0E239]. *Journal of Geophysical Research: Solid Earth*, *91*(B13), E239-E251. https://doi.org/https://doi.org/10.1029/JB091iB13p0E239
Nordenskjöld, C. E. (1937). Några sjötyper i Kalmar län. [A couple of lake-types in the district of Kalmar]. *Svensk Geografisk Arsbok*, *1937*, 108-118.
Nordenskjöld, C. E. (1944). Morfologiska studier inom övergångsområdet mellan Kalmar-slätten och Tjust. [Morphological studies in the transitionarea between the Kalmar-flat and Tjust]. *Meddelanden från Lunds Universitets Geografiska Institution*, *8*, 1-126.
O'Keefe, J. D., & Ahrens, T. J. (1993). Planetary cratering mechanics [https://doi.org/10.1029/93JE01330]. *Journal of Geophysical Research: Planets*, *98*(E9), 17011-17028. https://doi.org/https://doi.org/10.1029/93JE01330
Ormö, J., Sturkell, E., Blomqvist, G., & Törnberg, R. (1999). Mutually constrained geophysical data for the evaluation of a proposed impact structure: Lake Hummeln, Sweden. *Tectonophysics*, *311*(1), 155-177. https://doi.org/https://doi.org/10.1016/S0040-1951(99)00158-4
Osinski, G., Grieve, R., Collins, G., Marion, C., & Sylvester, P. (2008). The effect of target lithology on impact melting. *Meteoritics & Planetary Science*, *43*, 1939-1954. https://doi.org/10.1111/j.1945-5100.2008.tb00654.x
Osinski, G. R. (2004). Impact melt rocks from the Ries structure, Germany: An origin as impact melt flows? *Earth and Planetary Science Letters*, *226*, 529-543. https://doi.org/10.1016/j.epsl.2004.08.012
Osinski, G. R., Cockell, C. S., Pontefract, A., & Sapers, H. M. (2020). The Role of Meteorite Impacts in the Origin of Life. *Astrobiology*, *20*(9), 1121-1149. https://doi.org/10.1089/ast.2019.2203
Osinski, G. R., Grieve, R. A. F., Bleacher, J. E., Neish, C. D., Pilles, E. A., & Tornabene, L. L. (2018). Igneous rocks formed by hypervelocity impact. *Journal of Volcanology and Geothermal Research*, *353*, 25-54. https://doi.org/https://doi.org/10.1016/j.jvolgeores.2018.01.015
Osinski, G. R., Grieve, R. A. F., Ferrière, L., Losiak, A., Pickersgill, A. E., Cavosie, A. J., Hibbard, S. M., Hill, P. J. A., Bermudez, J. J., Marion, C. L., Newman, J. D., & Simpson, S. L. (2022). Impact Earth: A review of the terrestrial impact record. *Earth-Science Reviews*, *232*, 104112. https://doi.org/https://doi.org/10.1016/j.earscirev.2022.104112
Osinski, G. R., Tornabene, L. L., Banerjee, N. R., Cockell, C. S., Flemming, R., Izawa, M. R. M., McCutcheon, J., Parnell, J., Preston, L. J., Pickersgill, A. E., Pontefract, A., Sapers, H. M., & Southam, G. (2013). Impact-generated hydrothermal systems on Earth and Mars. *Icarus*, *224*(2), 347-363. https://doi.org/https://doi.org/10.1016/j.icarus.2012.08.030
Pickersgill, A. E., Mark, D. F., Lee, M. R., & Osinski, G. R. (2020). 40Ar/39Ar systematics of melt lithologies and target rocks from the Gow Lake impact structure, Canada. *Geochimica et Cosmochimica Acta*, *274*, 317-332. https://doi.org/https://doi.org/10.1016/j.gca.2020.01.025
Poelchau, M. H., & Kenkmann, T. (2011). Feather

features: A low-shock-pressure indicator in quartz [https://doi.org/10.1029/2010JB007803]. *Journal of Geophysical Research: Solid Earth*, *116*(B2). https://doi.org/https://doi.org/10.1029/2010JB007803

Rodhe, A. (1987). Depositional environments and lithostratigraphy of the middle Proterozoic Almesåkra Group, southern Sweden. *Sveriges Geologiska Undersökning*, *Ca 69*, 1-80.

Shoemaker, E.M., & Chao, E.C.T. (1961). New evidence for the impact origin of the Ries Basin, Bavaria, Germany. *J. Geophys. Res., 66*, 3371–3378.

Schulte, P., Alegret, L., Arenillas, I., Arz, J. A., Barton, P. J., Bown, P. R., Bralower, T. J., Christeson, G. L., Claeys, P., Cockell, C. S., Collins, G. S., Deutsch, A., Goldin, T. J., Goto, K., Grajales-Nishimura, J. M., Grieve, R. A. F., Gulick, S. P. S., Johnson, K. R., Kiessling, W., Willumsen, P. S. (2010). The Chicxulub Asteroid Impact and Mass Extinction at the Cretaceous-Paleogene Boundary. *Science*, *327*(5970), 1214-1218. https://doi.org/10.1126/science.1177265

Stöffler, D. (1984). Glasses formed by hypervelocity impact. *Journal of Non-Crystalline Solids*, *67*(1), 465-502. https://doi.org/https://doi.org/10.1016/0022-3093(84)90171-6

Stöffler, D. & Grieve, R. A. F. (2007). Impactites, Chapter 2.11 in Fettes, D. and Desmons, J. (eds.) Metamorphic Rocks: A Classification and Glossary of Terms, Recommendations of the International Union of Geological Sciences, *Cambridge University Press, Cambridge,* UK, 82-92, 111-125, and 126-242.

Stöffler, D., Hamann, C., & Metzler, K. (2018). Shock metamorphism of planetary silicate rocks and sediments: Proposal for an updated classification system [https://doi.org/10.1111/maps.12912]. *Meteoritics & Planetary Science*, *53*(1), 5-49. https://doi.org/https://doi.org/10.1111/maps.12912

Stöffler, D., & Langenhorst, F. (1994). Shock Metamorphism of quartz in nature and experiment: I. Basic observation and theory. *Meteoritics*, *29*, 155-181. https://doi.org/10.1111/j.1945-5100.1994.tb00670.x

Suuroja, K., Suuroja, S., All, T., & Floden, T. (2002). Kärdla (Hiiumaa Island, Estonia)—the buried and well-preserved Ordovician marine impact structure. *Deep Sea Research Part II: Topical Studies in Oceanography*, *49*(6), 1121-1144. https://doi.org/https://doi.org/10.1016/S0967-0645(01)00145-X

Svensson, N. B. (1966). Lake Hummeln, a possible astrobleme in southern Sweden. I. The bottom topography. *Sveriges Geologiska Undersökning*, *C*(608), 1-18.

Trepmann, C. A. (2008). Shock effects in quartz: Compression versus shear deformation — An example from the Rochechouart impact structure, France. *Earth and Planetary Science Letters*, *267*(1), 322-332. https://doi.org/https://doi.org/10.1016/j.epsl.2007.11.035

Trewin, N. H. F., Sune Rune. (2005). Cherts resulting from hydrothermal systems. *Encyclopedia of Geology*, 51-62.

Versh, E., Kirsimae, K., Jõeleht, A., & Plado, J. (2005). Cooling of the Kärdla impact crater: I. The mineral parasequence observations. *Meteoritics & Planetary Science*(40).

Wallace, C. J., & Maher, K. C. (2019). Phyllic alteration and the implications of fluid composition at the Copper Flat hydrothermal System, New Mexico, USA. *Ore Geology Reviews 104*, 273-293. https://doi.org/https://doi.org/10.1016/j.oregeorev.2018.11.009

Zack, T., Stockli, D.F., Luvizotto, G.L., Barth, M.G., Belousova, M.R., Hinton, R.W. (2011). In situ U–Pb rutile dating by LA-ICP-MS: 208Pb correction and prospects for geological applications. *Contributions to Mineralogy and Petrology volume 162*, p. 515–530

Appendix

Table A1. Field notes summarized for each locality
Table A2. Breccia-index used in field
Table A3. Localities with sedimentary blocks
Table A4. Localities with in-situ impactites
Table A5. Rock samples from Hummeln 2022
Table A6. Description of the Hummeln-1 drill core
Table A7. Description of the lowermost 7 meters of the Hummeln-1 drillcore
Figure A1. Scanned thin sections
Figure A2. Scanned thin sections
Figure A3. Scanned thin sections
Table A8. Petrographic descriptions, field samples 2022
Table A9. Petrographic descriptions, Hummeln-1 drill core.

Table A1. Field notations from Lake Hummeln August and October 2022. Summary of what was noted in each locality regarding rock types (Fig. 9), brecciation (Fig. 8) and serial number of samples. Most localities refer to an area of about 5-10 m^2 and not a point or specific boulder. A few localities refer to an area >20 m^2.

Locality	Description	Samples
1	Råsviks badplats. Sandy beach. Big boulders of granite are not brecciated. No IN-SITU found by the water. About 100 m from lake: pink granite huge boulders / IN-SITU.	
2*	Rather pink-red than grey granite.	
3	IN-SITU light colored granite, rather white than pink. Coarse grained but "rounded" due to iceage. Almost undeformed except for a few long fractures.	
4	80 m.a.s.l., >1km fr. SHORELINE. Rounded basaltic boulder, 7x5 m. Fine-grained and heavily weathered skin. Fractured but would not classify as breccia, similar to the "weak [Bi1]" as seen in locality Å. Fractures filled with granitic crystals (pegmatite). No IN-SITU. *57°20'42"N, 16°15'20"Ö*	
5*	The map over the nature reserve. No IN-SITU	
6	300 m fr SHORELINE. No IN-SITU found, shoreline consists of boulders. No deformation that looks like breccia found.	
7	250 m fr SHORELINE. No IN-SITU found, shoreline consists of boulders. No deformation that looks like breccia found.	
8	Shoreline. Sandy, gravelly. 20-50 cm boulders. [Bi5] is common here and [Bi1, Bi2] as well (H22 B13). No findings of sand- or limestone. Weird finding of calcite crystals on a breccia boulder (H22 B01). No IN-SITU found. *57°22'3"N, 16°15'52"Ö*	H22 B01 H22 B13
9	5 m fr SHORELINE. No IN-SITU but a few breccia boulders, especially [Bi2].	
10	At SHORELINE. No IN-SITU but breccia boulders [Bi1, Bi2]. Sandstones of different textures: yellow fine-grained, lighter yellow with bigger yellow clasts, light green fine-grained.	
11	At SHORELINE. IN-SITU granite just below water-level. Breccia [Bi2] with clasts 5-10 cm. Sandstone boulders are less mature (not well sorted). Approximately 50% of the boulders here are breccia.	
12	At SHORELINE. No IN-SITU but some boulders are brecciated [Bi2]. Limestones displaying the "blommiga bladet". Also fossils of orthocones and gastropods. Sandstone boulders with bioturbation.	
13	At SHORELINE. No IN-SITU and less than 50% of the boulders are brecciated [Bi2, Bi5]. Large limestone boulders.	H22 S01
14	At SHORELINE. IN-SITU granite breccia [Bi5]. Clasts approximately 10 cm. *57°21'55"N, 16°15'46"Ö.*	H22 F01

15	Small bay at SHORELINE. No IN-SITU but abundance of brecciated boulders [Bi5] and [Bi4]. Calcite mostly white but sometimes colored red, Fe-. Both coarse- and fine-grained granite present. Matrix sometimes consisting of this weird, grey-blue fine-grained mass…	H22 B02-B08
16	70 m. fr. SHORELINE. Granite breccia [Bi1, Bi2] occurring in meter-sized boulders and smaller. No IN-SITU.	
17	15 meters from SHORELINE, old lake rim. Boulders heavily overgrown with moss. Generally intact/undeformed but breccia occurs [Bi1, Bi2]. Sandstone also occurs. No IN-SITU.	
18	Shoreline. IN-SITU granite breccia [Bi1, Bi5] where some fragments >30 cm. Rock mostly big k-fsp crystals but also fine-grained weathered granite. Brecciated boulders [Bi0, Bi1, Bi4]. Limestone boulders >50 cm occurs.	H22 F04 H22 F05 H22 B09
19	Shoreline with dense / a lot of IN-SITU granite breccia [Bi2, Bi5]. Basalt boulders here are not brecciated. Sandstone. Limestone characteristic colors and shape.	H22 F06 H22 F07 H22 B10
20	Small sandy beach, redish coarse sand grains, very shallow waters. Big flat horizontal limestone boulders could potentially be in-situ, but could not investigate.	
21	Shoreline a lot of granite IN-SITU, brecciated. Low angle (around 5-10º) cliff. Breccia both [Bi2] coarse matrix and [Bi3] long axis 315º NW.	
22	IN-SITU shoreline cliff, low angle both coarse- and fine-grained granite, brecciated [Bi1, primarily Bi2]. Clasts 10 cm, matrix gravel sized. Sandstone boulders with ichno fossils occur.	
23	IN-SITU 10 meters from shoreline: granite breccia [Bi1]. Many breccia boulders [Bi1-Bi2] and sandstone boulders with ichno fossils and clay-holes.	
24	IN-SITU. Shoreline-cliff of about 19 x 7 meters. Low angle (10º) cliff primarily semi-fine-grained granite of varied brecciation [Bi1, Bi3]. Basaltic xenoliths and portions of finer grained granite occur, these are not fractured but seem intact [Bii]. In the IN-SITU breccia [Bi3] some fractures are >1 m long. Long axis measurements of [Bi3] from north to south: 328º NNW, 322º NNW, 330º NNW, 325º NNW, 325º NNW.	
25	Steep angle (20-25º) IN-SITU cliff of granite with varied brecciation. Many portions are intact [Bii], much is only fractured [Bi1]. In boulders breccia [Bi1] is common. Long axis measurements of [Bi3] from north to south: 340º N, 330º NNW, 320º NNW, 330º NNW.	
26	IN-SITU granite cliff, showing different modes of brecciated rock as well as intact [Bii]. Primarily [Bi1] & [Bi2] but smaller segments show [Bi3] and [Bi5]. In some areas thicker, longer fractures	H22 S07

	intersect both [Bi3] and [Bi1]. In the case of [Bi3] the longer fractures intersect at a high angle, sometimes perpendicular (?). *Axis orientation of [Bi3]-fractures: 320, 335, 270, 290, 330. Drawing (Fig. 12 B).* Important finding: sandstone boulder with fractures filled with calcite. The boulder is also "enveloped" in long crystals (of calcite?), displaying an unusual structure.	
27	IN-SITU granite breccia [Bi2]. Fragments are angular and 3-15 cm, matrix consists of 0,5 cm particles of the same rock type.	
28*	Brecciated granite boulder [Bi1], 150 meters from "normally measured" shoreline. No IN-SITU.	
29	IN-SITU granite, not very brecciated but displaying some [Bi1]. A few boulders of granite breccia [Bi1, Bi2].	
30	Big, granitic boulders showing traces of brecciation [Bi0].	
31	Boulders of granite breccia with calcite cement [Bi4].	
32	Granite IN-SITU breccia displaying [Bi3]. Orientation of axis not measured.	
A	Far from shoreline, lots of sediments and vegetation. No IN-SITU but a lot of granite boulders, some of basalt. Quite angular showing lack of transportation. No signs of brecciation. Weathered k-feldspar is whiteish.	
B	Far from shoreline, lots of sediments and vegetation. No IN-SITU but boulders of granite and basalt. Two main types of granite: a coarser red, a more fine-grained light red.	
C	By the shoreline in a bay, thus a little more than 100 m. from SHORELINE. No IN-SITU. Brecciated boulders [Bi1, Bi2]. Sandstone occurs. The majority of the boulders here are intact and of granite.	
D	IN-SITU a few meters from land in the same bay as locality C, about 5 meters from SHORELINE. The cliff consists of granite what is unevenly brecciated [Bi1, Bi2/Bi5], some parts are intact. Matrix is gravelly and weathered, granite is coarse-grained and weathered. Width 5 m, length 10 m. Continuing in both 290° NNW and 100° ESE direction under the surface. Dip: 10, 20, 30°. *57°21'43"N, 16°15'20"Ö*	H22 F02
E	At SHORELINE. Granite IN-SITU, some parts intact but mostly brecciated [Bi1, Bi2, Bi3, Bi4]. [Bi3] long axis towards 352º N and 358º N. Boulder with angular clasts of both granite and basalt [Bi1, Bi7], no matrix which suggests little transport. Sandstone boulder found. *57°21'43"N, 16°15'18"Ö*	H22 F03
F_1	More than 200 meters from lake shore. A >20 m wide area rich with basalt boulders. Light-colored veins. No brecciation. No IN-SITU.	

F	At SHORELINE. Basalt both in IN-SITU and boulders, brecciated [Bi1 and Bi4]. Calcite crystals bigger than most localities. Breccia is not well cemented and breaks apart easy. Boulder showing contact between granite and basalt (Fig X photo 6/10 09:43), makes you think basalt was there first (older rock).	H22 B11
G_1	More than 300 m. fr. SHORELINE: findings of sandstone. Correlates with earlier mappings of the glacial trail. No IN-SITU	
G	At SHORELINE. IN-SITU basalt, granite boulders. Breccia mostly [Bi1] but [Bi4] in some granite boulders. Close-to-shore-cliff (not examined closer than from a few meters distance) appears to be brecciated [Bi1], rock type is unclear due to lake water weathered surface.	
H	At SHORELINE. Both granite and basalt IN-SITU, brecciated [Bi0, Bi1, Bi3, Bi4]. Granite [Bi3] long axis towards 35º NNE.	
I	At SHORELINE. Granite and basalt IN-SITU. Granite intact and [Bi1]. Basalt IN-SITU [Bi3] long axis towards 350º NNW.	
J	At SHORELINE. Granite IN-SITU, breccia IN-SITU [Bi5].	H22 F08 H22 F09 H22 B12
K	At SHORELINE. Basaltic breccia [Bi4]. And very weird-shaped sandstone (photo 6/10 14:53) could it suggest brittle fraction? Sandstone older than impact? No IN-SITU.	
L	At SHORELINE. No IN-SITU. Boulder granite breccia [Bi2]	
M	At SHORELINE. Weird striations in sandstone boulder. No IN-SITU rock but many sandstone boulders.	
N	At SHORELINE. Lots of sandstone boulders, fractions, or stripes? Granite breccia [Bi1-Bi2].	
O	At SHORELINE. A small island ten meters from shore. Not examined closely but looks brecciated [Bi1-Bi2] and granitic. Most likely IN-SITU.	
P	At SHORELINE. Granite breccia in boulders mostly [Bi2] and partly [Bi1]. No IN-SITU	
Q	At SHORELINE. No IN-SITU. Large, rounded boulders close to shore. Breccia consisting sometimes more of matrix than clasts [Bi6] and different rock types [Bi7], indicating movement before cementation.	
R	Granite IN-SITU with basaltic veins. Not brecciated but fractures occur [Bi1]. Based on rock contact, basalt is older than granite.	
S	Several meters high cliff in granite, IN-SITU. Not brecciated but fractured [Bi1].	
T	Small sandy beach, mixed provenance. Is situated between the esker and esker islands. No IN-SITU	
U	Basaltic high cliff (IN-SITU), steep dip towards north-east. Competent veins that occur to be of a light-colored fracture filling mineral, but suffered plastic deformation.	
V	Granite boulders and IN-SITU, high and steep relief dipping towards north-east.	

X	IN-SITU at boulder beach. Basaltic breccia [Bii, Bi1, Bi4], decimeter-sized fragments. Photo of calcite 10:43.
Y	No IN-SITU. Granite boulders are generally undeformed while all basalt boulders bigger than 1.5 meters here are brecciated [Bi1]. A few granitic boulders show brecciation [Bi1, Bi4].
Z	No IN-SITU. Boulders primarily basalt [Bi1]. Also, basalt [Bi3]. One brecciated boulder consists of both basalt and granite and is classified as [Bi7], however the relationship between these rocks is probably of magmatic origin rather than clasts of different provenance.
Å	Less breccia. No IN-SITU. “Weak [Bi1]” is common. Mostly granite. One boulder of sandstone found, the only one from V to X. A few brecciated rocks: granite [Bi3], basalt [Bi1].
Ä	IN-SITU granitic cliff, strong dip (52-55º) strike (340º). Not brecciated but weakly fractured [Bi1]. Continues for >50 meters (measure in map?).
Ö	The peninsula north of L8. Generally low relief with an abundance of boulders, granitic. No IN-SITU found. Breccia is common, especially [Bi1]. A lot of [Bi2] and a few [Bi3] and [Bi5].

Table A2. Breccia-index used in field.

Index	Description
Bii	Intact crystalline rock, no signs of deformation.
Bi0	Rock is intact, free from cracks and fissures, and shows no sign of deformation. One or several sides are however covered in a thin layer of calcite crystals which are interpreted as fracture filling minerals. (Fig. 13b).
Biw	Fractures or cracks that are vague or weak and maybe unrelated to the impact event.
Bi1	Rock is fractured but contains no matrix, only fissures. The fissures are oriented chaotically and show no pattern. *Not only noted where the fissures are assumed to be related to the impact event, but also for fault related deformation.*
Bi2	Rock is fragmented and has matrix. The matrix consists of particles of sand and gravel size, most likely of target rock. No calcite present.
Bi3	Rock is fractured and the fractures show a pattern in orientation, so called *bookshelf-breccia*. Sets of fractures. (Fig. 11)
Bi4	Breccia with calcite matrix (Fig. 13).
Bi5	Breccia with a blueish matrix of clay size particles. (Fig. 13c-e)
Bi6	Breccia with more matrix than clasts or fragments (not used much).
Bi7	Breccia with fragments of two or more different provenances. Not used much (but see Fig. 14f, locality Q).

Table A3. Localities with sedimentary blocks.

L. 10
L. 11
L.12
L. 13
L. 14
L. 15
L. 18
L. 19
L. 20
L. 22
L. 26
L. 27
L. 32
L. C
L. E
L. K
L. M
L. N
L. Z
L. G1

Tab A4. Localities with in-situ impactites, what kind of breccia and how they are interpreted. Asterisk indicates the presence of fractures with parallel orientation. Locations are illustrated in Fig. 20.

Loc.	Breccia-index	Result	Interpretation: type of impactite and location in impact structure
L. 11	Bi2	Monomict clast sup. breccia	Lithic impact breccia, crater wall or crater fill
L. 14	Bi5	Polymict matrix sup. breccia	Melt bearing impact breccia, crater fill
L. 19	Bi2, Bi5	Monomict clast sup. breccia and polymict clast sup. breccia	Lithic impact breccia and melt bearing breccia, crater fill
L. 18	Bi1, Bi5	Fractured rock and polymict matrix sup. breccia	Fractured basement and melt bearing breccia, the lower part of the crater fill
L. 21	Bi3, Bi2	Parallel fractures and monomict clast sup. breccia	Fractured basement and lithic impact breccia. Crater wall*
L. 22	Bi1, Bi2	Fractured rock and monomict clast sup. breccia	Fractured basement and lithic impact breccia, crater wall
L. 23	Bi1	Fractured rock	Crater wall
L. 24	Bi1, Bi3	Weak fractures, non-parallel fractures and parallel fractured rocks	Fractured basement, crater wall
L. 25	Bii, Bi1, Bi3	Intact rock, fractured rocks and parallel fractures	Intact and fractured basement, crater wall
L. 26	Bii, Bi1, Bi2, Bi3, Bi5	Intact rock, fractured rocks, monomict clast sup. breccia, parallel fractures and polymict matrix sup. breccia	Intact and fractured basement, lithic and melt bearing impact breccia. Lowermost part of the crater fill.
L. 32	Bi3	Parallel fractures	Fractured basement, crater wall
L. 27	Bi2	Monomict clast supported breccia	Lithic impact breccia, crater fill or crater wall
L. D	Bi1, Bi2, Bi5	Fractured rock and monomict clast and matrix supported breccia	Lithic impact breccia and melt-bearing impact breccia, boundary between crater wall and crater fill
L. E	Bi1, Bi2, Bi3, Bi4	Fractured rocks both parallel and non-parallel, some fractures filled with calcite. Monomict clast supported breccia	Fractured basement and lithic impact breccias, at the boundary between crater wall and crater fill
L. F	Bi1, Bi4	Fractured mafic rock, some fractures are filled with calcite	Fractured basement, crater wall has been lithified by calcite during hydrothermal activity
L. G	Bi1, Bi4	Fractured mafic rock, a few fractures are filled with calcite	Fractured basement, crater wall
L. H	Bii, Bi1, Bi3	Intact and fractured rocks, some parallel fractures	Fractured basement, crater wall
L. J	Bi5	Polymict matric sup. breccia	Melt-bearing impact breccia, crater fill
L. X	Bii, Bi1, Bi4	Intact and fractured rocks, some parallel fractures	Fractured basement, crater wall
L. Ä	Bii	Intact rock, steeply dipping	Not impact-related, fault older than impact event
L. R	Bi1	Fractured rock	Basement rocks separated from severe impact-deformation by fault (Locality Ä)
L. S	Bi1	Fractured rock	Basement rocks separated from severe impact-deformation by fault (Locality Ä)
L. U	Bii	Intact rock	Basement rocks separated from severe impact-deformation by fault (Locality Ä)
L. V	Bii	Intact rock	Basement rocks separated from severe impact-deformation by fault (Locality Ä)

Table A5. Rock samples from Hummeln 2022
For samples noted with asterisk, the petrographic description is in Tab. 8.

Serial number	Locality	Description
H22 F01	14	Polymict matrix supported breccia [Bi5]. Very fine grained, blueish matrix. Angular clasts of semi-fine-grained rock fragments, primarily granite, 2-20 mm big, also calcite crystals. Interpretation: suevitic impact breccia, crater fill.
H22 F02	D	Heavily weathered matrix supported breccia [Bi2] and/or [Bi5]. Light color and grainy, feldspar crystals are evident. Falls apart when handled. Interpretation: melt-bearing impact breccia
H22 F03	E	Matrix supported granitic breccia; calcite is matrix [B4]. Maybe biotite in granite. Surface is black from air and/or water contact.
H22 F04*	18	Polymict clast- and matrix supported breccia [Bi5] from IN-SITU. Similar to H22-F06 and containing at least three types of rock fragments: crystals of dark red k-feldspar, clasts of a fine grained light red granite, clasts of a fine grained dark grey claystone and a lighter grey rock. Calcite veins occur in in fissures in big clasts of the fine-grained granite. Interpretation: suevitic impact breccia (crater fill)
H22 F05	18	Fine-grained granite with a weathered rim, no matrix [Bi1]. The rock that it is sample from had other parts with fine-grained matrix [Bi5]. An example of very different grade of brecciation in the same rock. Interpretation: suevitic impact breccia.
H22 F06*	19	Polymict matrix supported breccia [Bi5] from IN-SITU. Similar to H22-F04. Types of clasts: both dark and light granite, one containing biotite crystals of mm-size. Also, dark brown clasts that looks like claystone. Brittle fractures with calcite in the dark brown clasts. Interpretation: suevitic impact breccia (crater fill)
H22 F07	19	Granite clast was part of breccia, displaying both [Bi1] and [Bi5].
H22 F08	J	Clast- and matrix supported breccia [Bi5] with angular k-feldspar fragments. One side is weathered the other displays the blue/grey fine-grained matrix. Interpretation: suevitic impact breccia (crater fill)
H22 F09	J	Polymict clast supported breccia [Bi5], fine-grained matrix. Fragments are primarily light colored and fine-grained granite. Also has some calcite in fractures [Bi4].
H22 B01	8	Granite breccia [Bi0, 4]. Dark-red, fine-grained rock with bigger k-fsp crystals in some parts. The rock (100 x 200 mm) is intact but for the big calcite filled fractures. The calcite crystals have a strange texture which is probably because of the lake water suffering. There are also rounded / nodular quartz crystals adjacent to the calcite.
H22 B02	15	Breccia of granite with a lot of calcite crystals [Bi4].
H22 B03	15	Breccia of granite with a lot of calcite crystals [Bi4]. Some crystals are huge, around 20 mm. Host rock granite is fine-grained.
H22 B04	15	Granite breccia [Bi4]. Weathered surface on both granite and calcite crystals bears witness of lake water weathering: rounded and a bit smochi.
H22 B05	15	Granite breccia [Bi4]. Dark red granite and big veins. Some of the calcite crystals has a pink color on the surface, looks delicious. Turned out to be iron on it according to the SEM.
H22 B06	15	Granite breccia [Bi4]. Dark red TIB granite, big clasts. Some bigger fractures filled with calcite but some only with smaller fragments of the mother rock [Bi2]. On some parts of the calcite on the surface, there is a pink color just like H22-B05.
H22 B07	15	Blue breccia [Bi5] the matrix is fine-grained, and the rock has more matrix than clasts [Bi6?]. Clasts are generally red and of gravel size (2-5 mm) but one is 40 mm and light colored granite. Triangle!

H22 B08*	15	Blue-breccia [Bi5] with both fine-grained blue/grey matrix and calcite in some veins. Granite clasts of both big, dark-red k-fsp (some qz probably) and finer-grained lighter granite. Also light grey very fine-grained clast, angular, not the same as matrix. Excited about thin sections!!!
H22 B09	18	Granite breccia [Bi4] cement calcite. Rusty oxidation weathering.
H22 B10	19	Intact basalt from a boulder. No brecciation and most sides are fresh.
H22 B11	F	Granite breccia [Bi4] with a blackened weathered surface.
H22 B12	J	Fine-grained granite breccia [Bi4] that looks black on the weathered surface. Wide calcite veins with very big calcite (5-10 mm) crystals.
H22 B13	8	Monomict clast supported (crushed and cemented) granite breccia [Bi1, Bi4]. Clasts of homogenous reddish, fine-grained k-feldspar rich granite. No grainy matrix but small calcite crystals on surfaces of clasts, cementing the rock. Epidote on surfaces and in fractures. Interpretation: fractured crater wall, autochthonous
H22 S01	13	Limestone
H22 S02	19	Limestone
H22 S03	18	Limestone
H22 S04	20	Sandy limestone
H22 S05	18	Sandstone
H22 S06	19	Sandstone
H22 S07	26	“dark” calcite crystals from a sandstone boulder. Mineralizations both in fractures and surrounding/ enveloping the sandstone. Calcite has grown along the side of the boulder, forming pillar like long crystals.

Table A6. Description of Hummeln-1 drill core. For box 21 and 22 there are more detailed descriptions in Tab. A7.

Box	*m. below lake surface*	*Lithology*	*Signs of shock and/ or deformation*
1	17.10-23.57	Un-deformed granite boulder >10 cm overlies dark grey mudstone. Quite homogenous in color and grain-size, except for 10 cm at 22 meters which is dark green from high concentration of glauconite.	When bedding is visible it is not horizontal but rather slumpy.
2	23.57-30.12	Dark grey mudstone. Homogenous grain-size. Some parts are darker and coarser grains. Other parts appear as if they were not fully lithified when the core was retrieved – crumbling.	Some slumping visible despite the little difference in grain-size and color.
3	30.12-36.88	Mudstone, calcareous breccia and light-colored limestone. Echinoderm fossils in the lowermost limestone. Big (>5 cm) cephalopod-fossils.	Slumping in the upper part (mudstone), breccia of limestone. Some stylolites.
4	36.88-43.58	Homogenous light-colored limestone, grey with some glauconitic parts. Horizontal bedding. Not a lot of fossils but some brachiopods, trilobites and cephalopods.	A few stylolites.
5	43.58-50.40	Limestone with varying colors: 43-46 m is light grey, 46-48 m is reddish and very hard, 48-50 m is a darker shade of grey and some areas are greenish due to glauconite grains. Abundance of macrofossils (brachiopods, trilobites and cephalopods) is greater than in overlying strata. Fossils are generally replaced or filled with calcite. “Blommiga bladet” and “Blodläget” are located in the red part.	The light grey uppermost part contains stylolites, one which is oriented perpendicular to the core (almost vertical). The lowermost part displays brecciation: clasts of limestone in a fine-grained lime mud. Transport of older limestone.
6	50.40-57.00	Dominated by dark grey mudstone. In the lowermost two meters there are sections with sand displaying slump-structures. The lowermost 30 cm consists of a coarse-grained lithic arkose. Color, size, and roundness varies in the sandstone.	Slumping occurs in the mudstone. Flow structures in the sandstone.
7	57.00-64.10	Homogenous sandstone with a small portion of mudstone-sandstone interlayered.	Slumping.
8	64.10-70.70	Mostly light-colored sandstone but one meter contains fine mudstone-sandstone layers.	Slumping.
9	70.70-77.44	Mostly light-colored sandstone with some layers of darker mudstone.	Slumping.
10	77.44-84.40	Grey sandstone and greenish mudstone interbedded. Some sections of sandstone are 20-30 cm long while the majority displays laminated sand/mud dipping >30 degrees.	Slump structures cut by faults.
11	84.40-90.80	A little bit more than 50% is dark mudstone. Mudstone is interfingered with massive light-colored sandstone.	Slumping.
12	90.80-97.63	Dark mudstone interfingered with light-colored sandstone. Sharp contrasts between the two lithologies. Fractures contains zink-sulphide (SEM).	Slumping.
13	97.63-104.69	Light colored fine-grained sandstone.	Slumping.
14	104.69-111.15	Light, creamy white sandstone with dark seams of varied orientation. Grain size varies from fine- to coarse sand.	Slump structures. A few of the dark seams are horizontal but most dip >30 degrees or are chaotically deformed.

15	111.15-117.87	Light colored sandstone, fine-grained. Some layers appear almost orange.	Slumping.
16	117.87-124.67	Light colored sandstone. Mostly fine-grained but contains some layers of coarser grains, distinct difference.	Some slumping.
17	124.67-131.53	Rather homogenous sandstone. Light, beige white. A few thin layers of fine-grained black grains.	Slumping and micro-faulting.
18	131.64-138.67	Arkosic sandstone displaying sharp contrasts in color: light-beige, greenish and pink dots (feldspar grains?) in an almost black sandstone.	Slumping.
19*	138.67-144.18	Fine-grained and coarse grained arkosic sandstone. Generally light colored but some darker minerals.	Slumping. Petrographic studies show PF in qz-grains (139.90 m).
20	144.18-151.95	Light yellow-beige sandstone and green-grey mudstone, lots of slumping. Quartz and feldspar rock fragments around 151-152 m.	Slumping of sand and mud.
21*	151.95-158.70	152-155 cm is a generally light colored, coarse-grained arkose with flow patterns of dark-grey and orange sand. 155-157 cm is more homogenous coarse-grained sandstone. 157-158.5 is heavily fractured / brecciated granite [Bi2], containing small sections (>10 cm) of lithic arkose.	Brecciation in granite. Flow structures in the sand-rich parts.
22*	158.70-164.25	159-160 is fractured granite [Bi2], 160-161 shows some flow- or melt structures. 161-162 has a dark, blueish fine-grained matrix [Bi5], with big, isolated feldspar crystals and some calcite filled fractures [Bi4]. Granite breccia with some fragments >30 cm.	Brecciation Fractures with calcite Melt? PF in rounded qz-grains Kink bands in biotite (161.30)

Table A7. Core logging of the lowermost 7 meters (164.25-156.00 m), Fig. 17.

Box number	*Meters below lake surface*	*Description of lithology*	*Signs of shock, alteration, and deformation*
22	164.25-162	164.25-163.50 m consists of monomict, clast supported granite breccia. Matrix contains clay minerals. 163.50-163.20 m polymictic matrix supported breccia, clasts of mostly granite but also mafic rocks containing a lot of chlorites. 163.20-162.50 is monomict matrix supported granite breccia, overlain by a fractured granite boulder (> 0.5 m big). 162.50-162.25 polymict matrix supported breccia, clay in matrix 162.25-162.00 is dominated by "matrix": dark, fine-grained, dense rock (plagioclase and chlorite) that could be either melt or mafic rock. Cutting the dark rock is a granite vein and cutting both granite and mafic rocks are calcite filled fractures.	Breccia Fractures, some calcite filled Chloritization Melt? Flow in granite?
22	162-160	162.00-161.80 continuation of 162.25-162.00. The calcite filled fractures "end abruptly" towards the overlying breccia. 161.80-160.90 polymictic matrix supported breccia, clasts of granite and mafic rock. Matrix does not contain any clays 160.90-160.60 sand-rich breccia with clay and flow structures 160.60-160.00 matrix supported monomict granite breccia overlain by clast supported breccia, overlain by fractured massive granite boulder.	(161.30 A): kind bands in biotite PF and FFL in quartz (160.69, 160.68) Basal PDFs Breccia Fractures, some calcite filled
21	160-158	160.00-159.00 fractured, granite boulder overlain by clast supported monomict granite breccia, no clay in matrix. 159.00-158.40 clast supported granite breccia; matrix contains clay. 158.40-158.10 increasingly more sand in the matrix, overlain by arkosic sandstone with flow patterns. 158.10-158.00 monomict clast supported granite breccia, no clay in matrix.	Fractures Breccia PF in quartz grains (158.27)
21	158-156	158.00-157.58 monomict matrix supported breccia, matrix contains only granite fragments and no visible clay. 157.85-157.25 fractured granite with veins of monomict breccia 157.25-157.10 monomict clast supported breccia overlain by a gradually more matrix supported breccia. 157.10-157.00 light-yellow, coarse-grained arkose sandstone. Bigger grains of mainly quartz but also feldspar, massive and no flow patterns visible. 157.00-156.60 gradually more fine-grained, grey arkose sandstone (massive). 156.60-156.00 fine-grained dark grey and coarse-grained lighter grey arkose sandstone interfingering in flow patterns. Some patterns have massive texture and contains round, light-colored grains.	Fractures Breccia

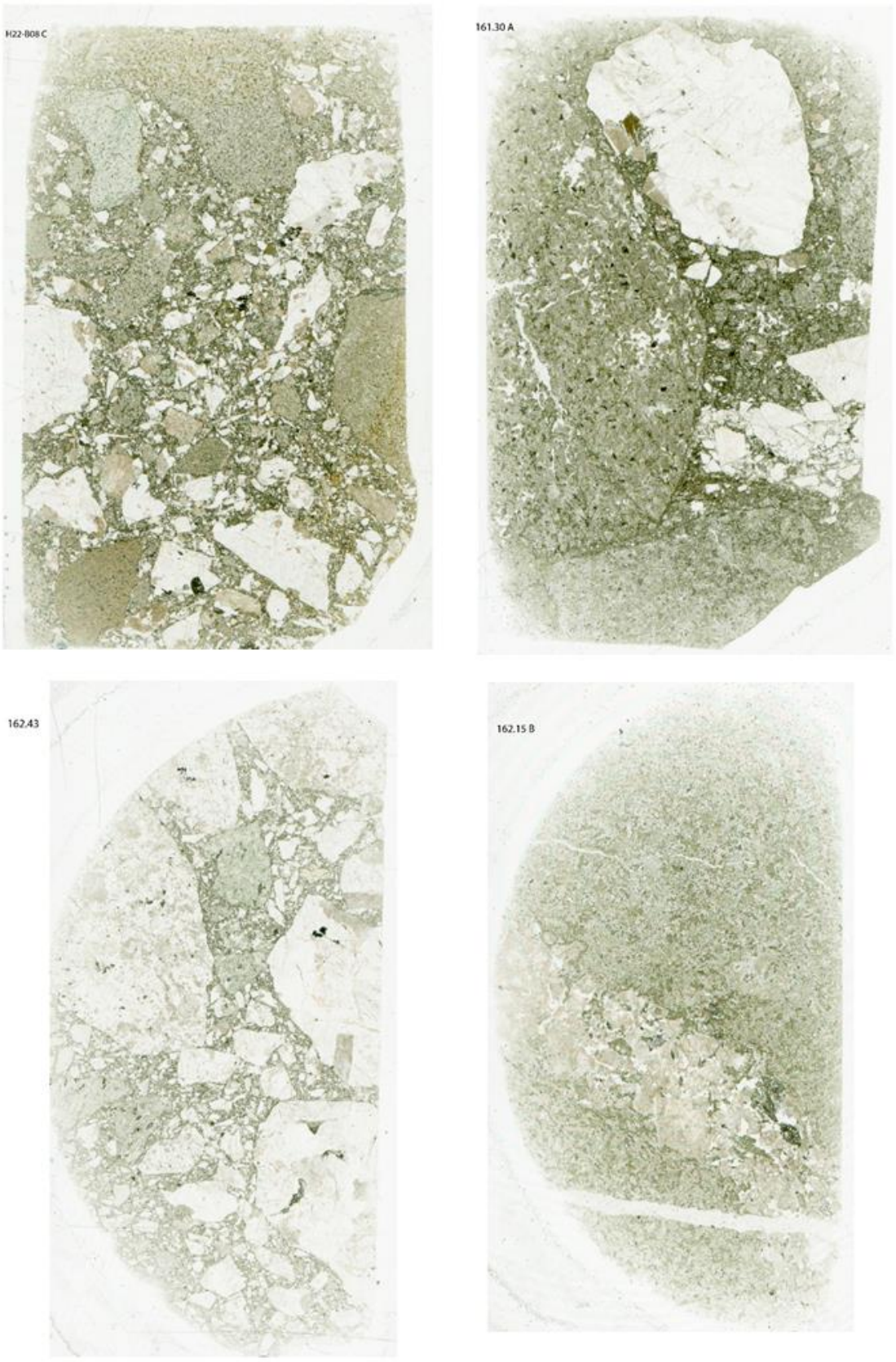

Figure A1. Thin sections showing suevitic impact breccia with chloritized rock fragments (H22-B08 C), suevitic impact breccia with kink bands in biotite (161.30 A), suevitic impact breccia (162.43) and clast-poor impact melt with calcite filled fractures (162.15 B).

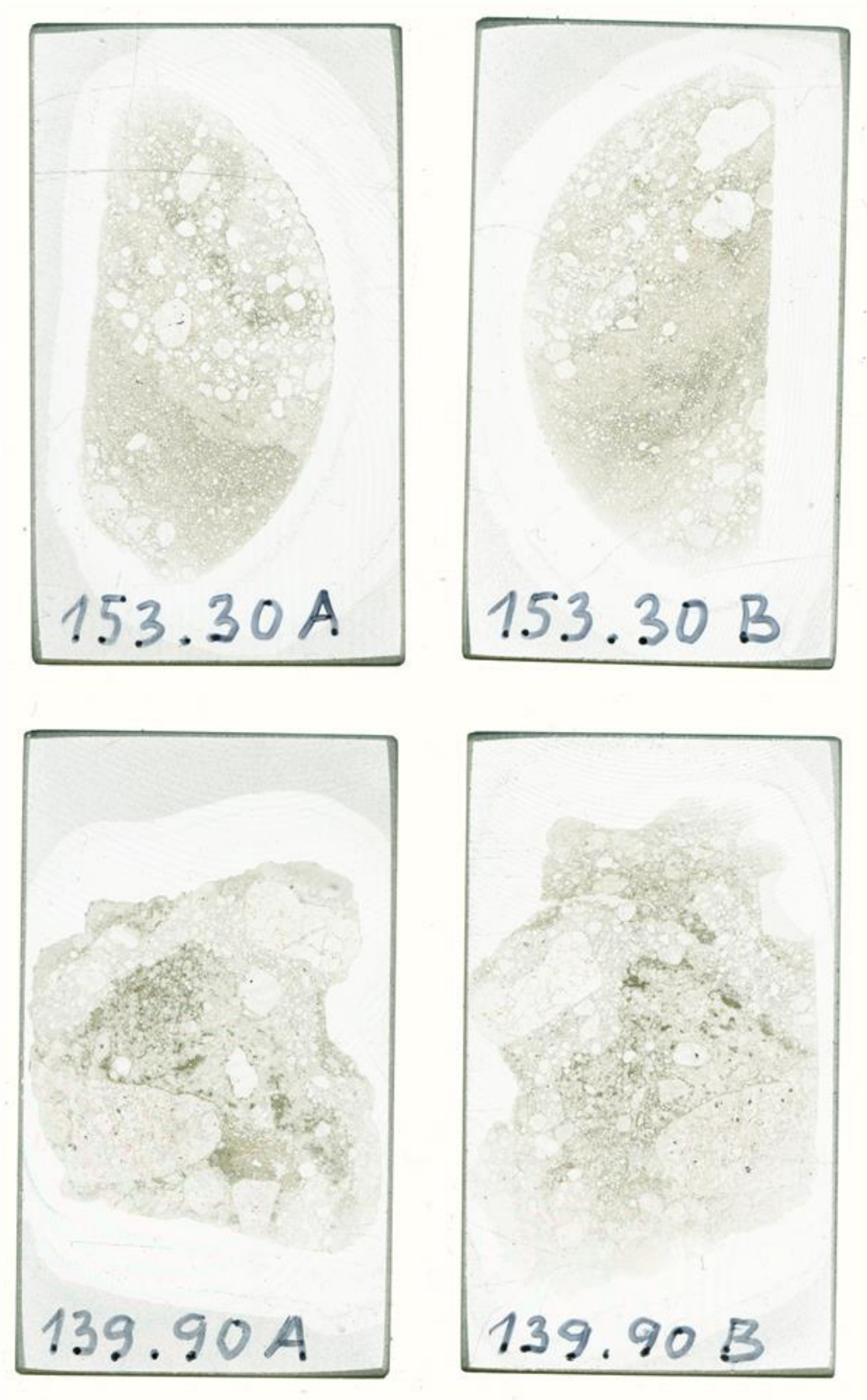

Figure A2. Thin sections from the Hummeln-1 drill core showing different types of arkosic sandstone in the lowermost part of the sedimentary infill. (i.e., above the transition from crater fill till post-impact sediments).

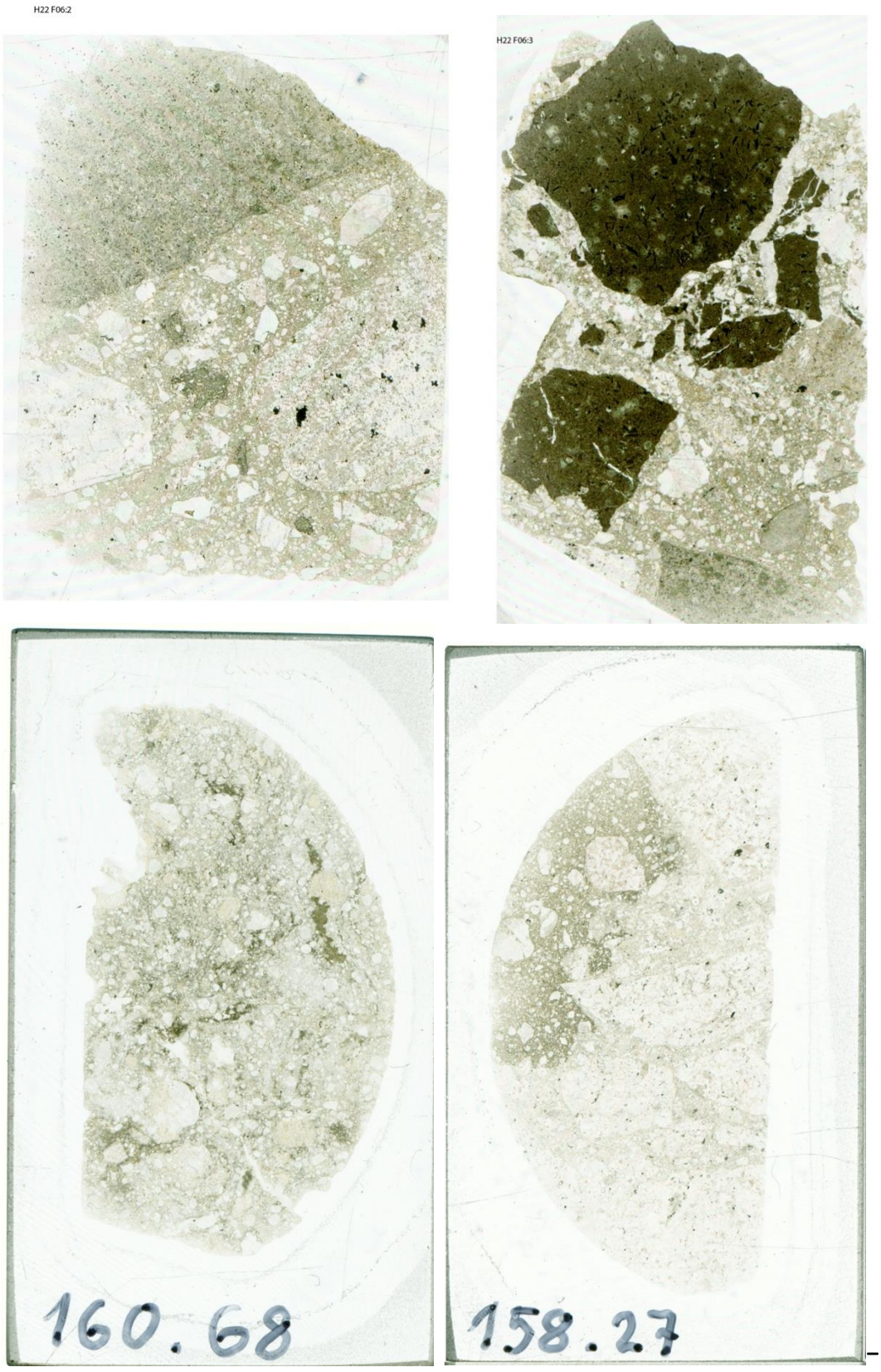

Figure A3. Thin sections from the field samples and the Hummeln-1 drill core. H22-F06:2) Suevitic impact breccia. H22-F06:3) Clasts of claystone displaying chloritized crystals. 160.68) sand-rich impact melt. 158.27) Suevitic impact breccia, the dark area contains clay and rounded quartz-grains with PFs.

Table A8. Petrographic descriptions of hand samples from Hummeln.

Sample	*Description of thin section*	*Shock?*
H22-B08 A	Polymict clast supported breccia. Quartz, microcline, plagioclase, chlorite, calcite, and opaque minerals. Clast type 1: rock fragments of TIB-granite, big euhedral crystals of quartz, feldspars, and a small portion of opaques. Clast type 2: fine-grained rock fragments, more opaques and chlorite, highly altered plagioclase. Big, euhedral calcite crystals. Big, angular quartz crystals that display weird extinction patterns – probably because of alteration. Also, a sawtooth pattern from intergrown quartz and calcite. Calcite filling voids?	No signs of shock.
H22-B08 B	Polymictic matrix supported breccia. Quartz, microcline, plagioclase, chlorite, calcite. Minor: opaques and rutile needles. Big, fine-grained, altered rock fragments. Opaque minerals and maybe biotite, partly altered. Bigger crystals of quartz and microcline are less altered. Some quartz crystals seem to fill out voids. Melted? Matrix is dark and probably consists of clay minerals.	Maybe PF in rounded and / or angular quartz grain.
H22-B08 C	Polymictic, mostly clast supported, breccia. Altered clast contains chlorite. Biotite present in matrix. Microcline crystals displays stretchmarks but also with fresh tartan pattern.	
H22-B08 D	Polymictic, mostly clast supported, breccia. Quartz, microcline, altered plagioclase, micas showing different grades of chloritization, calcite, and opaque minerals. Coarse-grained granite dominates the sample, with fresh looking quartz and microcline, but sericitized plagioclase. Matrix contains a few rounded quartz grains, also many angular quartz grains and clay minerals.	PF in rounded quartz grains.
H22-B08 E	Polymictic, mostly clast supported, breccia. Quartz, microcline, plagioclase, calcite, chlorite, biotite, and opaque minerals. Rock fragments vary in clast-size, angularity, and state of alteration. Plagioclase is more altered than microcline, showing light brown colors. Fine-grained clasts are more altered than big euhedral crystals, plagioclase and biotite have suffered most. Matrix consists of heterogenous fragments. Opaques, chlorite, rounded quartz grains and angular quartz grains.	PF in rounded quartz grains.
H22-B08 F	Polymictic clast supported breccia. Quartz, microcline, sericitized plagioclase, micas showing different grades of chloritization, calcite and opaque minerals. Calcite occurs as filled fractures in rock fragments. Rock fragments primarily have granitic mineralogy but vary from fine-grained to big euhedral crystals. Matrix is dark,	PF in rounded quartz grains.

	fine-grained, and probably contain clay minerals. There are a few sand-grains in matrix. A peculiar mineral grain has chlorite stripes.	
H22-F04:1	Polymictic clast- and matrix supported breccia. Quartz, microcline, plagioclase, biotite, chlorite, calcite, and opaque minerals. Rock fragments are sub-angular to angular, some granitic but most rocks are mafic showing chlorite alteration. One of the rock-fragments is similar to the rock type in H22-F06:4, with abundant elongated crystals. Matrix consists of clay minerals and contains rounded quartz grains.	PF in rounded quartz grains.
H22-F04:2	Polymictic clast- and matrix supported breccia. Quartz, microcline, plagioclase, biotite, chlorite, calcite, and opaque minerals. Rock fragments are prominently angular, but some are angular. Half of the sample consists of a mafic, coarse-grained rock-fragment made up by chlorite, sericitized plagioclase and opaques. There are also several smaller, fine-grained mafic and highly altered rock-fragments. The rest of the mm-big fragments consist of big microcline crystals. There are small portions of clay in matrix, but less than in H22-F04:1, and only a few rounded quartz grains.	No.
H22-F04:3	Generally, the same mineralogy as in H22-F04:2. But also containing an elongated clast of dark, fine-grained, partly chloritized, probably mudstone. Biggest coarse-grained rock fragment contains calcite filled fracture. Also: in the upper left corner: an angular fragment that could potentially be a carbonate clast. Altered, striated, broken in two, and darker along the edges. SEM-studies confirms Ca-mineralogy. Surface has fractures. Not much rounded quartz grains.	No
H22-F06:1	Polymictic matrix supported breccia. Quartz, microcline, plagioclase, biotite, chlorite, calcite, and opaque minerals. The zonation in the granite rock fragments is due to more intense alteration of plagioclase and micas, probably to sericite and chlorite, closer to the rim. Mafic rock fragments are also present but displaying more thorough and even alteration. Matrix consists of clay minerals and contains sand grains.	PF in rounded quartz grains.
H22-F06:2	Polymictic matrix supported breccia. Quartz, microcline, plagioclase, chlorite, calcite, and opaque minerals. Much of the sample consists of sub-rounded fragments of different rock types. A. Mafic rock. The most common mineral makes up elongated, euhedral, dark-grey and light-grey crystals displaying twins. There is some chloritization as well. B. Granite fragment displaying zonation (same as H22 F06:1). Matrix consists of clay minerals and contains sand grains.	PF in rounded quartz grains.
H22-F06:3	Polymictic, mostly matrix supported breccia. Quartz, microcline, altered plagioclase, chlorite, calcite, and opaque minerals Two of the rock fragments are identified as granitic and chlorite-altered mafic rocks. The third type is dark,	PF in rounded quartz grains.

	angular, and fine-grained, probably clay minerals. These also contain chloritized minerals and elongated opaque crystals and some of them contain calcite filled fractures. Matrix consists of clay minerals and contains sand grains.	
H22-F06:4	Sample consists primarily of one rock-fragment. One of the edges contain a quartz rich matrix, with rounded to angular grains. This rock-fragment type is also found, in a smaller fragment, in H22-F04:1. The most common mineral is needle shaped with distinctive twinning. The “fuzzy” surface makes it look altered. Could be a feldspar. SEM: yes, this is oligoclase. Other present minerals in this rock are chloritized, plus plenty of opaque minerals, so it is probably mafic.	-

Table A9. Petrographic descriptions of thin sections from the Hummeln-1 drill core.

m. below lake surface	*Description of thin section*	*Shock?*
164.25 A	Fractured and crushed granite, partly displaying monomict clast supported breccia. Quartz, microcline, altered plagioclase, chlorite. Minor minerals: white mica and opaque minerals. Some small fractures filled with calcite. Clasts are generally angular. Big microcline crystals are fractured.	No sign of shock.
164.25 B	Same as 164.25 A. *SEM: potential melts, two rounded grains noted.*	No sign of shock.
163.21 A	Polymictic (matrix supported?) breccia. Clasts are angular, mostly granitic (big crystals of quartz, microcline, plagioclase, and chlorite) but some show a mafic composition (smaller crystals of chlorite, plagioclase and opaque minerals). Plagioclase is altered to sericite (?) both in big and smaller crystals. Bigger quartz crystals are fractured. Matrix is dark and probably made up of clay minerals.	No sign of shock.
163.21 B	Same as 163.21 A.	No sign of shock.
162.45	Matrix supported polymictic breccia. Two types of angular rock fragments: **A.** Chlorite, altered plagioclase, (micas?) and opaques. **B.** Quartz and microcline, altered plagioclase and opaques. Matrix is dark, probably clay minerals (or glass?).	No sign of shock.
162.43	Matrix supported polymictic breccia. Three types of rock fragments identified, A and B similar to 162.45. **B.** some of the B-fragments contain more opaques and adjacent chlorite. **C.** Big microcline crystal containing small mica crystals. Matrix is the same as in 162.45.	No sign of shock.
162.15 A	More than 70% percent of the sample consists of fine-grained mafic and partly altered rock (plagioclase, chlorite and opaque minerals). A vein of coarser rock consists primarily of quartz, altered plagioclase crystals and opaque minerals. Calcite filled fractures cuts through both. Biotite and plagioclase are more altered close to the vein, suggesting reactions have happened in the weaker zones. Plagioclase is fresher further away from quartz and calcite. White mica and zircon are present in minor amounts.	No sign of shock.
162.15 B	Same as 162.15 A except more and bigger calcite filled fractures.	Same as 162.15 A.
161.80 A	Polymictic clast/matrix supported breccia. Quartz, microcline, plagioclase, calcite, biotite, chlorite, and opaque minerals. Rock fragments are angular and altered to different degrees. **A.** Altered plagioclase and chlorite, also opaques. **B.** Quartz, micas and opaque minerals. Strained. **C.** TIB. Quartz, altered plagioclase and microcline, big crystals. Matrix is dark and consists of clay minerals and opaques, no sand grains present in the matrix. Calcite fills fractures of a rock fragment.	No sign of shock.
161.80 B	Same as 161. 80 A.	No sign of shock.

161.30 A	Polymictic, primarily clast supported, breccia. Matrix is dark. Two types of angular rock fragments: **A.** Heavily altered feldspar and micas, also opaques. Relatively small crystals. **B.** Big crystals of quartz, and microcline and a minor amount of altered plagioclase. These big crystals have shattered and are found adjacent to the rock fragments. By the plagioclase in B there is a big, altered biotite crystal with kink-bands. Fig. A1.	Shock-trace: kink-bands in biotite.
161.30 B	Polymictic, both clast and matrix supported, breccia. Same rock fragments as in 161.30 A but no XXX-mineral. One rock fragment seems to have Fe-impregnation. Same type of matrix as in 161.30 A.	No signs of shock.
160.69	Lithic arkose (there are rock fragm., right?) with smaller domains of wacke, making a flow pattern. Dominant minerals are quartz and microcline making up rounded grains and rock fragments. Also minor amounts of plagioclase, chlorite, micas, opaques. Rutile, pyrite and zircon. Matrix consists of clay minerals and possibly weathered melt. There are also angular grains (feldspar, micas, quartz) present in the matrix.	Shock is present: basal PDF in rock fragment, lots of PF and in rounded quartz grains, several FF (dextral shearing).
160.68	Lithic arkose with clay parts. Quartz, microcline, clay minerals + pyrite, rutile, and zircon. Breccia in the clay parts of the sample is polymictic and matrix supported, angular clasts.	PF in many rounded quartz grains. PFs with several orientations. PDF in one rounded quartz grain and in one rock fragment (quartz and microcline). FFLs.
160.36	Clast supported granite breccia. Big crystals of heavily fractured microcline and quartz. A lot of altered plagioclase. Matrix is not abundant but consists of clay minerals, opaques and micas.	Shock: maybe 1 PF.
158.29	Monomict (matrix and clast supported) granite breccia. Quartz, microcline, both fresh and altered plagioclase, chlorite, minor elements: muscovite and opaque minerals. Altered minerals: plagioclase to sericite (?) and biotite to chlorite. Matrix does not differ in composition from the clasts, and it is locally more concentrated with opaques. Clasts are angular.	No sign of shock found.
158.28	Same as 158.29.	No sign of shock.
158.27	Same as 158.29 to 75%. The lst 25% has a matrix of clay-minerals where some of the clasts are rounded.	Shock traces: PF in rounded quartz grains in the clay-part of the sample.
154.60 A	Lithic arkose. Rounded grains of quartz, microcline and plagioclase. Angular grains of micas. Rock fragments of quarts, feldspars and micas. Quite fresh muscovite and plagioclase. Some chlorite (Fig. 18e).	Shock traces: PF in rounded quartz grains. FF (sinistral or dextral?)
154.60 B	Same as 154.60 A.	Shock traces: PF in rounded quartz grains.
153.85 A	Lithic arkose with rounded to sub-rounded grains in a partly clay matrix. Mostly quartz and microcline, some	Shock traces: PF in rounded quartz grains.

	micas and opaques. Rock fragments consists primarily of either quartz or microcline, but a few of quartz, micas and (probably) altered feldspars. The rock fragments of quartz are (?) probably older generations of sandstone (?). *discuss with S or A*	
153.85 B	Same as 153.85 A.	Shock traces: PF in rounded quartz grains.
153.85 C	Same as 153.85 A.	Shock traces: PF in rounded quartz grains.
153.30 A	Lithic arkose with wacke interfingering in a flow pattern. Very uneven distribution in grain size. Parts with clay matrix contain mostly feldspars and micas, some opaques and clay minerals and a small portion of quartz grains. Parts with less clay contain big, rounded quartz grains and a smaller portion of feldspars. No evident mineral alterations.	No traces of shock.
153.30 B	Same as 153.30 A, but a bigger part of the sample consists of wacke.	No traces of shock.
153.30 C	Same as 153.30 A, but with focus on one altered rock fragment. Mineralogy unclear. *Melted?*	No traces of shock.
139.90 A	Lithic arkose with wacky parts. Mostly quartz and microcline. Some altered minerals, probably feldspars and micas. Green crystals could be glauconite.	Shock traces: a lot (>20) PF found in rounded quartz grains, never in rock fragments. Some grains display three or more orientations of planar fractures.
139.90 B	Same as 139.90 A.	Same as 139.90 A.

Tidigare skrifter i serien ”Examensarbeten i Geologi vid Lunds universitet”:

610. Lindberg Skutsjö, Love, 2021: Geologiska och hydrogeologiska tolkningar av SkyTEM-data från Vombsänkan, Sjöbo kommun, Skåne. (15 hp)
611. Hertzman, Hanna, 2021: Odensjön - A new varved lake sediment record from southern Sweden. (45 hp)
612. Molin, Emmy, 2021: Rare terrestrial vertebrate remains from the Pliensbachian (Lower Jurassic) Hasle Formation on the Island of Bornholm, Denmark. (45 hp)
613. Höjbert, Karl, 2021: Dendrokronologi - en nyckelmetod för att förstå klimat- och miljöförändringar i Jämtland under holocen. (15 hp)
614. Lundgren Sassner, Lykke, 2021: A Method for Evaluating and Mapping Terrestrial Deposition and Preservation Potential-for Palaeostorm Surge Traces. Remote Mapping of the Coast of Scania, Blekinge and Halland, in Southern Sweden, with a Field Study at Dalköpinge Ängar, Trelleborg. (45 hp)
615. Granbom, Johanna, 2021: En detaljerad undersökning av den mellanordoviciska ”furudalkalkstenen” i Dalarna. (15 hp)
616. Greiff, Johannes, 2021: Oolites from the Arabian platform: Archives for the aftermath of the end-Triassic mass extinction. (45 hp)
617. Ekström, Christian, 2021: Rödfärgade utfällningar i dammanläggningar orsakade av *G. ferruginea* och *L. ochracea* - Problemstatistik och mikrobiella levnadsförutsättningar. (15 hp)
618. Östsjö, Martina, 2021: Geologins betydelse i samhället och ett första steg mot en geopark på Gotland. (15 hp)
619. Westberg, Märta, 2021: The preservation of cells in biomineralized vertebrate tissues of Mesozoic age – examples from a Cretaceous mosasaur (Reptilia, Mosasauridae). (45 hp)
620. Gleisner, Lovisa, 2021: En detaljerad undersökning av kalkstenslager i den mellanordoviciska gullhögenformationen på Billingen i Västergötland. (15 hp)
621. Bonnevier Wallstedt, Ida, 2021: Origin and early evolution of isopods - exploring morphology, ecology and systematics. (15 hp)
622. Selezeneva, Natalia, 2021: Indications for solar storms during the Last Glacial Maximum in the NGRIP ice core. (45 hp)
623. Bakker, Aron, 2021: Geological characterisation of geophysical lineaments as part of the expanded site descriptive model around the planned repository site for high-level nuclear waste, Forsmark, Sweden. (45 hp)
624. Sundberg, Oskar, 2021: Jordlagerföljden i Höjeådalen utifrån nya borrningar. (15 hp)
625. Sartell, Anna, 2021: The igneous complex of Ekmanfjorden, Svalbard: an integrated field, petrological and geochemical study. (45 hp)
626. Juliusson, Oscar, 2021: Implications of ice -bedrock dynamics at Ullstorp, Scania, southern Sweden. (45 hp)
627. Eng, Simon, 2021: Rödslam i svenska kraftdammar - Problematik och potentiella lösningar. (15 hp)
628. Kervall, Hanna, 2021: Feasibility of Enhanced Geothermal Systems in the Precambrian crystalline basement in SW Scania, Sweden. (45 hp)
629. Smith, Thomas, 2022: Assessing the relationship between hypoxia and life on Earth, and implications for the search for habitable exoplanets. (45 hp)
630. Neumann, Daniel, 2022: En mosasaurie (Reptilia, Mosasauridae) av paleocensk ålder? (15 hp)
631. Svensson, David, 2022: Geofysisk och geologisk tolkning av kritskollors utbredning i Ystadsområdet. (15 hp)
632. Allison, Edward, 2022: Avsättning av Black Carbon i sediment från Odensjön, södra Sverige. (15 hp)
633. Jirdén, Elin, 2022: OSL dating of the Mesolithic site Nilsvikdalen 7, Bjorøy, Norway. (45 hp)
634. Wong, Danny, 2022: GIS-analys av effekten vid stormflod/havsnivåhöjning, Morupstrakten, Halland. (15 hp)
635. Lycke, Björn, 2022: Mikroplast i vattenavsatta sediment. (15 hp)
636. Schönherr, Lara, 2022: Grön fältspat i Varbergskomplexet. (15 hp)
637. Funck, Pontus, 2022: Granens ankomst och etablering i Skandinavien under postglacial tid. (15 hp)
638. Brotzen, Olga M., 2022: Geologiska besöksmål och geoparker som plattform för popularisering av geovetenskap. (15 hp)
639. Lodi, Giulia, 2022: A study of carbon, nitrogen, and biogenic silica concentrations in *Cyperus papyrus*, the sedge dominating the permanent swamp of the Okavango Delta, Botswana, Africa. (45 hp)
640. Nilsson, Sebastian, 2022: PFAS- En sammanfattning av ny forskning, med ett fokus på föroreningskällor, provtagning, analysmetoder och saneringsmetoder. (15 hp)
641. Jägfeldt, Hans, 2022: Molnens påverkan på jordens strålningsbalans och klimat-

system. (15 hp)

642. Sundberg, Melissa, 2022: Paleontologiska egenskaper och syreisotopsutveckling i borrkärnan Limhamn-2018: Kopplingar till klimatförändringar under yngre krita. (15 hp)
643. Bjermo, Tim, 2022: A re-investigation of hummocky moraine formed from ice sheet decay using geomorphological and sedimentological evidence in the Vomb area, southern Sweden. (45 hp)
644. Halvarsson, Ellinor, 2022: Structural investigation of ductile deformations across the Frontal Wedge south of Lake Vättern, southern Sweden. (45 hp)
645. Brakebusch, Linus, 2022: Record of the end-Triassic mass extinction in shallow marine carbonates: the Lorüns section (Austria). (45 hp)
646. Wahlquist, Per, 2023: Stratigraphy and palaeoenvironment of the early Jurassic volcaniclastic strata at Djupadalsmölla, central Skåne, Sweden. (45 hp)
647. Gebremedhin, G. Gebreselassie, 2023: U-Pb geochronology of brittle deformation using LA-ICP-MS imaging on calcite veins. (45 hp)
648. Mroczek, Robert, 2023: Petrography of impactites from the Dellen impact structure, Sweden. (45 hp)
649. Gunnarsson, Niklas, 2023: Upper Ordovician stratigraphy of the Stora Sutarve core (Gotland, Sweden) and an assessment of the Hirnantian Isotope Carbon Excursion (HICE) in high-resolution. (45 hp)
650. Cordes, Beatrix, 2023: Vilken ny kunskap ger aDNA-analyser om vegetationsutvecklingen i Nordeuropa under och efter Weichsel-istiden? (15 hp)
651. Bonnevier Wallstedt, Ida, 2023: Palaeocolour, skin anatomy and taphonomy of a soft-tissue ichthyosaur (Reptilia, Ichthyopterygia) from the Toarcian (Lower Jurassic) of Luxembourg. (45 hp)
652. Kryffin, Isidora, 2023: Exceptionally preserved fish eyes from the Eocene Fur Formation of Denmark – implications for palaeobiology, palaeoecology and taphonomy. (45 hp)
653. Andersson, Jacob, 2023: Nedslagskratrars inverkan på Mars yt-datering. En undersökning av Mars främsta yt-dateringsmetod ”Crater Counting". (15 hp)
654. Sundberg, Melissa, 2023: A study in ink – the morphology, taphonomy and phylogeny of squid-like cephalopods from the Jurassic Posidonia Shale of Germany and the first record of a loligosepiid gill. (45 hp)
655. Häggblom, Joanna, 2023: En patologisk sjölilja från silur på Gotland, Sverige. (15 hp)
656. Bergström, Tim, 2023: Hur gammal är jordens inre kärna? (15 hp)
657. Bollmark, Viveka, 2023: Ca isotope, oceanic anoxic events and the calcareous nannoplankton. (15 hp)
658. Madsen, Ariella, 2023: Polycykliska aromatiska kolväten i Hanöbuktens kustnära sediment - En sedimentologisk undersökning av vikar i närhet av pappersbruk. (15 hp)
659. Wangritthikraikul, Kannika, 2023: Holocene Environmental History of Warming Land, Northern Greenland: a study based on lake sediments. (45 hp)
660. Kurop, Anna, 2023: Reconstruction of the glacier dynamics and Holocene chronology of retreat of Helagsglaciären in Central Sweden. (45 hp)
661. Frisendahl, Kajsa, 2023: Holocene environmental history of Washington Land, NW Greenland: a study based on lake sediments. (45 hp)
662. Ryan, Cathal, 2023: Luminescence dating of the late Quaternary loess-palaeosol sequence at Velika Vrbica, Serbia. (45 hp)
663. Lindow, Wilma, 2023: U-Pb datering av zirkon i metasediment tillhörande Stora Le-Marstrand, SV Sverige. (15 hp)
664. Bengtsson, Kaisa, 2023: Geologisk karaktärisering av den kambriska Faluddensandstenen i Östersjön och dess lämplighet för koldioxidlagring. (15 hp)
665. Granbom, Johanna, 2023: Insights into simple crater formation: The Hummeln impact structure (Småland, Sweden). (45 hp)

LUNDS UNIVERSITET

Geologiska institutionen
Lunds universitet
Sölvegatan 12, 223 62 Lund